Department of Signal Processing and Acoustics

Contributions to time-frequency synchronization in wireless systems

Tommi Koivisto

Aalto University

DOCTORAL DISSERTATIONS

Aalto University publication series
DOCTORAL DISSERTATIONS 114/2015

Contributions to time-frequency synchronization in wireless systems

Tommi Koivisto

A doctoral dissertation completed for the degree of Doctor of Science (Technology) to be defended, with the permission of the Aalto University School of Electrical Engineering, at a public examination held at the lecture hall S1 of the school on 16 October 2015 at 12.

Aalto University
School of Electrical Engineering
Department of Signal Processing and Acoustics

Supervising professor
Academy Prof. Visa Koivunen

Thesis advisor
Academy Prof. Visa Koivunen

Preliminary examiners
Prof. Mounir Ghogho, University of Leeds, United Kingdom
Dr. Man-On (Simon) Pun, Huawei Technologies, USA

Opponents
Prof. Helmut Bölcskei, ETH Zürich, Switzerland
Prof. Mounir Ghogho, University of Leeds, United Kingdom

Aalto University publication series
DOCTORAL DISSERTATIONS 114/2015

ISBN 978-952-60-6332-4 (printed)
ISBN 978-952-60-6333-1 (pdf)
ISSN-L 1799-4934
ISSN 1799-4934 (printed)
ISSN 1799-4942 (pdf)
http://urn.fi/URN:ISBN:978-952-60-6333-1

Unigrafia Oy
Helsinki 2015

Finland

441 697
Printed matter

Aalto University

Abstract

Aalto University, P.O. Box 11000, FI-00076 Aalto www.aalto.fi

Author
Tommi Koivisto

Name of the doctoral dissertation
Contributions to time-frequency synchronization in wireless systems

Publisher School of Electrical Engineering

Unit Department of Signal Processing and Acoustics

Series Aalto University publication series DOCTORAL DISSERTATIONS 114/2015

Field of research Signal Processing for Communications

Manuscript submitted 16 March 2015 **Date of the defence** 16 October 2015

Permission to publish granted (date) 2 June 2015 **Language** English

☐ **Monograph** ☒ **Article dissertation (summary + original articles)**

Abstract

Time and frequency synchronization is an indispensable task for all wireless transceivers and systems. In modern wireless systems, such as 4G and future 5G systems, new wireless technologies set new challenges also to synchronization. In particular, new solutions for time and frequency synchronization are needed in multiantenna and cooperative systems. New research areas arise also in context of interference cancellation and cognitive radio systems where the transmission parameters of the signal of interest may not be known to the receiver. Similar applications can be found also in the military domain. Obviously, synchronization in such cases poses significant challenges.

In this thesis, new methods for time and frequency synchronization in wireless systems are developed and analyzed. Both orthogonal frequency division multiplexing (OFDM) -based as well as direct sequence spread spectrum (DSSS) -based systems are considered. The thesis consists of seven publications and a summary which contains also an extensive literature review on the topic.

Synchronization acquisition methods in DSSS-based systems without the knowledge of the spreading sequence are developed. A subspace -based method for asynchronous multi-user DSSS systems is proposed and shown to achieve nearly optimal processing gain corresponding to that of the conventional matched filter. The studied methods find applications in interference cancellation, cognitive radio as well as in military applications.

Multiantenna methods for synchronization are analyzed. Probabilities of synchronization acquisition and false alarm are derived analytically for the multiantenna case where transmit, receive and time diversity schemes are used. The analytical results are verified by simulations. Also optimum synchronization sequence transmission schemes are derived. Extensive simulation results for various scenarios in terms of signal-to-noise ratio, spatial correlation and Doppler spread are provided. The results can be used to facilitate practical design of wireless multiantenna systems.

The impacts of time and frequency offsets in cooperative OFDM wireless systems are analyzed and quantified and shown to be, in some cases, much more severe than in traditional OFDM systems. Solutions to estimation of multiple frequency offsets in cooperative OFDM systems are then studied. A method enabling low complexity algorithms to be used for the estimation is proposed and shown to achieve mean square error performance close to the Cramér-Rao bound.

Keywords synchronization, OFDM, spread spectrum, MIMO

ISBN (printed) 978-952-60-6332-4	**ISBN (pdf)** 978-952-60-6333-1	
ISSN-L 1799-4934	**ISSN (printed)** 1799-4934	**ISSN (pdf)** 1799-4942
Location of publisher Helsinki	**Location of printing** Espoo	**Year** 2015
Pages 138	**urn** http://urn.fi/URN:ISBN:978-952-60-6333-1	

Aalto-yliopisto

Aalto-yliopisto, PL 11000, 00076 Aalto www.aalto.fi

Tiivistelmä

Tekijä
Tommi Koivisto

Väitöskirjan nimi
Kontribuutioita aika- ja taajuussynkronointiin langattomissa järjestelmissä

Julkaisija Sähkötekniikan korkeakoulu

Yksikkö Signaalinkäsittelyn ja akustiikan laitos

Sarja Aalto University publication series DOCTORAL DISSERTATIONS 114/2015

Tutkimusala Tietoliikenteen signaalinkäsittely

Käsikirjoituksen pvm 16.03.2015 **Väitöspäivä** 16.10.2015

Julkaisuluvan myöntämispäivä 02.06.2015 **Kieli** Englanti

☐ **Monografia** ☒ **Yhdistelmäväitöskirja (yhteenveto-osa + erillisartikkelit)**

Tiivistelmä

Aika- ja taajuussynkronointi on oleellinen toiminto kaikissa langattomissa vastaanottimissa ja järjestelmissä. Nykyaikaisissa langattomissa järjestelmissä, kuten 4G- sekä tulevissa 5G-järjestelmissä, uudet langattomat teknologiat asettavat uusia haasteita myös synkronoinnille. Uusia synkronointiratkaisuja tarvitaan erityisesti moniantennijärjestelmissä sekä yhteistoiminnallisissa järjestelmissä. Joissain sovelluksissa, esimerkiksi häiriönpoistossa ja kognitiivisissa radioissa, synkronointi on tehtävä vastaanottimessa tuntematta kaikkia signaalin lähetysparametreja, jolloin synkronointi on erityisen haastavaa. Myös sotilassovelluksissa, esimerkiksi tiedusteluvastaanottimien synkronoinnissa, on vastaavia tilanteita.

Tässä väitöskirjassa tutkitaan ja analysoidaan uusia menetelmiä aika- ja taajuussynkronointiin langattomissa järjestelmissä. Tutkimuksen kohteena ovat sekä monikantoaaltomodulaatioon perustuvat OFDM-järjestel\-mät että suorahajotukseen perustuvat hajaspektrijärjestelmät. Työ koostuu seitsemästä erillisestä julkaisusta sekä yhteenvedosta, johon on koottu myös laaja kirjallisuuskatsaus aiheesta.

Suorahajotushajaspektrijärjestelmiin liittyen väitöskirjassa on tutkittu menetelmiä, joilla synkronointi voidaan tehdä tuntematta hajotuskoodia. Työssä on kehitetty aliavaruusmenetelmiin pohjautuva algoritmi synkronointiin ja hajotuskoodin estimointiin asynkronisissa monen käyttäjän hajaspektrijärjestelmissä. Menetelmällä voidaan saavuttaa lähes sovitettua suodatinta vastaava optimaalinen prosessointivahvistus. Tutkittuja menetelmiä voidaan käyttää häiriönpoistossa, kognitiivisissa radioissa sekä sotilassovelluksissa.

Väitöskirjassa on tutkittu myös synkronointimenetelmiä moniantennijärjestelmissä. Työssä on johdettu analyyttisiä tuloksia synkronoinnin onnistumisen todennäköisyydelle tilanteissa, joissa useampaa antennia käytetään sekä lähetys- että vastaanottopäässä lähetys-, vastaanotto- ja aikadiversiteetin parantamiseen. Analyyttisten tulosten on myös näytetty vastaavan simuloituja tuloksia. Työssä on myös tutkittu optimaalisia lähetystapoja. Menetelmiä on simuloitu laajasti eri signaalikohinatasoilla, erilaisilla radiokanavan korrelaatioilla sekä Doppler-hajeilla. Tuloksilla on käyttöä esimerkiksi moniantennijärjestelmien suunnittelussa.

Työssä on tutkittu myös aika- ja taajuuspoikkeamien vaikutuksia yhteistoiminnallisissa OFDM-järjestelmissä, ja näytetty vaikutusten olevan merkittävästi haitallisempia kuin perinteisissä OFDM-järjestelmissä. Näiden ongelmien ratkaisemiseksi työssä on tutkittu menetelmiä taajuuspoikkeamien estimointiin ja kehitetty uusia menetelmiä, joiden avulla taajuuspoikkeamat voidaan estimoida laskennallisesti yksinkertaisilla algoritmeilla. Menetelmillä saavutetaan alhainen estimoinnin keskineliövirhe, joka on hyvin lähellä Cramér-Raon alarajaa.

Avainsanat synkronointi, OFDM, hajaspektritekniikka, MIMO

ISBN (painettu) 978-952-60-6332-4 **ISBN (pdf)** 978-952-60-6333-1

ISSN-L 1799-4934 **ISSN (painettu)** 1799-4934 **ISSN (pdf)** 1799-4942

Julkaisupaikka Helsinki **Painopaikka** Espoo **Vuosi** 2015

Sivumäärä 138 **urn** http://urn.fi/URN:ISBN:978-952-60-6333-1

Preface

The research work leading to this thesis has been carried out under the supervision of Academy Prof. Visa Koivunen from the Department of Signal Processing and Acoustics, Aalto University School of Electrical Engineering (formerly Helsinki University of Technology).

First and foremost, I would like to express my gratitude to Prof. Visa Koivunen for supporting and guiding the work throughout its lengthy history, and for giving me the freedom to choose my research topics while still giving valuable advice to keep the thesis work focused. It has been a great honor to work under the supervision of such a dedicated and distinguished scientist.

Secondly, I wish to thank the pre-examiners of this thesis, Prof. Mounir Ghogho and Dr. Man-On (Simon) Pun for the careful examination of the thesis and for the good comments that helped me improve the quality of the work.

Most of my research work was done while working primarily on 4G wireless system standardization within Nokia, Renesas Mobile Europe Ltd and NVIDIA. During this work, I have had the pleasure of working with the most inspiring and brightest people, all world-class experts in the field of wireless communications. Out of these people, I would in particular like to thank Dr. Kari Pehkonen, my former superior and the leader of the wireless systems research group in Nokia and Renesas Mobile Europe Ltd. I greatly appreciate his support, understanding and encouraging attitude towards academic publishing and finishing my thesis work. In addition, I would like to thank my current and former colleagues, especially Timo Roman and Tero Kuosmanen with whom I also co-authored Publication VI, as well as Mikko Rinne, Pekka Jänis, Kari Hämäläinen, Antti Rasmus, Karol Schober and Mihai Enescu for all the technical advice, non-technical discussions and friendship throughout the years.

Furthermore, from the Department of Signal Processing and Acoustics at Aalto, I want to thank my former colleagues Jarmo Lundén and Keijo Pölönen for all the interesting discussions and advice especially in the early days of my research work.

Finally, special thanks belong to my family. I would like to express my warmest thanks to my parents Tiina and Harri as well as to my siblings Anna-Kaisa and Teemu for all the support. My three little rascals Veeti, Vilho and Väinö deserve my deepest gratitude and love for reminding me of the more important things in life. Lastly, I wish to express my heartfelt thanks and love to my wife Satu for providing understanding, love, comfort and support without which the work would never have been possible.

Espoo, August 19, 2015,

Tommi Koivisto

Contents

List of publications

This thesis consists of an overview and of the following publications which are referred to in the text by their Roman numerals.

I T. Koivisto and V. Koivunen. Blind despreading and synchronization of short-code DS-CDMA signals. In *39th Annual Conference on Information Sciences and Systems*, Baltimore, MD, USA, March 2005.

II T. Koivisto and V. Koivunen. Blind despreading of short-code DS-CDMA signals in asynchronous multi-user systems. *Signal Processing*, vol. 87, no. 11, pp. 2560-2568, November 2007.

III T. Koivisto and V. Koivunen. Diversity transmission for correlation-based slot synchronization with noncoherent combining . In *IEEE 69th Vehicular Technology Conference*, Barcelona, Spain, September 2009.

IV T. Koivisto and V. Koivunen. Diversity transmission of synchronization sequences in MIMO systems. *IEEE Transactions on Wireless Communications*, vol. 11, no. 11, pp. 4048-4057, November 2012.

V T. Koivisto and V. Koivunen. Impact of time and frequency offsets on cooperative multi-user MIMO-OFDM systems. In *IEEE 20th International Symposium on Personal, Indoor and Mobile Radio Communications*, Tokyo, Japan, pp. 3119-3123, September 2009.

VI T. Koivisto, T. Kuosmanen and T. Roman. Estimation of time and frequency offsets in LTE coordinated multi-point transmission. In *IEEE*

78th Vehicular Technology Conference, Las Vegas, NV, USA, September 2013.

VII T. Koivisto and V. Koivunen. Low complexity estimation of multiple frequency offsets using optimized training signals. In *IEEE 11th International Symposium on Spread Spectrum Techniques and Applications*, Taichung, Taiwan, October 2010.

Author's contribution

In all publications, the author has written the first draft and derived all the theoretical studies as well as performed the simulations, except in Publication VI the link-level throughput results were based on simulations run by Mr. Tero Kuosmanen. Also all simulation tools used to perform the simulations have been developed by the author (with the exception of the simulator used for the mentioned link-level throughput results in Publication VI). The co-authors have helped with planning the research and writing the publications.

List of abbreviations

3G	third generation
3GPP	3rd Generation Partnership Project
4G	fourth generation
5G	fifth generation
AIC	Akaike information criterion
BER	bit error rate
BPSK	binary phase shift keying
CDMA	code division multiple access
CFO	carrier frequency offset
CoMP	coordinated multi-point
CRB	Cramér-Rao bound
CRE	cell range expansion
CSI	channel state information
DSSS	direct sequence spread spectrum
DVB-T	digital video broadcasting, terrestrial
EGC	equal gain combining
EM	expectation maximization
ESPRIT	estimation of signal parameters via rotational invariance technique
FFT	fast Fourier transform
GLRT	generalized likelihood ratio test
GPS	global positioning system
ICI	inter-carrier interference
ICIC	inter-cell interference coordination
IEEE	institute of electrical and electronics engineers
IFDMA	interleaved frequency division multiple access
IFFT	inverse fast Fourier transform
ISI	inter-symbol interference

LLR	log-likelihood ratio
LO	local oscillator
LPI	low probability of intercept
LS	least squares
LTE	long term evolution
MDL	minimum description length
MIMO	multiple input multiple output
ML	maximum likelihood
MMSE	minimum mean square error
MRC	maximum ratio combining
MSE	mean square error
MUSIC	multiple signal classification
NLS	nonlinear least squares
OFDM	orthogonal frequency division multiplexing
OFDMA	orthogonal frequency division multiple access
OTDOA	observed time difference of arrival
OTD-S	orthogonal transmit diversity - simulcast
PDP	power delay profile
PIC	parallel interference cancellation
PN	pseudorandom noise
PSS	primary synchronization signal
PVS	precoding vector switching
QAM	quadrature amplitude modulation
QPSK	quadrature phase shift keying
SAGE	space-alternating generalized expectation maximization
SC	selection combining
SIMO	single input multiple output
SINR	signal to interference and noise ratio
SIR	signal to interference ratio
SISO	single input single output
SNR	signal to noise ratio
SSS	secondary synchronization signal
TDD	time division duplexing
TDM	time division multiplexing
TSTD	time-switched transmit diversity
UE	user equipment
WCDMA	wideband code division multiple access
WiMAX	worldwide interoperability for microwave access

WLAN	wireless local area network
ZF	zero forcing
ZZB	Ziv-Zakai bound

List of symbols

$(\cdot)^*$	conjugate
$(\cdot)^H$	conjugate transpose
$(\cdot)^T$	transpose
$\jmath$	imaginary unit, $\jmath = \sqrt{-1}$
$\otimes$	matrix Kronecker product
$E\{\cdot\}$	expected value
$\Im\{\cdot\}$	imaginary part of a complex variable
$\Re\{\cdot\}$	real part of a complex variable
$\lambda_i(\boldsymbol{A})$	the i:th eigenvalue of matrix $\boldsymbol{A}$
$\mathrm{tr}\{\boldsymbol{A}\}$	trace of matrix $\boldsymbol{A}$
$\lvert\boldsymbol{A}\rvert$	determinant of matrix $\boldsymbol{A}$
$\lVert\boldsymbol{A}\rVert_F$	Frobenius norm of matrix $\boldsymbol{A}$
$\mathrm{vec}(\boldsymbol{A})$	vectorization of matrix $\boldsymbol{A}$
$\tilde{a}$	a scalar representing a time domain quantity
a	a scalar representing a frequency domain quantity
$\tilde{\boldsymbol{a}}$	a vector representing a time domain quantity
$\boldsymbol{a}$	a vector representing a frequency domain quantity
$\tilde{\boldsymbol{A}}$	a matrix representing a time domain quantity
$\boldsymbol{A}$	a matrix representing a frequency domain quantity
$\mathbb{C}(\boldsymbol{\mu}, \boldsymbol{R})$	complex normal distribution with mean $\boldsymbol{\mu}$ and covariance $\boldsymbol{R}$
D	decision statistic
f_ν	frequency offset
f_s	sampling rate
$f(x\lvert\mathcal{H})$	probability distribution function conditioned on $\mathcal{H}$
$F(x\lvert\mathcal{H})$	cumulative distribution function conditioned on $\mathcal{H}$
$\boldsymbol{F}$	the Fourier matrix
G	cyclic prefix length

$\mathcal{H}_0$	null hypothesis
$\mathcal{H}_1$	alternative hypothesis
$\tilde{h}$	time domain SISO channel
$\tilde{\boldsymbol{h}}$	time domain SIMO channel
$\tilde{\boldsymbol{H}}$	time domain MIMO channel
$\boldsymbol{I}_N$	identity matrix of size $N \times N$
K	number of transmitters
L	channel impulse response length
N	number of subcarriers, size of fast Fourier transform
N_c	spreading code length
N_d	diversity order
N_r	number of receive antennas
N_s	length of an OFDM symbol
N_{seq}	number of synchronization sequences transmitted in parallel
N_{ss}	number of synchronization sequence transmission repetitions
N_t	number of transmit antennas
N_u	length of the timing uncertainty region
$\tilde{\boldsymbol{r}}$	received signal in time domain
$\boldsymbol{r}$	received signal in frequency domain
$\mathcal{S}$	modulation alphabet
T	symbol period
T_c	chip period
T_s	sampling period
$\tilde{\boldsymbol{v}}$	received noise signal (vector) in time domain
$\tilde{v}_0$	noise under the null hypothesis in time domain
$\tilde{v}_1$	noise under the alternative hypothesis in time domain
$\tilde{\boldsymbol{x}}$	transmitted signal in time domain
Δf	subcarrier spacing
ε	frequency offset normalized by subcarrier spacing
η	threshold value used in hypothesis testing
ν	frequency offset normalized by sampling rate
σ_v^2	noise variance
τ	discrete-time time offset
τ_c	continuous-time time offset
$\Phi(\omega\|\mathcal{H})$	characteristic function conditioned on $\mathcal{H}$

1. Introduction

Fourth generation (4G) wireless communication networks are currently being deployed world-wide, while the third generation (3G) mobile communication systems are already supported by practically every mobile handset. Furthermore, preliminary investigations on the next generation (5G) wireless systems have already started [1]. The latest advancements in wireless systems are necessitated by the proven exponential growth of wireless traffic driven by new applications, in particular by heavily increased mobile video data traffic, by an increase in the number of subscribers as well as by the sheer number of different wireless devices [2]. Meeting all future requirements calls for novel wireless technologies to be explored.

The third (3G) and fourth (4G) generation wireless technologies are based on code division multiple access (CDMA) and orthogonal frequency division multiple access (OFDMA) technologies, respectively. When writing this thesis, for the fifth generation (5G) wireless standards the multiple access scheme selection remains an open topic. In the 3G systems, such as WCDMA [3] [4] [5] and cdma2000 [6], so called direct sequence spread spectrum (DSSS) technologies are used, which enable the CDMA-based multiple access. In CDMA, the users are separated by means of (quasi-)orthogonal spreading codes. In contrast, in OFDMA, which is utilized in the 4G systems such as 3GPP LTE [7] [8], the users are separated in frequency domain. Orthogonal frequency division multiplexing (OFDM) is also utilized as a transmission scheme in IEEE 802.11 -based wireless local area network (WLAN) systems [9], in the IEEE 802.16 WiMAX systems [10][11] as well as in digital video broadcasting (DVB-T) systems [12].

OFDM is generally considered superior to CDMA especially in connection with multiple-input multiple-output (MIMO) technologies as it en-

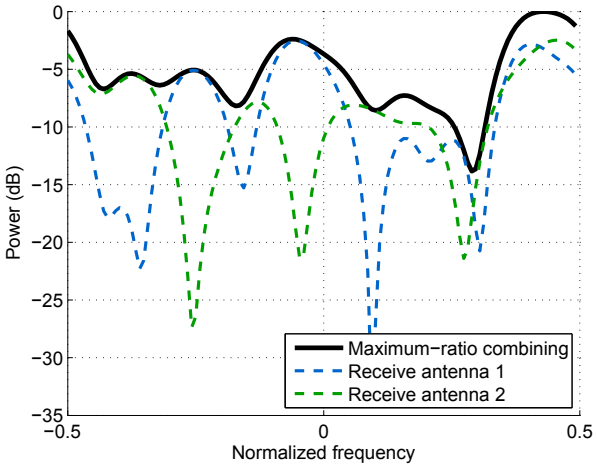

Figure 1.1. Illustration of receive diversity impact in terms of frequency-domain channel power when maximum ratio combining is used. Basically, receive diversity provides protection from deep channel fades as the probability of all antennas facing deep fades simultaneously decreases as the number of antennas is increased.

ables very simple receiver implementation. However, in addition to its importance in the commercial legacy 3G systems, DSSS/CDMA technology remains very important in the military wireless communication domain due to its low probability of intercept properties. The DSSS/CDMA technology enables communication even below the noise level, hence making such communications difficult to detect and intercept. Furthermore, the signal properties of DSSS signals make them well suitable for ranging. Thus the GPS positioning system also utilizes DSSS signaling [13].

One basic technology component of 3G, 4G and future 5G systems is and will be MIMO antenna technology [14][15]. By utilizing multiple antennas at the transmitter and/or the receiver side the spectral efficiency (bits/s/Hz), the link reliability and the coverage can be improved. For instance, a typical 4G LTE base station as well as a typical UE receiver may be equipped with two antennas for enabling 2x2 MIMO transmission and reception. By information-theoretic considerations [14][15], spectral efficiency (bits/s/Hz) can be expected to grow linearly with $\min\{N_t, N_r\}$, N_t and N_r denoting the number of transmit and receive antennas, respectively. To illustrate the improvement in link reliability, Figure 1.1 shows the impacts of a maximum ratio combining -based receiver in terms of frequency-domain radio channel power at the combiner output.

In addition to the MIMO techniques, in order to be able to provide

the required spectral efficiency per area ($\mathrm{bits/s/Hz/km^2}$), also more dense networks and thus reduced cell sizes are required. With smaller cell sizes and more dense networks, inter-cell interference is bound to increase and limit the performance of the network and the benefits obtained by the network densification. Therefore, methods for inter-cell interference coordination are required. One possibility is cooperative transmission schemes in which the different transmitters (e.g. base stations) coordinate their transmissions such as, for example, to minimize interference towards each other, or transmit the data jointly to the receiver in order to combat the interference [16][17].

An important prerequisite for taking advantage of the wireless technologies discussed above is that the receiver has achieved time and frequency synchronization towards one or more transmitters. This thesis addresses time and frequency offset estimation and synchronization in DSSS/CDMA as well as in OFDM-based wireless systems.

1.1 Motivation of the thesis

Time and frequency offset estimation and synchronization are, obviously, required for coherent reception of the transmitted data and for reducing self-interference, but also for many other purposes: For example, several positioning methods rely on the knowledge of the timing of the received signal from several transmitters, e.g. satellites in the GPS system [13], or base stations in mobile wireless systems. Time synchronization enables methods such as observed time difference of arrival (OTDOA) -based positioning which is already utilized in 3G and 4G systems [18] for supporting emergency situations as well as for enabling different location-aware applications. In addition to positioning, another use case requiring time and frequency synchronization towards multiple transmitters arises in cooperative systems which, as mentioned, are considered for 4G and 5G systems. In cooperative systems, the receiver may need to synchronize to multiple transmitters for coherent reception, or may need to, for example, provide feedback about time and frequency synchronization errors between the transmitters in order to enable distributed network synchronization [19][20]. Such aids for network synchronization may be important simply to synchronize the transmissions at frame/subframe/slot level, or for more advanced applications such as for phase-coherent joint cooperative transmissions from multiple transmitters [16][17]. Finally, in

wireless multi-cell systems, cell search is also often done using the same procedures as initial time synchronization [21].

Basic time/frequency synchronization schemes, in particular for single-link single-antenna cases, have been studied for decades for both CDMA and OFDM and are already well known. However, the new developments towards more advanced wireless systems introduce new challenges also in the area of time/frequency offset estimation and synchronization.

For instance, while MIMO communication schemes have been rather thoroughly studied and even deployed in practical networks, there is fairly little research made on the utilization and the actual benefits of multiple antennas at the transmitter and receiver side for synchronization. Since multiple antennas will be deployed in different network entities for purposes of boosting the data rates, it would be very important to understand their utilization also for synchronization purposes. In particular, when multiple (N_t) antennas are deployed at the transmitter side, it would be desirable from both cost and complexity perspective to dimension the corresponding power amplifiers only for a power of P_{tot}/N_t with P_{tot} denoting the total transmit power which needs to be split between the antennas. While it is well known that such an approach can boost the data rates and improve the reliability of the data transmission, it is not obvious that the coverage of synchronization can be improved or even maintained in the same way. Hence studies of multi-antenna schemes for synchronization are necessary.

Cooperative systems also impose additional challenges to time and frequency synchronization. In cooperative systems (or in any other multi-link applications such as positioning), the receiver may need to obtain time and frequency offset estimates corresponding to multiple different transmitters. In cooperative systems, even the impacts of time and frequency offsets and hence the time and frequency synchronization accuracy requirements remain largely unknown. In addition to studying the time and frequency synchronization requirements of these new applications, obviously some efficient methods for estimation of multiple time and frequency offsets are needed.

Finally, related to DSSS/CDMA systems, research has been conducted for several decades and basic concepts and methods are very well known. Typically the time and frequency synchronization in DSSS/CDMA systems is done using known spreading codes. However, there are some unexplored research areas mainly related to cases where spreading codes

are not known to the receiver. In particular, in the military domain there are applications in signal and communications intelligence, such as non-cooperative interception of low probability of intercept DSSS data transmissions, as well as localization of the transmitters, where the spreading codes and other transmission parameters may be a priori unknown. Similarly in the civilian domain, techniques not requiring any kind of a priori knowledge of the spreading codes are important in spectrum surveillance and in detection, characterization and localization of interference sources. Even in commercial systems, applications may be found in interference cancellation where the parameterization of the interfering transmissions may be unknown to the receiver. As an example of this, as of writing this thesis 3GPP has just started investigating network-assisted interference cancellation (IC) for the UMTS system [22]. Some of the envisioned IC methods require estimation of the used channelization codes of the interfering cell.

1.2 Scope and objectives

The first objective of this thesis is developing blind algorithms for synchronization and despreading in non-cooperative CDMA applications. Typically in DSSS/CDMA reception the spreading codes are known to the receiver. The goal here is to consider the very challenging case where the spreading codes are not a priori known to the receiver. Hence, synchronization and despreading needs to be done at very low signal-to-noise ratio conditions via, for instance, blind estimation of the spreading code. Estimation of the spreading code allows for obtaining processing gain even if the code is not exactly known. As mentioned, such methods have use cases in both military and civilian applications in intercept receivers, spectrum surveillance and interference cancellation receivers. However, the scope in this thesis is limited to initial synchronization and spreading code estimation, i.e. blind estimation of other transmission parameters such as modulation order is not considered. Mainly short-code DSSS/CDMA systems are considered, however also a brief review of methods in long-code DSSS/CDMA systems is given.

The second objective of the thesis is finding out the benefits of multi-antenna schemes on initial synchronization. In particular, transmit diversity algorithms and their benefits are studied, in addition to receive and time diversity which have been mainly studied earlier. The goal is to

analyze how different methods of utilizing the multiple antennas at both the transmitter and the receiver side impact the probability of correct synchronization acquisition. Both DSSS/CDMA as well as OFDM-based systems are considered, while the studies are applicable also to any other systems utilizing known synchronization sequences for synchronization. Thus the obtained results are of interests to a wide variety of existing and future wireless MIMO systems. The study is done under the assumption that the receiver is aware of the synchronization sequence(s) used by the transmitter. Also some optimum schemes under long-term channel state information knowledge are considered in the work.

The third objective of the thesis is in analyzing and quantifying the impacts of imperfect time-frequency synchronization on cooperative MIMO-OFDM systems. The corresponding impacts have been already studied earlier thoroughly for single-antenna cases considering only a single transmitter, see e.g. [23] for a thorough review. Hence, the main focus in this thesis is in analyzing the impacts in cooperative MIMO-OFDM systems in which multiple MIMO-OFDM transmitters are serving the receiver in a joint manner. In such cases the receiver has to cope with multiple different time and frequency offsets. Specifically, the main focus is on cooperative transmission schemes that have been considered for example for 4G systems, such as phase-coherent joint transmission and dynamic cell (or transmission point) selection [17].

Finally, once the impacts of time and frequency offsets in cooperative MIMO-OFDM systems are known, the fourth objective of the thesis is in developing methods and algorithms for estimation of the multiple time and frequency offsets in cooperative MIMO-OFDM systems where multiple transmitters coordinate their transmissions, and analyzing the performance of the estimators. The coordination among the transmitters could be done in order to improve the signal strength and/or to reduce interference, for example. As mentioned earlier, such time and frequency offset estimation for multiple transmitters could be also needed for purposes of distributed synchronization of the network with the aid of the receivers [19][20]. Also a review of possible methods for utilizing the time and frequency offset estimates in cooperative systems is provided.

1.3 Contributions of the thesis

The contributions of this thesis are related to blind initial synchronization and despreading in DS-CDMA systems, as well as to time and frequency synchronization in multi-antenna OFDM and CDMA systems, and to time and frequency offset estimation in cooperative MIMO-OFDM systems. The contributions of the thesis in the field of time and frequency synchronization in wireless systems can be listed as follows:

- Algorithms for blind estimation of spreading sequences in direct sequence spread spectrum systems are developed, and an algorithm for asynchronous multi-user short-code DS-CDMA systems is proposed. The algorithm works for non-cooperative applications in which no prior information of the spreading sequences exists. The algorithm is able to provide almost optimal processing gain. In the examples, high resolution direction of arrival estimation of a DSSS signal buried in noise is performed, showing that the estimation performance at low SNR can be significantly improved by using the proposed blind despreading algorithm. Blind algorithms for long-code DS-CDMA systems are also reviewed.

- Multi-antenna schemes for transmission of synchronization sequences are analyzed. The impacts of transmit, receive and time diversity are evaluated using analytical and numerical methods. In particular, the distribution of the synchronization decision statistic is derived under various radio channel conditions and under various diversity schemes, and the probabilities of correct synchronization acquisition and false alarm are derived for frequency-selective channels. A relation between the detection performance and the synchronization correlator output covariance matrix is established. The performance of various practical spatial diversity schemes is characterized using analytical tools as well as in simulation considering various scenarios in terms of spatial correlation, signal to noise ratio and Doppler spread.

- Optimum spatial diversity schemes for synchronization sequence transmission are derived given knowledge of channel spatial correlation, Doppler spread and signal to noise ratio (SNR). Cost functions for studying optimum transmission schemes given such knowledge are formu-

lated. Based on numerical optimization of the cost functions, it is shown how the optimum transmission strategy depends on the channel statistics listed above. Extensive simulations are provided on the optimum schemes.

- The impacts of time and frequency offsets in cooperative MIMO-OFDM systems are analyzed. The impacts are characterized in terms of SINR degradation in case of phase-coherent cooperative systems, for which an analytical expression is derived. It is shown that such systems impose very stringent time and frequency synchronization accuracy requirements on the transmitters. In particular, the frequency synchronization accuracy needs to be of several orders of magnitude more accurate than in typical single-link OFDM systems. In addition, the impacts on channel estimation performance are studied in context of practical LTE coordinated multi-point transmission. In dynamic cell (or transmission point) selection systems, new challenges appear as the receiver may need to very rapidly change the transmitter to which it is locked. The impacts of time and frequency offsets are studied at link throughput level. Part of these results have also been contributed to and made an impact in 3GPP LTE standardization.

- Finally, methods are proposed for estimation of multiple frequency offsets in cooperative MIMO-OFDM systems. The focus is on training-based methods, where typically the frequency offsets cause loss of orthogonality between the training sequences (in addition to inter-carrier interference) and consequent error floors in the estimator performance. Training signal design criteria are introduced for avoiding these problems, and three different methods for achieving designs with these criteria are proposed. It is shown that using the proposed training signals, the estimation of multiple frequency offsets can be decoupled, enabling the utilization of low complexity estimation methods, including some of the well-known single CFO estimation methods.

1.4 Structure of the thesis and summary of the publications

This thesis consists of a summary and seven original publications. The summary is organized as follows: In Chapter 2, an overview of synchro-

nization in wireless systems is given, serving as a background for the forthcoming chapters. In Chapter 3, a literature review of blind methods for DS-CDMA despreading and spreading code estimation is provided. Furthermore, the blind despreading method proposed in Publications I and II is described in Chapter 3. Chapter 4 reviews receive and transmit diversity schemes for synchronization in multi-antenna systems, and summarizes the findings from Publications III and IV regarding the benefits of multi-antenna schemes on synchronization. In Chapter 5, a review of the effects of time and frequency offsets on MIMO-OFDM systems is provided. Also the effects on cooperative systems as analyzed in Publications V and VI are described. Chapter 6 provides an overview of existing methods for multiple frequency offset estimation in cooperative MIMO-OFDM systems, as well as a review of methods of utilizing the multiple frequency offset estimates. Moreover, a summary of the methods proposed in Publication VII is presented in Chapter 6. Finally, Chapter 7 provides the concluding remarks.

The original publications are summarized as follows:

- Publications I and II address the problem of blind initial synchronization and despreading in asynchronous short-code multi-user DS-CDMA systems. An iterative subspace-based algorithm is proposed for estimating the timing offsets and the spreading codes. It is shown that in case of a moderate number of users, it is possible to achieve nearly ideal processing gains already at a low SNR regime using the proposed method. As an application example, in Publication II it is further demonstrated that the performance of non-cooperative direction of arrival estimation in DS-CDMA systems can be significantly improved using the proposed algorithm despite the low SNR of the spread spectrum signal.

- Publications III and IV consider initial synchronization using synchronization signals (training signals) in case of multiple antennas at the transmitter side. In Publication III, the probabilities of false alarm and missed detection are derived analytically for cases where both receive and transmit diversity as well as time diversity are utilized for initial synchronization. A threshold-based correlation detector with noncoherent combining over the diversity branches is employed. The established analytical expressions are verified in simulation. The analytical and simulated results are on par. Furthermore the expressions are utilized

to analyze different transmit diversity schemes in a simulation setup similar to 3GPP LTE synchronization signal transmission [24]. The results show that at low SNR regime, transmit diversity may in fact degrade the performance, and hence it is better to utilize the available degrees of freedom for increasing time diversity, for instance by transmit antenna or precoder switching. In contrast at high SNR a clear performance benefit is observed.

- Publication IV extends the analysis done in Publication III by providing further analytical results and an analysis of optimum transmission schemes given knowledge of the long-term channel statistics such as channel spatial correlation, Doppler spread and signal-to-noise ratio. In order to find the optimum transmission scheme and power allocation, a cost function for maximizing the probability of detection is formulated assuming a genie knowledge of the mentioned statistics, and solved numerically. Moreover, extensive simulation results on practical spatial diversity schemes as well as on the optimum schemes are demonstrated.

- In Publication V, the impacts of small time and frequency offsets on cooperative MIMO-OFDM systems are analyzed. Initial time synchronization is assumed to roughly align the OFDM symbol timing with the FFT window at the receiver side. Also coarse frequency synchronization is assumed such that any residual frequency offsets are clearly smaller than the employed subcarrier spacing in the system. An expression for the SINR in presence of time and frequency offsets is derived, demonstrating that in addition to inter-carrier and inter-symbol interference, multi-user interference is introduced in such systems as well. Furthermore, this multi-user interference is shown to be the dominant source of interference. The results show that in cooperative MIMO-OFDM systems that rely on channel state information feedback from the receiver to the transmitter to achieve phase coherence, very strict time and frequency synchronization accuracy requirements are imposed on the transmitters.

- Publication VI addresses additional problems introduced by time and frequency offsets in cooperative MIMO systems, in particular in the context of 3GPP LTE coordinated multi-point transmission (CoMP). It is shown that time and frequency offsets may cause significant perfor-

mance degradation to certain types of channel estimators. This may cause the employed channel estimators to fail. Thus, also demodulation performance will be degraded. In the paper, the applicability of different LTE reference signals to estimation of the time and frequency offsets is analyzed assuming certain well-known time-frequency tracking algorithms. It is shown that the offsets can be almost perfectly compensated and thus the performance restored.

- In Publication VII, estimation of frequency offsets for multiple transmitters is considered. The transmitters are assumed to be transmitting training signals simultaneously, and methods for the training signal design are proposed such that low complexity frequency offset estimators become applicable. In particular, the proposed methods enable design of training signals that remain nearly orthogonal even in presence of time and frequency offsets. In such case, the estimation of multiple frequency offsets can be done utilizing existing algorithms developed for the single transmitter case. Good performance close to the Cramér-Rao lower bound (see Chapter 6) is demonstrated.

2. Overview of synchronization in wireless systems

In this chapter, a brief overview of synchronization procedures in CDMA and OFDM -based wireless systems is presented. As discussed in Chapter 1, in addition to coherent data reception, time and frequency offset estimation and synchronization may be required for various applications ranging from positioning to aiding distributed network synchronization. Sources of synchronization errors, in addition to the inaccuracies in initial access, are relative motion between the transmitter and the receiver, moving scatterers and changing multipath propagation, Doppler spread of the radio channel, RF unidealities such as local oscillator drifts at the transmitter and the receiver and so on. Also various levels of synchronization can be identified, from coarse and fine symbol-level synchronization to slot or frame level synchronization. In this thesis the interest resides in both the coarse synchronization achieved during initial access as well as the fine synchronization needed to combat the abovementioned effects and to keep the receiver synchronized. In this chapter, basic methods for coarse synchronization are reviewed, and also a brief review of the fine synchronization methods in OFDM systems is provided.

This chapter is organized as follows: In section 2.1, a general overview of the synchronization task is given, in particular focusing on OFDM and CDMA systems. In section 2.2, a review of the relevant theoretical performance bounds is given. Next, in section 2.3, some widely used methods for gaining the initial synchronization are presented. Then, in section 2.4 some specific synchronization methods developed for OFDM systems are considered. The chapter is then concluded with a discussion in section 2.5.

2.1 Overview of synchronization in OFDM and CDMA systems

Let us consider a single link of a multiple input multiple output (MIMO) wireless system in presence of time and frequency offsets. The transmitted continuous-time signal $\tilde{\boldsymbol{x}}_c(t)$ can be modeled at reception with N_r receive antennas as a $N_r \times 1$ vector

$$\tilde{\boldsymbol{r}}(t) = e^{\jmath 2\pi f_\nu t} \int_0^{T_d} \tilde{\boldsymbol{H}}_c(t;\tau_h)\tilde{\boldsymbol{x}}_c(t-\tau_h-\tau_c) + \tilde{\boldsymbol{v}}(t), \tag{2.1}$$

where f_ν is a frequency offset, T_d is the delay spread of the generally time-variant $N_r \times N_t$ continuous-time MIMO channel $\tilde{\boldsymbol{H}}_c(t;\tau_h)$ and τ_c is the (continuous) time offset. Sampling this at the sampling rate of $f_s = 1/T_s$, this becomes in discrete-time

$$\tilde{\boldsymbol{r}}[n] = e^{\jmath 2\pi\nu n} \sum_{l=0}^{L-1} \tilde{\boldsymbol{H}}[n;l]\tilde{\boldsymbol{x}}[n-l-\tau] + \tilde{\boldsymbol{v}}[n], \tag{2.2}$$

where $\nu = f_\nu T_s$ is a frequency offset normalized by the sampling rate, L is the length of the channel impulse response in samples, $\tilde{\boldsymbol{H}}[n;l]$ is the discrete-time counterpart of $\tilde{\boldsymbol{H}}_c(t;\tau_h)$ and τ is the discrete-time time offset. It is noted that the fractional part of the time offset τ_c is modeled as part of the channel matrix in this case. Interference and thermal noise are modeled as an additive white circular Gaussian distributed random noise process $\tilde{\boldsymbol{v}}[n] \sim \mathbb{C}\left(\boldsymbol{0}, \sigma_v^2 \boldsymbol{I}\right)$, where σ_v^2 is the noise variance.

In this thesis, both OFDM and DSSS/CDMA systems are considered. In an OFDM systems, the frequency-selective channel is converted to multiple parallel flat fading channels via fast Fourier transforms (FFT), enabling low complexity equalization of the channel. Additionally, a cyclic prefix is inserted to each OFDM symbol to combat inter-symbol interference and to maintain orthogonality of the subchannels. Thus the time-domain transmitted OFDM signal from a single transmit antenna t can be further written as

$$\tilde{x}_{m,t}[n] = \frac{1}{\sqrt{N}} \sum_{k=0}^{N-1} s_{m,t}[k] e^{\jmath 2\pi \frac{nk}{N}}, \quad n = -G, \ldots, N-1 \tag{2.3}$$

$$\tilde{x}_t[n] = \sum_{m=-\infty}^{\infty} \tilde{x}_{m,t}[n - mN_s] \tag{2.4}$$

where G is the cyclic prefix length, N is the FFT size, $N_s = N + G$ and the modulation symbols transmitted on the subcarriers in OFDM symbol m from transmit antenna t are denoted as $s_{m,t}[k]$.

In contrast, in DSSS/CDMA systems the information-bearing symbols are modulated by pseudo-random code sequences prior to transmission,

resulting in a wideband signal robust to narrowband interference and impacts of multipath propagation. By filtering (despreading) the received signal with a filter matched to the pseudo-random code sequence, the receiver can recover the signal even if the signal power is below the noise level. This gives the DSSS signals their low probability of intercept (LPI) property. The transmitted DSSS/CDMA signal from a single transmit antenna t can be written as

$$\tilde{x}_t[n] = \sum_{m=-\infty}^{\infty} \tilde{s}_{m,t}\tilde{u}_{m,t}[n - mN_c], \tag{2.5}$$

where $\tilde{s}_{m,t}$ are the transmitted modulation symbols and N_c is the length of the spreading code sequence that is written as

$$\tilde{u}_{m,t}[n] = \sum_{k=0}^{N_c-1} \tilde{c}_{m,t}[k]\tilde{p}[n-k]. \tag{2.6}$$

where $\tilde{c}_{m,t}[k]$ denotes the (typically BPSK-modulated) code symbols and $\tilde{p}[n]$ is the pulse shaping function, for instance the root-raised cosine function. In Chapter 3, we separate DSSS/CDMA systems into short-code and long-code systems, based on the length of the code sequence period.

In the synchronization process, the task of the receiver is to obtain estimates of ν and τ in equation (2.2). For purposes of data reception, another task is to synchronize to the transmitted signal using the estimates. Other use cases may involve for instance reporting the acquired estimates to another node, e.g. a base station, forming an equalizer (see section 6.2), or localizing a device based on the estimates. The synchronization task is often divided into two subtasks, i.e. initial synchronization, where the receiver obtains a coarse symbol timing, and fine synchronization (or time and frequency tracking) where the receiver continuously performs more precise time and frequency offset estimation and corrects any residual time and frequency offsets for instance prior to demodulation. The latter procedure is specifically needed in mobile wireless systems where changes in the relative motion between the receiver and the transmitter, moving scatterers, changing multipath channel as well as local oscillator drifts may cause the receiver to otherwise quickly lose synchronization.

In OFDM systems, the main focus is typically on frequency synchronization since even small residual frequency offsets may cause loss of orthogonality among the subcarriers and consequently, significant inter-carrier interference (ICI). As will be further discussed in Chapter 5, in OFDM systems the interest resides in the frequency offset ε that is normalized by the OFDM subcarrier spacing Δf, i.e. $\varepsilon = f_\nu/\Delta f$. The estimation of the

frequency offset ε is typically further split into estimation of the integer and fractional parts of the frequency offset such that $\varepsilon = i_\varepsilon + \delta_\varepsilon$ where i_ε is an integer and δ_ε is the fractional part belonging to the half-open interval $\delta_\varepsilon \in [-1/2, 1/2[$. In most practical cases the problem is mainly in the estimation of δ_ε. Time synchronization on the other hand typically has not been that problematic in OFDM systems due to utilization of the cyclic prefix that provides protection from ISI even in case of imperfect time synchronization. In Chapter 5, the effects of time and frequency offsets on OFDM systems are explored in more detail.

In contrast in DSSS systems, similarly to any other single-carrier systems, more focus is put on time synchronization as imperfect time synchronization would cause significant inter-symbol interference (ISI). For DSSS systems, the main focus in this thesis is on the initial (coarse) time synchronization.

2.2 Performance limits and lower bounds

The limits of achievable estimation performance, e.g. mean square estimation error, are often characterized using various lower bounds. Such limits are useful in predicting the achievable estimation performance in terms of mean square estimation error, and in measuring the efficiency of different estimators. The most commonly used bound is the Cramér-Rao lower bound (CRB), which gives a lower bound on the achievable mean square estimation error using any unbiased estimator. For example, the mean square estimation error achieved by maximum likelihood estimators is known to approach the CRB asymptotically as the observation period tends to infinity.

The Cramér-Rao bound for the time synchronization problem has been presented for instance in [25]. In a flat-fading SISO channel, the Cramér-Rao bound for any unbiased estimator $\hat{\tau}$ of the time delay τ can be expressed as follows:

$$\mathrm{CRB}(\hat{\tau}) = \frac{1 + \mathrm{SNR}^{-1}}{2(2\pi B)^2 \mathrm{SNR}} \tag{2.7}$$

where $\mathrm{SNR} = E_s/N_o$, $E_s = \int_0^T |\tilde{x}(t)|^2 dt$, N_o is the two-sided power spectral density of the additive noise, T is the observation period and

$$B = \frac{\int f^2 |X(f)|^2 df}{E_s} \tag{2.8}$$

is the mean square signal bandwidth. Term $\tilde{x}(t)$ is the continuous-time counterpart of $\tilde{x}[n]$ and $X(f)$ is the Fourier transform of $\tilde{x}(t)$. As seen from

the CRB expression, the achievable time delay estimation mean square error is a function of the observation period, signal bandwidth and signal to noise ratio. Essentially, the mean square error is decreasing as any of these quantities increases.

However, the CRB fails to characterize the performance correctly at low to moderate signal to noise ratios where timing ambiguities start to appear [26]. As will be discussed in more detail in the next section, the maximum-likelihood timing detector involves a cross-correlator. At low to medium SNR, the cross-correlator may produce ambiguous timing peaks which are not taken into account by the CRB. Therefore, the performance predicted by the CRB is too optimistic, i.e. the bound is not tight. Furthermore, the CRB does not take into account any a priori information about the parameter, such as the range of the parameter τ. It is also only applicable to unbiased estimators.

The Ziv-Zakai bound (ZZB) was developed to tackle these problems, and has been used in particular to predict time delay estimation performance [26][27][28]. The ZZB is expressed as follows assuming that the delay is uniformly distributed in the range $\tau \in [0, D]$ [28]:

$$\mathrm{ZZB}(\hat{\tau}) = \frac{1}{D}\int_0^D \theta(D-\theta)P_e(\theta)d\theta, \tag{2.9}$$

where $P_e(\theta)$ is the minimum error probability associated with the following hypothesis testing problem:

$$\mathcal{H}_0 \quad : \quad \tilde{r}(t) = \tilde{h}\tilde{x}(t-a) + \tilde{v}(t) \tag{2.10}$$

$$\mathcal{H}_1 \quad : \quad \tilde{r}(t) = \tilde{h}\tilde{x}(t-(a+\theta)) + \tilde{v}(t). \tag{2.11}$$

In other words, $P_e(\theta)$ is the minimum error probability associated with detecting whether the delay is $\tau = a$ or $\tau = a+\theta$. In evaluating $\mathrm{ZZB}(\hat{\tau})$, $P_e(\theta)$ is derived from a likelihood ratio test. A closed-form expression for the $\mathrm{ZZB}(\hat{\tau})$ typically does not exist, rather evaluating the bound requires numerical computation. In [25], the bound is evaluated and compared with $\mathrm{CRB}(\hat{\tau})$ as well as with the maximum likelihood estimator performance. The results clearly illustrate that $\mathrm{ZZB}(\hat{\tau})$ is a rather tight bound also at low to moderate SNR. In contrast, the lower bound given by $\mathrm{CRB}(\hat{\tau})$ is too optimistic at low SNR. At high SNR, both bounds as well as the performance of the ML estimator approach the same value.

For frequency offset estimation, the Cramér-Rao bound is derived for instance in [29], and is expressed as follows:

$$\mathrm{CRB}(\hat{\nu}) = \frac{3\sigma_v^2}{2\pi^2 M^3} \tag{2.12}$$

where M is the number of samples used for estimation.

2.3 Initial synchronization

Typically receivers perform first an initial or coarse synchronization in order to obtain a rough symbol timing. In practical wireless systems, often at least a frame-level synchronization is obtained by the same procedure. This allows reception of, for example, certain broadcast channels that enable access to the system. Furthermore, in wireless multi-cell systems, cell search is often performed using the same procedure.

In this section, the basic methods of obtaining initial synchronization are briefly reviewed. Very good overviews are given also in [30][31][32] which describe the code acquisition process in spread spectrum systems. However, the same methods are applicable to training signal or preamble -based initial synchronization in any other systems, including OFDM-based systems. A nice overview of the synchronization problem is given also in [33].

In principle, initial time synchronization is a problem of estimating the time delay τ, which is in general a continuous parameter. The single-user maximum likelihood (ML) estimator for the time delay parameter involves correlating the received signal with a known signal [31], such as a preamble or a pseudo-random code sequence, and finding a time delay that maximizes this correlation. Let us consider a single input single output (SISO) system for simplicity (initial synchronization in MIMO systems is discussed in Chapter 4). The correlator output signal can be written as follows:

$$\tilde{y}[n] = \frac{1}{P} \sum_{p=0}^{P-1} \tilde{r}[n+p]\tilde{s}^*[p] \tag{2.13}$$

where P is the correlator length and $\tilde{s}[n]$ is the known synchronization sequence. Then the ML estimator is

$$\hat{\tau} = \arg\max_n |\tilde{y}[n]|^2. \tag{2.14}$$

Typically the correlation is performed only for a set of discrete time delay values n, and the maximum is chosen within this range. The set of values depends on the range of timing uncertainty which depends on the particular application. A sufficient synchronization accuracy is achieved if the time delay is found within a certain window from its correct value such that fine time tracking (and also channel estimation and equalization) is able to handle the remaining synchronization uncertainty.

The above ML-based timing acquisition is applicable when there is a priori knowledge of the presence of a signal. However, often the initial synchronization problem involves also detecting the signal, i.e. deciding whether the signal is present. In such case, the problem boils down to a binary hypothesis testing problem, where the null hypothesis is that the signal is absent or not synchronized and the alternative hypothesis is that the signal is present and synchronized. Thus formally this can be presented as the following hypothesis testing problem:

$$\begin{aligned} \mathcal{H}_0 &: \text{signal absent and/or not synchronized} \\ \mathcal{H}_1 &: \text{signal present and synchronized.} \end{aligned}$$

For purposes of choosing between the hypotheses, the receiver generates a test statistic which is compared against a threshold value to determine whether the alternative hypothesis should be accepted, in which case synchronization can also be declared. In terms of the signal model in (2.13), neglecting frequency offsets and assuming a time-invariant flat-fading SISO channel, the same can be expressed as

$$\mathcal{H}_0 : \tilde{y}[n] = \tilde{v}_0[n] \tag{2.15}$$

$$\mathcal{H}_1 : \tilde{y}[n] = \tilde{h}[n] + \tilde{v}_1[n]. \tag{2.16}$$

where $\tilde{v}_0[n]$ and $\tilde{v}_1[n]$ denote the noise under hypothesis $\mathcal{H}_0$ and $\mathcal{H}_1$, respectively. Choosing between the two hypotheses now follows traditional decision theory. Often the Neyman-Pearson approach is employed to maximize the detection probability under a given constraint on false alarm rate. This leads to a likelihood ratio test [34]. Assuming both the noise and the channel term $\tilde{h}[n]$ complex Gaussian -distributed, the log-likelihood ratio for this problem can be written in a simplified form as

$$D = |\tilde{y}|^2. \tag{2.17}$$

This decision statistic compared to a threshold value η and hypothesis $\mathcal{H}_1$ is declared correct if $D \geq \eta$. In order to find an appropriate threshold value, one needs to establish the distribution of test statistic under hypothesis $\mathcal{H}_0$. It is noted that one may utilize also other hypothesis testing strategies that typically lead to a similar likelihood ratio test but a possibly different threshold value.

The above hypothesis testing is performed on N_u distinct time offset values, called here the timing uncertainty region. As mentioned before, the timing uncertainty region depends on the application. Typically in wireless systems such as 3GPP WCDMA [4][21] and LTE [7][24], the receiver

Table 2.1. Expressions for probabilities of detection P_D and false alarm P_{FA} with different detection strategies assuming a flat-fading channel.

	Threshold-based	ML-based
P_D	$1 - F_D(\eta\|\mathcal{H}_1)$	$\int_0^\infty f_D(x\|\mathcal{H}_1)\,[F_D(x\|\mathcal{H}_0)]^{N_u-1}\,dx$
P_{FA}	$1 - F_D(\eta\|\mathcal{H}_0)$	$1 - P_D$

(UE, user equipment) first acquires the synchronization to the downlink signals transmitted by the base station. In this stage there may be no prior knowledge of the timing, hence the uncertainty region equals the whole repetition period of the known training or synchronization signal. In contrast, for uplink synchronization, there are typically pre-defined slots in which the UE will transmit its (random access) preamble based on the obtained downlink timing. Therefore, at the uplink receiver (base station) side the timing uncertainty region may be rather small as it depends basically only on the maximum propagation delay.

The performance of initial time synchronization is measured by the probability of detecting the signal within a correct time window, as well as by the probability of false alarm, i.e. the probability of choosing hypothesis $\mathcal{H}_1$ when the signal is absent or not synchronized (type I error). These probabilities depend on the chosen timing acquisition strategy: In purely ML-based timing acquisition the receiver would declare synchronization based on the maximum of the decision statistic within the timing uncertainty region, while in the threshold-based acquisition the receiver would declare synchronization whenever the threshold is exceeded, i.e. $D > \eta$. Additionally, a hybrid decision strategy could be chosen such that synchronization is declared whenever the maximum decision statistic within the uncertainty region exceeds the threshold.

Expressions for probabilities of detection and false alarm for the threshold-based as well as the ML-based synchronization detectors are summarized in Table 2.1 in case of flat-fading channels. The expressions are given in terms of probability and cumulative distribution functions $f_D(\eta|\mathcal{H}_i)$ and $F_D(\eta|\mathcal{H}_i)$ of the detection statistic D under different hypotheses, respectively. Note that the explicit expressions of $f_D(\eta|\mathcal{H}_i)$ and $F_D(\eta|\mathcal{H}_i)$ are not provided here — for SIMO and MIMO cases, expressions are presented later in Chapter 4.

In case of frequency-selective channels, synchronization can be declared in principle for any of the L channel taps, provided that the related decision statistic exceeds the threshold. In this case, one may be interested on

the overall detection probability, which in case of threshold-based decision strategy can be expressed as follows:

$$P_D = 1 - \prod_{l=0}^{L-1} F_D(\eta|\mathcal{H}_1^{(l)}) \tag{2.18}$$

where $F_D(\eta|\mathcal{H}_1^{(l)})$ denotes the cumulative distribution function of D evaluated at η under the hypothesis that the local signal is synchronized with the l:th path of the received signal. It is noted that equation (2.18) is based on the assumption of independently fading channel taps.

Especially in CDMA systems, mean acquisition time is also often used as a performance measure in addition to the P_{FA} and P_D [31]. This is essentially the mean of the time needed to acquire synchronization. The time needed to acquire synchronization is a random variable depending on, for example, probabilities of detection and false alarm, initial uncertainty of the timing, size of the uncertainty region N_u, channel conditions and the penalty time due to false alarms. Obviously, different measures of timing offset estimation error are of interest as well.

It is noted that the initial synchronization procedure as described above is similar in both CDMA and OFDM systems whenever there is a known synchronization sequence or a preamble transmitted for synchronization purposes. However, some OFDM-specific methods for initial synchronization are reviewed in the next section, whereas CDMA-specific approaches are covered in section 2.3.1.

In addition to time synchronization, initial acquisition may involve also acquiring an initial estimate of the frequency offset ν. One way to achieve this is the maximum likelihood -based correlation search in frequency, i.e. correlating the received signal with frequency-shifted copies of the synchronization signal [31]. The frequency shifts are chosen from the initial frequency uncertainty region with a desired frequency granularity. Obviously, this approach is rather complex as it involves a two-dimensional search over both time and frequency offsets. A simpler approach is to decouple the time and frequency offset estimation problems. Cross-correlating the received signal with the synchronization signal is not very sensitive to frequency offsets as long as the correlation length is kept short enough. Thus, the impact of frequency offset on the time acquisition can be mitigated by keeping the correlation length P short by performing partial correlations with different parts of the synchronization signal [21][35]. Consequently, the time offset can be estimated using either noncoherent [21] or differential [35] combining of the correlator outputs corresponding to

the different partial correlations. The frequency offset can be estimated using the phase differences between the partial correlator outputs.

In case of OFDM, where dealing with frequency offsets is most important, there exist more specific methods for frequency offset estimation and compensation upon initial acquisition. These methods will be looked at in section 2.4 in more detail.

2.3.1 CDMA-specific aspects of initial synchronization

In contrast to OFDM (see section 2.4), CDMA-specific initial synchronization methods are less common in the literature. The main focus has been on the code acquisition search strategies which essentially specify the order in which the code timing candidates are searched over in threshold-based timing acquisition. More specifically, methods to minimize the mean acquisition time have been studied by optimizing the acquisition search strategy, as well as by optimizing the probability of false alarm and impacts of false alarm by so called multi-dwell search. Good overviews of these are given for instance in [32] and references therein, as well as in [30][36]. Some aspects are briefly reviewed here.

Typically the full uncertainty region needs to be searched through in the code acquisition process, and the search strategy has a direct impact on how long it takes for the receiver to search through all code timing candidates in the timing uncertainty region. The simplest search strategy is serial search in which the receiver goes through all code timing candidates in a serial manner. This is obviously also very time-consuming. Therefore, the search can also be done (at least partly) in parallel such that multiple code timing candidates are tested simultaneously [31]. While M-fold parallelization decreases the search time by a factor of M, it also requires M times the hardware. Thus, parallel search also increases receiver complexity. For instance in a mobile terminal with certain complexity limitations, only serial search or (limited) hybrid serial/parallel search may be feasible. Other (modified) search strategies are well summarized in [31].

In multi-dwell search, instead of declaring acquisition immediately once the threshold ν is exceeded, multiple hypothesis tests are performed, with possibly different dwell (correlation) lengths and threshold values. This allows utilizing lower thresholds, and thus a higher probability of false alarm, in the first search phase(s), since the impact of false alarm is lowered by the later verification phase(s). By optimizing the dwell lengths and the corresponding threshold values, the mean acquisition time can be

reduced [36].

2.4 Synchronization methods in OFDM systems

As mentioned, the correlation -based methods for synchronization as described above are equally applicable for OFDM-based systems in case there is a known preamble or a synchronization sequence transmitted in specific slots with a known location in the frame structure. The difference to many CDMA systems with continuous spreading sequence transmission is mainly in the search strategy as the sequences may be only periodically transmitted (e.g. a preamble). For instance, the 3GPP LTE system relies on periodically transmitted synchronization signals [24]. In Chapter 4 extensions of the correlation-based methods to MIMO case are discussed, where the discussion is kept generic to cover the applicability of the method to both CDMA and OFDM -based systems.

In addition to the correlation-based methods, there are also several methods in the literature that are specific to initial time and frequency synchronization in OFDM systems. Very nice summaries of such methods are presented in [23][37][38], for example. Still, some of the well-known methods are briefly reviewed here.

First, in a seminal work by van de Beek et al. in [39], the redundancy introduced by the cyclic prefix was taken advantage of by a maximum-likelihood -based method. The resulting time and frequency offset estimators are expressed

$$\hat{\tau}_{\mathrm{B}} = \arg\max_{\tau} \{|\gamma(\tau)| - \rho\Phi(\tau)\} \tag{2.19}$$

$$\hat{\varepsilon}_{\mathrm{B}} = -\frac{1}{2\pi} \arg\{\gamma(\tau)\} \tag{2.20}$$

where

$$\gamma(\tau) = \sum_{m=\tau}^{\tau+G-1} \tilde{r}[m]\tilde{r}^*[m+N] \tag{2.21}$$

$$\Phi(\tau) = \frac{1}{2} \sum_{m=\tau}^{\tau+G-1} |\tilde{r}[m]|^2 + |\tilde{r}[m+N]|^2 \tag{2.22}$$

and $\rho = SNR/(SNR+1)$. The estimation range is within $[-1/2, 1/2[$ of the normalized subcarrier spacing, hence additional methods may be needed in the acquisition phase to resolve the integer part of the frequency offset.

Also several methods based on repetitive symbol or training structures have been introduced: A method in which a known synchronization signal

is repeated twice within one OFDM symbol was studied specifically in [40] and [41]. For time synchronization, the method is essentially the same as the usual correlation-based timing acquisition described in the previous section. Frequency offsets may be then estimated from the phase difference between the repeated slots once the timing has been acquired. It is noted that the method of repetitive slots as in [40] [41] was studied for multiple CFO estimation in Publication VII. This is discussed in detail in Chapter 6 and hence a more elaborate discussion is omitted here.

One of the most widely known methods based on repetitive slots is the one developed by Schmidl and Cox [42]. The method is based on OFDM symbols that contain two repetitions of the same signal in time domain. The repetition within an OFDM symbol can be achieved by utilizing only every second subcarrier as illustrated in Figure 2.1. However, the difference to the pure training-based methods in [40] [41] is that the actual transmitted symbols do not need to be known. Still, the method could be classified as data-aided since it requires null subcarriers to be inserted on every second subcarrier, and the receiver is aware of this signal structure. With this structure, the time synchronization may be obtained as

$$\hat{\tau}_{\mathrm{SC}} = \arg\max_{\tau} \frac{|P_{\mathrm{SC}}(\tau)|^2}{(R_{\mathrm{SC}}(\tau))^2} \tag{2.23}$$

where

$$P_{\mathrm{SC}}(\tau) = \sum_{m=0}^{N/2} \tilde{r}^*[\tau+m]\tilde{r}[\tau+m+N/2] \tag{2.24}$$

$$R_{\mathrm{SC}}(\tau) = \sum_{m=0}^{N/2} |\tilde{r}[\tau+m+N/2]|^2. \tag{2.25}$$

A coarse frequency offset estimate may be then obtained as

$$\hat{\varepsilon}_{\mathrm{SC}} = \frac{1}{\pi} \arg\left\{P_{\mathrm{SC}}(\hat{\tau})\right\}. \tag{2.26}$$

Similarly to the estimator by Schmidl and Cox, Moose's estimator in [43] is based on a repetitive symbol structure. However, instead of relying on a single repetitive OFDM symbol, two OFDM symbols are utilized where the latter one is transmitted without a cyclic prefix. Originally in [43] (and also in [23]), the algorithm is presented based on a frequency-domain received signal. However, due to the Fourier transform being unitary, the algorithm can be equivalently presented in time-domain, revealing the resemblance with the Schmidl and Cox's algorithm:

$$\hat{\varepsilon}_{\mathrm{M}} = \frac{1}{2\pi} \arg\left\{\sum_{m=0}^{N-1} \tilde{r}_1^*[m]\tilde{r}_2[m]\right\}. \tag{2.27}$$

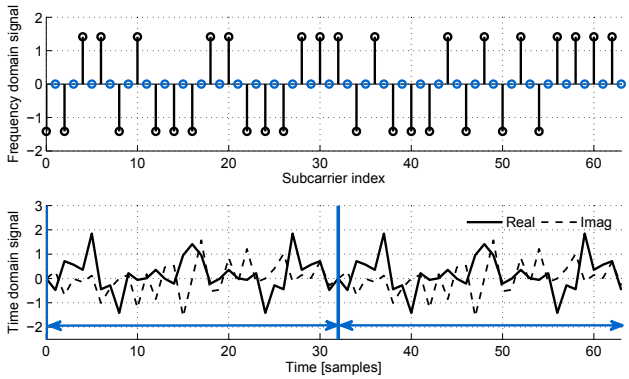

Figure 2.1. Illustration of an OFDM symbol with the repetitive slot -based structure. In frequency domain (top figure), the signal is mapped only to every second subcarrier. This results in a time domain signal (bottom figure) that repeats twice within the OFDM symbol duration.

In the above expression, $\tilde{r}_1[n]$ and $\tilde{r}_2[n]$, $n = 0, \ldots, N-1$ are the two OFDM symbols in time-domain. It is noted that the algorithm is in fact a maximum likelihood estimator of ε [43]. The main difference between Moose's and Schmidl and Cox's estimators is in the symbol structure, resulting in a different frequency offset estimation range. The Schmidl and Cox estimator has a range of $[-1, 1[$ of subcarrier spacing, while the range of the Moose estimator is only $[-1/2, 1/2[$ of subcarrier spacing.

The method of repetitive slots has been also extended to support a larger number of repetitions, such as the training sequences used in IEEE 802.11 -based systems [9] [44]. For instance, in [45], the best linear unbiased estimator (BLUE) was derived as an extension of the Schmidl and Cox method. In the proposed method, the correlations between the repeated slots are first calculated as

$$\tilde{z}[m] = \frac{1}{N - mQ} \sum_{n=mQ}^{N-1} \tilde{r}[n]\tilde{r}^*[n - mQ], \; m = 0, \ldots, H-1. \tag{2.28}$$

where $Q = N/P$ is the length of each of the P slots and $H \leq P - 1$ is a design parameter. The idea is then to combine angles

$$\phi[m] = \arg\{\tilde{z}[m]\} - \arg\{\tilde{z}[m-1]\}, \; m = 1, \ldots, H-1 \tag{2.29}$$

as follows:

$$\hat{\varepsilon}_{\mathrm{ESC}} = \frac{P}{2\pi} \sum_{m=1}^{H} w_{ESC}[m]\phi[m] \tag{2.30}$$

where the weights $w_{ESC}[m]$ are chosen as

$$w_{ESC}[m] = 3\frac{(P-m)(P-m+1) - H(P-H)}{H(4H^2 - 6PH + 3P^2 - 1)} \tag{2.31}$$

The main benefit of this estimator over the Schmidl and Cox estimator is extended frequency offset estimation range which becomes now $[-P/2, P/2]$. It was shown in [45] that the choice $H = P/2$ minimizes the variance of the estimator.

Another method for multiple repetitive slots was proposed in [46], where a nonlinear least squares (NLS) -based method was developed. The estimator can be expressed as follows:

$$\hat{\varepsilon}_{\mathrm{NLS}} = \arg\max_{\varepsilon} \sum_{n=0}^{Q-1} \frac{1}{P} \left| \sum_{p=1}^{P-1} e^{-\jmath 2\pi p\varepsilon/P} \tilde{r}[n+pQ] \right|^2 \tag{2.32}$$

$$= \arg\max_{\varepsilon} \sum_{p=1}^{P-1} \Re\left\{ \tilde{z}[pQ] e^{-\jmath 2\pi p\varepsilon/P} \right\}, \tag{2.33}$$

where $\tilde{z}[\tau]$ is the sample correlation

$$\tilde{z}[\tau] = \sum_{n=0}^{N-\tau-1} \tilde{r}^*[n]\tilde{r}[n+\tau]. \tag{2.34}$$

Interestingly, for $P = 2$ the method has a closed-form solution which reduces to the Schmidl and Cox's method $\hat{\varepsilon} = \frac{1}{\pi} \arg\{\tilde{z}[N/2]\}$. In contrast, there is no closed-form solution for $P > 2$. Therefore, in [46] an approximate NLS-based method was also proposed, however, the details are omitted here.

Another category of OFDM-specific methods for frequency synchronization is based on utilization of null subcarriers. In OFDM systems, typically virtual (zero) subcarriers are inserted at least to band edges to simplify filtering of the received signal. As in case of repetitive slot -type of OFDM symbols, other null subcarriers can be inserted additionally.

A null subcarrier -based algorithm was originally proposed in [47]. It is based on the observation that in presence of CFO, part of the signal energy leaks to the null subcarriers. Therefore, the algorithm targets at minimizing the signal energy on the null subcarriers:

$$\hat{\varepsilon}_{\mathrm{NSC}} = \arg\min_{\varepsilon} \sum_{k \in \mathcal{K}_Z} |r[k+\varepsilon]|^2 \tag{2.35}$$

where $\mathcal{K}_Z$ denotes the set of null subcarriers and $r[k]$ is the received signal in frequency-domain (after FFT), i.e. $r[k] = \frac{1}{\sqrt{N}} \sum_{n=0}^{N-1} \tilde{r}[n] \exp(-\jmath 2\pi nk/N)$. In absence of CFO, due to the null subcarriers the received signal is confined within a subspace spanned by the columns of the Fourier matrix corresponding to the data subcarriers. Therefore, the columns of the Fourier matrix corresponding to the null subcarriers can be used to project the received signal to the subspace corresponding to the null subcarriers, i.e. to

the null space. Thus minimizing the signal energy on the null subcarriers as in equation (2.35) corresponds basically to the MUSIC algorithm [48]. It was further shown in [23][48][49] that this algorithm is in fact a deterministic ML estimator of the CFO.

Further analysis of the null subcarrier -based methods was conducted in [23] and [46]. It was shown that without virtual subcarriers at the band edges, the NLS-based method is equivalent to the method of repetitive slots by Schmidl and Cox. Additionally, the method is in fact equivalent to the null subcarrier -based method described above and is thus ML. In case virtual subcarriers are present, the null subcarrier -based method is still ML. However, it is no longer equivalent to the method of repetitive slots. In this case the method of repetitive slots is only approximately ML as not all needed time-domain correlation lags are taken into account.

Note that since this thesis focuses mainly on data-aided methods for OFDM, this section has mainly covered data-aided methods for OFDM synchronization. All above methods may be characterized as data-aided since they rely either on actual training signals or at least on a certain type of OFDM symbol structure, and in such cases the number of required null subcarriers may in fact be rather large. Fully blind synchronization methods have been omitted here; thorough overview of blind methods is given in [23], for example.

2.4.1 Pilot-assisted time and frequency offset tracking

The methods reviewed above are suitable for time and frequency acquisition. However, as discussed in the beginning of this chapter, the receiver may have to continuously track the estimates in order to avoid losing synchronization due to, for example, changing radio conditions, mobility or local oscillator drifts. For this purpose, many practical OFDM systems broadcast scattered pilots among the data subcarriers. For instance, Figure 2.2 illustrates the cell-specific reference signals utilized in 3GPP LTE [24]. This section reviews the methods for utilizing scattered pilots for time and frequency offset tracking.

The algorithms for time and frequency tracking essentially take advantage of the phase shifts that time and frequency offsets induce between adjacent pilot symbols in frequency and time, respectively. For instance, the conventional algorithm for time offset estimation is based on calculating the phase differences between frequency-adjacent scattered pilots and averaging those. Time offset is then obtained from the averaged phase dif-

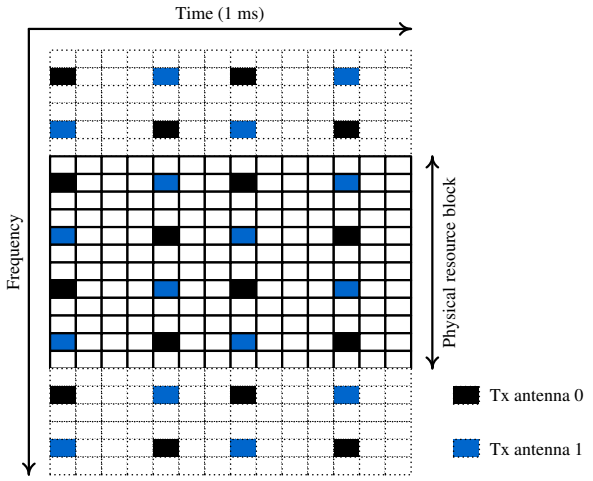

Figure 2.2. Illustration of the cell-specific reference signals (scattered pilots) used in the 3GPP LTE system in case of two transmit antennas [24]. In LTE, the OFDM time-frequency grid is split in time domain in subframes of 1 ms (14 OFDM symbols) and in frequency domain in physical resource blocks of 12 subcarriers.

ference. This method is studied for instance in [50], and its extension to multiple-input multiple-output (MIMO) case was studied in Publication VI for LTE CoMP. The estimator can be expressed as

$$\hat{\tau}_c = -\frac{N}{2\pi\Delta_{p,f}} \arg\left\{ \sum_{k=0}^{N_{p,f}-2} \hat{g}[k,l]\hat{g}^*[k+1,l] \right\} \tag{2.36}$$

where $\Delta_{p,f}$ is the spacing of two pilot subcarriers in frequency, $N_{p,f}$ is the total number of pilot subcarriers in one OFDM symbol and $\hat{g}[k,l]$ is the raw channel estimate on pilot subcarrier k in symbol l, obtained for instance as the least squares estimate as $\hat{g}[k,l] = r[k,l]s^*[k,l]/|s[k,l]|^2$, $s[k,l]$ being the pilot symbol on subcarrier k in symbol l.

Similarly, the frequency offset estimator can be expressed as

$$\hat{\varepsilon} = \frac{N}{2\pi N_s \Delta_{p,t}} \arg\left\{ \sum_{k=0}^{N_{p,f}-1} \sum_{l=0}^{N_{p,t}-2} \hat{g}[k,l]\hat{g}^*[k,l+1] \right\} \tag{2.37}$$

where $\Delta_{p,t}$ is the spacing of two pilot symbols in time and $N_{p,t}$ is the total number of OFDM symbols containing pilot subcarriers.

Maximum-likelihood estimators have been studied in [51] [52] [53] [54] [55] [56]. In [51], it was pointed out that the estimation of the time offset in frequency domain from scattered pilot symbols corresponds to the classical problem of estimating the frequency of a sinusoid. An ML estimator was presented for the time offset. The ML solution for the frequency offset was studied in [52] [53]. It was shown that the optimum

ML estimator does not have a simple closed-form solution, and approximate ML solutions were studied. A closed-form estimator was found by approximating the derivative of the ML cost function by a Taylor series expansion truncated to the linear term, resulting in an estimator similar to (2.37). Furthermore, in [54][55][56], ML-based methods based on scattered pilots were studied by modeling the data subcarriers as additional Gaussian noise.

Finally, in [57] a method also taking advantage of the phase slope introduced by time and frequency offsets in frequency and time, respectively, was studied. The phase slope was estimated using a weighted least squares method, and the offsets were derived from the phase slope. The optimal weights for the weighted LS problem depend on channel conditions. However, in [57] also a simplified set of weights was derived and shown to still perform better than normal LS-based slope matching.

2.5 Discussion

In this chapter, a brief overview of synchronization in OFDM- and CDMA-based wireless systems was provided. Initial time synchronization is typically done by cross-correlating the received signal with a known synchronization or spreading sequence. Based on the correlation, synchronization can be achieved either by finding the maximum correlation peak (ML), or by means of hypothesis testing. For instance, in the 3GPP LTE and WCDMA systems, the initial synchronization is typically done by cross-correlating the received signal against a known periodically transmitted synchronization sequence, and performing hypothesis testing for the correlator outputs [21][24]. Fine time and frequency tracking is crucial in particular in mobile wireless applications in which the time and frequency offsets may be time-varying due to changing channel conditions and local oscillator drifts.

While the techniques discussed in this chapter assume knowledge of the synchronization or spreading sequence, there are applications in which this knowledge can not be assumed, as discussed in the introduction chapter. This leads to very challenging problems that have not been widely studied in the existing literature. Chapter 3 addresses despreading of DSSS/CDMA signals without a priori knowledge of the spreading codes.

Furthermore, SISO links have been assumed in this chapter. Chapter 4 discusses methods for initial synchronization in MIMO systems. In

particular, transmitter side techniques for diversity transmission of synchronization signals in MIMO systems are developed and analyzed in this thesis, which have not been thoroughly studied before.

In OFDM systems, time and frequency offset estimation has often been performed using some of the basic techniques introduced in section 2.4. These techniques are intended for single-link SISO cases, while they are not equally well applicable to (e.g. cooperative) systems with multiple links, where the receiver may need to estimate time and frequency offsets associated with multiple transmitters. This thesis addresses the impacts of imperfect time and frequency offset estimation in cooperative OFDM systems in Chapter 5. Methods for estimating multiple frequency offsets in OFDM systems are studied in Chapter 6.

3. Blind methods for DS-CDMA synchronization

The synchronization methods presented in Chapter 2 rely on a known synchronization or *spreading* sequence. In most typical applications, this is a fair assumption as the signaling waveforms including the synchronization sequences and other pilot sequences may be either explicitly specified, e.g. in a standard specification, or alternatively signaled to the receiver beforehand. However, there are also applications, where such an assumption can not be made. For example, military applications include interception of unknown signals and localization of transmission sources, in which case the synchronization sequences may not be known a priori. Even in civilian applications, similar cases arise for instance in spectrum surveillance. Furthermore, in commercial domain, applications of blind synchronization sequence estimation and synchronization could be envisioned in interference cancellation as well as in cognitive radio systems.

Obviously, the problem of synchronizing without a priori knowledge of the synchronization sequence is a rather difficult one. Basically, in the blind case one has to rely on structural properties of the signal, e.g. constant modulus or finite alphabet properties, or statistical properties of the signal, e.g. higher order statistics or cyclostationarity. The problem is made even more challenging by the fact that in the above-mentioned applications the signal-to-noise ratio may be very low, far below 0 dB. Furthermore, in addition to estimating the synchronization sequence and performing the synchronization, depending on the application the receiver may for instance need to estimate the synchronization sequence length as well as the chip and symbol periods, or perform modulation recognition.

In this chapter, blind methods for initial synchronization and despreading are discussed. As mentioned in Chapter 2, DS-CDMA systems can be split into short-code (periodic) and long-code (aperiodic) systems depending on whether the code sequence spans over multiple symbols or not. The

methods for blind synchronization and despreading in case of short-code DS-CDMA systems are discussed in section 3.1. Long-code DS-CDMA systems are discussed then in section 3.2. The chapter ends with concluding remarks in section 3.3.

3.1 Blind synchronization and code estimation in short-code DS-CDMA systems

Throughout this chapter, a SISO channel, which is quasi-stationary, i.e. time invariant during the observation period, is assumed. The received signal can then be written as

$$\tilde{r}[n] = \sum_{l=0}^{L-1} \tilde{h}[l]\tilde{x}[n-l-\tau] + \tilde{v}[n] \tag{3.1}$$

where τ is the unknown delay. The transmitted DSSS signal can be written as follows:

$$\tilde{x}[n] = \sum_{m=-\infty}^{\infty} \tilde{s}_m \tilde{u}[n-mN_c] \tag{3.2}$$

$$\tilde{u}[n] = \sum_{k=0}^{N_c-1} \tilde{c}[k]\tilde{p}[n-k]. \tag{3.3}$$

where $\tilde{s}_m$ are the transmitted modulation symbols, $\tilde{u}[n]$ is the spreading code of length N_c and $\tilde{c}[k]$ denotes the k:th chip of the spreading code. Note that in contrast to the more general DS-CDMA signal model in equations (2.5) and (2.6), here the spreading code $\tilde{u}[n]$ does not depend on the symbol index m. Such systems where the same spreading code repeats in every symbol are called short-code systems. The problem addressed in this chapter is basically to estimate τ and the spreading code $\tilde{u}[n]$, in order to (blindly) despread the signal. Practically all methods require synchronization (i.e. estimation of τ) to be achieved first, after which the spreading code can be estimated.

The chip period T_c as well as the symbol period $T = T_c N_c$ are assumed known in the following discussion of various blind synchronization and spreading code estimation methods. However, methods exist for estimating these quantities: For instance, the cyclostationarity of the signal can be exploited as proposed in [58][59][60], as well as more recently in [61] for multi-rate DS-CDMA signals. Short-code DSSS signals exhibit cyclostationarity due to the periodicity of the spreading code. Furthermore, if the signal is oversampled with respect to the chip rate, cyclostationarity

arises also due to the chip-level pulse shaping. Hence, chip and symbol periods can be estimated utilizing the cyclic frequencies of the signal. Symbol period estimation as well as rough synchronization can also be achieved using autocorrelation or cyclic autocorrelation -based methods as discussed in [59][62][63]. Finally, it is noted that imperfect chip-level synchronization in the sampling process may cause up to 3 dB loss [64]. However, if needed, this problem can be alleviated by sampling the signal with a rate higher than the chip rate [64].

The methods can be classified into blind channel identification and equalization -based methods, dominant eigenmode -based methods and maximum likelihood -based methods. These are discussed in detail in sections 3.1.1, 3.1.2 and 3.1.3, respectively.

3.1.1 Methods based on blind channel identification and equalization

The first class of methods are based on well-known blind channel identification and equalization algorithms. In the literature there is an abundance of different blind channel identification and equalization methods available and a thorough review of those is outside the scope of this thesis. For instance, in [65], Tong et al. provide a thorough review of blind channel identification methods, including maximum likelihood and subspace -based methods. They also discuss channel identifiability conditions for different approaches. Blind equalization methods are presented for instance in [66][67]. Nevertheless, some of the most important methods are reviewed here.

The methods based on blind channel identification and equalization are based on the fact that the received signal (3.1) can be written as

$$\tilde{r}[n] = \sum_{m=-\infty}^{\infty} \tilde{s}_m \tilde{h}_{\tilde{u}}[n - mN_c - \tau] + \tilde{v}[n] \tag{3.4}$$

where $\tilde{h}_{\tilde{u}}[n]$ is the combined impulse response of the channel and the spreading code, expressed as follows:

$$\tilde{h}_{\tilde{u}}[n] = \sum_{l=0}^{L-1} \tilde{h}[l]\tilde{u}[n-l]. \tag{3.5}$$

Hence in these methods, the underlying idea is to blindly estimate $\tilde{h}_{\tilde{u}}[n]$ instead of just $\tilde{h}[l]$ or $\tilde{u}[n]$. The methods require code synchronization prior to the estimation task, i.e. $\tau = 0$.

Code-blind DSSS signal interception was first considered in [60]. The spread spectrum signal model is cast into a multi-rate or multi-channel

framework, and known blind SIMO channel identification methods are utilized to estimate the joint channel-code impulse response (3.5). The method utilized in [60] is a subspace method based on second-order statistics of the received signal.

The other approach is to perform direct blind equalization of the symbols $\tilde{s}_m$. Blind equalization has been thoroughly studied since 1970's [68], however its application to blind despreading has never been studied to the best knowledge of the author. Similarly to the blind channel identification -based methods, these methods require prior code synchronization, i.e. $\tau = 0$. With this assumption, let us form vectors of N_c samples of the received signal as $\tilde{\boldsymbol{r}}[m] = [\tilde{r}[mN_c], \ldots, \tilde{r}[mN_c + N_c - 1]]^T$. Now, the equalizer output for symbol m can be expressed as

$$\tilde{\boldsymbol{z}}[m] = \boldsymbol{w}^H \tilde{\boldsymbol{r}}[m]. \tag{3.6}$$

Typically these methods find a suitable adaptive filter $\boldsymbol{w}$ by minimizing a certain cost function $J(\boldsymbol{w})$, relying only on the statistical or structural properties of the desired signal (i.e. without any training signal) [68][69] [66]. The minimization can be done for instance by using the well-known method of steepest (gradient) descent which updates the filter coefficients at each step towards the negative gradient as follows:

$$\boldsymbol{w}(i+1) = \boldsymbol{w}(i) - \mu \nabla_{\boldsymbol{w}} J(\boldsymbol{w}(i)). \tag{3.7}$$

Above, parameter μ determines the step size, which impacts the rate of convergence of the algorithm towards the correct solution, and on the other hand also the achievable accuracy (remaining excess error).

The accuracy of the obtained solution as well as the rate of convergence towards the solution also depend on the choice of the cost function $J(\boldsymbol{w})$. A few choices for the cost function are presented here. The most well known blind equalization algorithm is the constant modulus algorithm [69], in which the cost function essentially penalizes deviations of the magnitude of the equalizer output from a pre-defined value as

$$J_{CMA}(\boldsymbol{w}) = E\left\{ \left(|\boldsymbol{w}^H \tilde{\boldsymbol{r}}[m]|^p - R_p \right)^2 \right\}. \tag{3.8}$$

In [69], the choice of R_p is given as $R_p = E\{|\tilde{s}_k|^{2p}\} / E\{|\tilde{s}_k|^p\}$, i.e. it depends on the employed modulation scheme. Obviously, the algorithm is motivated by the fact that many modulation constellations exhibit a constant modulus property, and thus the equalizer output should ideally (in absence of noise) have a constant modulus. However, it is shown that the

Table 3.1. Summary of cost functions for blind equalization.

Cost	$J(\boldsymbol{w})$	References
Constant modulus	$E\left\{\left(\lvert\tilde{\boldsymbol{z}}[m]\rvert^p - R_p\right)^2\right\}$	[69] [66]
Constellation matching	$E\left\{\prod_{k=1}^{\lvert\mathcal{S}\rvert}\lvert\tilde{\boldsymbol{z}}[m] - s_k\rvert^2\right\}$	[70]
Alphabet matching	$E\left\{1 - \sum_{k=1}^{\lvert\mathcal{S}\rvert} e^{-\lvert\tilde{z}[m]-s_k\rvert^2/2\sigma^2}\right\}$	[71]

algorithm also works for non-constant modulus signals such as higher-order QAM modulations [69]. In [66], a thorough introduction into constant modulus -based algorithms for blind equalization is provided.

A slightly different approach to forming the cost function is to match the equalizer output to a known constellation. This approach was first studied by Li et al. in [70] where the proposed cost function penalizes deviations from the known constellation points as

$$J_{Li}(\boldsymbol{w}) = E\left\{\prod_{k=1}^{|\mathcal{S}|}|\tilde{\boldsymbol{z}}[m] - \tilde{s}_k|^2\right\}, \tag{3.9}$$

where $\mathcal{S}$ is the (known) set of constellation points, $|\mathcal{S}|$ denotes its cardinality and $\tilde{s}_k$ is the k:th symbol of the modulation alphabet. In [71] it is shown that the method in (3.9) converges to the correct solution only if the filter is well-initialized. Instead, the following cost function is proposed for matching the equalizer output to the known constellation:

$$J_{AMA}(\boldsymbol{w}) = E\left\{1 - \sum_{k=1}^{|\mathcal{S}|} e^{-|\tilde{z}[m]-\tilde{s}_k|^2/2\sigma^2}\right\}. \tag{3.10}$$

Parameter σ controls the width of the nulls of the cost function, and is chosen such that $e^{-|\tilde{s}(l)-\tilde{s}_k|^2/2\sigma^2} \approx 0$ for $\forall k \neq l$. Of course, using either (3.9) or (3.10) for blind equalization requires prior knowledge of the modulation scheme. A summary of the cost functions discussed in this section is provided in Table 3.1.

An example of utilization of the above methods for blind despreading is illustrated in Figure 3.1 and Figure 3.2. The constant modulus (eq. (3.8)) and alphabet matching -based (eq. (3.10)) adaptive algorithms are used to calculate the filters in case of a short-code DSSS system with $N_c = 31$ at an SNR of -6 dB in a flat Rayleigh fading channel. Figure 3.1 illustrates the convergence of the algorithms while Figure 3.2 shows one snapshot of the real part of the resulting filter coefficients. Note that for illustration purposes the unavoidable phase ambiguity has been removed from the

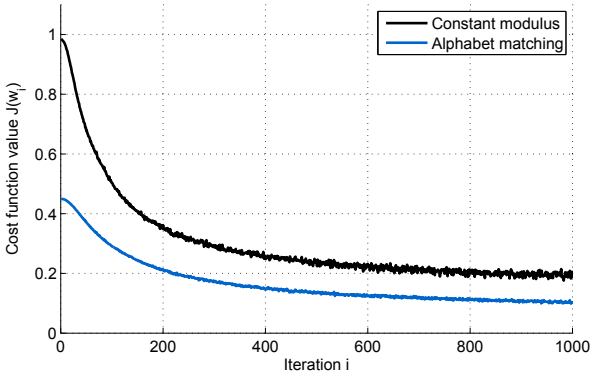

Figure 3.1. Convergence of the constant modulus and alphabet matching -based adaptive blind equalization algorithms in context of blind despreading.

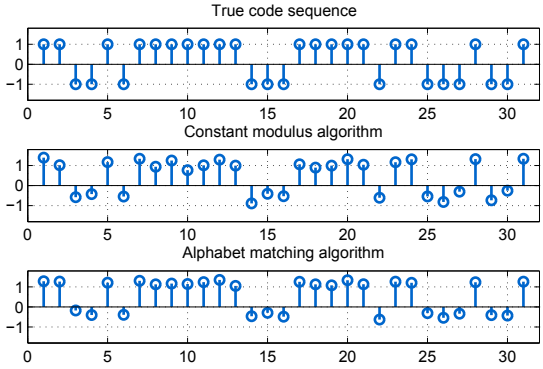

Figure 3.2. True spreading sequence and the (phase-normalized) spreading sequences obtained using the constant modulus and alphabet matching -based adaptive blind equalization algorithms.

filter coefficients. With this normalization, it is seen how the filter coefficients resemble very closely the true spreading sequence, thus enabling despreading of the signal (up to the phase ambiguity).

3.1.2 Dominant eigenmode -based methods

Dominant eigenmode -based methods, originally introduced in [72], are based on the low rank structure of the received signal. Unlike the blind channel identification or equalization -based methods, these methods estimate both the delay as well as the spreading sequence $\tilde{u}[n]$ (up to a phase ambiguity). Let us form vectors of N_c samples of the received signal (in presence of delay τ_c) as $\tilde{\boldsymbol{r}}[m;\tau_c] = [\tilde{r}[mN_c] \dots \tilde{r}[mN_c + N_c - 1]]^T$. These blocks are offset by τ_c with respect to the ideal spreading code timing as

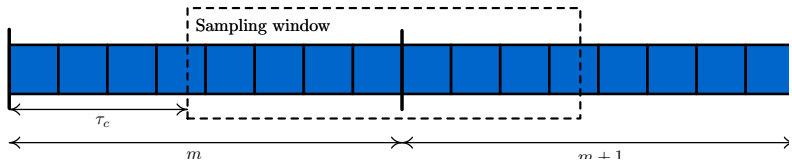

Figure 3.3. Taking N_c samples of the received short-code DSSS signal (with sampling period equal to chip period) when there is a time offset of τ_c results in a vector that contains samples from two consecutive symbols. Therefore, the latter part of the spreading code is in the first part of the received vector, and the first part of the spreading code is in the latter part of the received vector.

illustrated in Figure 3.3. Thus, $\tilde{\boldsymbol{r}}[m;\tau_c]$ can be written as follows:

$$\tilde{\boldsymbol{r}}[m;\tau_c] = \tilde{s}_m \tilde{\boldsymbol{h}}_{\tilde{u},r}(\tau_c) + \tilde{s}_{m+1}\tilde{\boldsymbol{h}}_{\tilde{u},l}(\tau_c) + \tilde{\boldsymbol{v}}[m;\tau_c] \tag{3.11}$$

where $\tilde{\boldsymbol{h}}_{\tilde{u},l}(\tau_c)$ and $\tilde{\boldsymbol{h}}_{\tilde{u},r}(\tau_c)$ correspond to first and second part of the joint channel-code sequence $\tilde{h}_{\tilde{u}}[n]$, respectively, when a delay of τ_c is present. The correlation matrix of the received signal can then be written as follows:

$$\begin{aligned} \boldsymbol{R}_{\tilde{\boldsymbol{r}}\tilde{\boldsymbol{r}}}(\tau_c) &= E\{\tilde{\boldsymbol{r}}(\tau_c)\tilde{\boldsymbol{r}}^H(\tau_c)\} && (3.12)\\ &= P_{\tilde{s}}\left(\tilde{\boldsymbol{h}}_{\tilde{u},r}(\tau_c)\tilde{\boldsymbol{h}}^H_{\tilde{u},r}(\tau_c) + \tilde{\boldsymbol{h}}_{\tilde{u},l}(\tau_c)\tilde{\boldsymbol{h}}^H_{\tilde{u},l}(\tau_c)\right) + \sigma^2_{\tilde{v}}\boldsymbol{I}_{N_c} && (3.13)\end{aligned}$$

where $P_{\tilde{s}} = E\{|\tilde{s}_m|^2\}$. Assuming that the energy transmitted during the spreading sequence transmission is uniformly distributed over the spreading sequence, it can be noted that

$$\begin{aligned} \|\tilde{\boldsymbol{h}}_{\tilde{u},r}(\tau_c)\|^2 &= \frac{T-\tau_c}{T}\|\tilde{\boldsymbol{h}}_{\tilde{u}}\|^2 && (3.14)\\ \|\tilde{\boldsymbol{h}}_{\tilde{u},l}(\tau_c)\|^2 &= \frac{\tau_c}{T}\|\tilde{\boldsymbol{h}}_{\tilde{u}}\|^2 && (3.15)\end{aligned}$$

where $\tilde{\boldsymbol{h}}_{\tilde{u}}$ corresponds to the case $\tau_c = 0$, and thus $\|\tilde{\boldsymbol{h}}_{\tilde{u}}\|^2 = |\tilde{h}|^2 N_c$ (assume flat fading, i.e. $L = 1$, and $\tilde{h}[0] = \tilde{h}$). Using these, the expression of the correlation matrix in (3.13) can be further written as

$$\boldsymbol{R}_{\tilde{\boldsymbol{r}}\tilde{\boldsymbol{r}}}(\tau_c) = \frac{P_{\tilde{s}}N_c|\tilde{h}|^2}{T}\left((T-\tau_c)\tilde{\boldsymbol{u}}_r(\tau_c)\tilde{\boldsymbol{u}}_r^H(\tau_c) + \tau_c\tilde{\boldsymbol{u}}_l(\tau_c)\tilde{\boldsymbol{u}}_l^H(\tau_c)\right) + \sigma^2_{\tilde{v}}\boldsymbol{I}_{N_c}. \tag{3.16}$$

where

$$\begin{aligned} \tilde{\boldsymbol{u}}_r(\tau_c) &= \frac{\tilde{\boldsymbol{h}}_{\tilde{u},r}(\tau_c)}{\|\tilde{\boldsymbol{h}}_{\tilde{u},r}(\tau_c)\|} && (3.17)\\ \tilde{\boldsymbol{u}}_l(\tau_c) &= \frac{\tilde{\boldsymbol{h}}_{\tilde{u},l}(\tau_c)}{\|\tilde{\boldsymbol{h}}_{\tilde{u},l}(\tau_c)\|}. && (3.18)\end{aligned}$$

Because of orthogonality between these vectors $\tilde{\boldsymbol{u}}_r^H(\tau_c)\tilde{\boldsymbol{u}}_l(\tau_c) = 0$, equation (3.16) in facts forms the eigendecomposition of the correlation matrix

$\boldsymbol{R}_{\tilde{\boldsymbol{r}}\tilde{\boldsymbol{r}}}(\tau_c)$. The eigenvalues are

$$\lambda_1(\boldsymbol{R}_{\tilde{\boldsymbol{r}}\tilde{\boldsymbol{r}}}(\tau_c)) = \frac{P_{\tilde{s}} N_c (T-\tau_c)|\tilde{h}|^2}{T} + \sigma_{\tilde{v}}^2 \tag{3.19}$$

$$\lambda_2(\boldsymbol{R}_{\tilde{\boldsymbol{r}}\tilde{\boldsymbol{r}}}(\tau_c)) = \frac{P_{\tilde{s}} N_c \tau_c |\tilde{h}|^2}{T} + \sigma_{\tilde{v}}^2 \tag{3.20}$$

$$\lambda_i(\boldsymbol{R}_{\tilde{\boldsymbol{r}}\tilde{\boldsymbol{r}}}(\tau_c)) = \sigma_{\tilde{v}}^2,\ i = 3, \ldots, N_c. \tag{3.21}$$

This shows the low rank of the signal subspace, which is the basis of the methods.

As seen from the eigenvalues in (3.19)-(3.21), the time offset can be estimated by finding the delay that maximizes the largest eigenvalue of the correlation matrix. In [62], it has been shown that maximizing the largest eigenvalue is equivalent to maximizing the squared Frobenius norm of the matrix. Thus, the algorithm for blind code synchronization is based on the following:

$$\|\boldsymbol{R}_{\tilde{\boldsymbol{r}}\tilde{\boldsymbol{r}}}(\tau_c)\|_F^2 = \sum_{i=0}^{N_c-1} \lambda_i\big(\boldsymbol{R}_{\tilde{\boldsymbol{r}}\tilde{\boldsymbol{r}}}(\tau_c)\big) \tag{3.22}$$

$$\hat{\tau}_c = \arg\max_{\tau_c} \|\boldsymbol{R}_{\tilde{\boldsymbol{r}}\tilde{\boldsymbol{r}}}(\tau_c)\|_F^2. \tag{3.23}$$

Once the code timing is established, the spreading code can be estimated (up to a phase ambiguity) from the principal eigenvector of $\boldsymbol{R}_{\tilde{\boldsymbol{r}}\tilde{\boldsymbol{r}}}(\hat{\tau}_c)$. Results on this algorithm have been presented in [62][72] as well as in Publication II. In [73] it is noted that in presence of covariance matrix estimation errors, maximizing the Frobenius norm as in (3.23) is no longer the same as using the maximum eigenvalue. Based on matrix perturbation theory, it is shown that it is in fact better to maximize the largest eigenvalue directly. This is also confirmed by numerical simulations [73].

A similar algorithm is proposed in [74] using frequency domain signals. The received signal is frequency-channelized, and the correlation matrix of the frequency-channelized signal is estimated. The dominant eigenvector of the correlation matrix is calculated, and the frequency-channelized signal is despread using the eigenvector. The performance of the algorithm is shown to approach the conventional code-matched filter based despreading even at low SNR.

Extensions to asynchronous multi-user DS-CDMA case

In [75] as well as in Publication I and Publication II, extensions of the method in [62][72] were studied for the case where multiple DSSS signals (e.g. multiple users) are received. Similarly to (3.4), the model for receiving multiple short-code DSSS signals asynchronously can be written in

case of K signals as follows:

$$\tilde{r}[n] = \sum_{j=0}^{K-1} \sum_{m=-\infty}^{\infty} \tilde{s}_m^{(j)} \tilde{h}_{\tilde{u}}^{(j)}[n - mN_c - \tau_c^{(j)}] + \tilde{v}[n]. \tag{3.24}$$

Furthermore, similarly to (3.11), the $N_c \times 1$ received blocks $\tilde{\boldsymbol{r}}[m; \boldsymbol{\tau}_c]$ can be written as follows ($\boldsymbol{\tau}_c = [\tau_c^{(1)}, \ldots, \tau_c^{(K)}]^T$):

$$\tilde{\boldsymbol{r}}[m; \boldsymbol{\tau}_c] = \sum_{j=1}^{K} \left[\tilde{s}_m^{(j)} \tilde{\boldsymbol{h}}_{\tilde{u},r}^{(j)}(\tau_c^{(j)}) + \tilde{s}_{m+1}^{(j)} \tilde{\boldsymbol{h}}_{\tilde{u},l}^{(j)}(\tau_c^{(j)}) \right] + \tilde{\boldsymbol{v}}[m; \boldsymbol{\tau}_c]. \tag{3.25}$$

The method in [75] essentially follows the method of [62][72]. The eigenvalues of $\boldsymbol{R}_{\tilde{\boldsymbol{r}}\tilde{\boldsymbol{r}}}(\boldsymbol{\tau}_c)$ can be derived for the multi-user case similarly to (3.19)-(3.21). Multiple asynchronous DSSS signals result in multiple local maxima in the squared Frobenius norm of $\boldsymbol{R}_{\tilde{\boldsymbol{r}}\tilde{\boldsymbol{r}}}(\boldsymbol{\tau}_c)$ as a function of τ_c. The method proposed in [75] attempts to locate these maxima in order to estimate the time offsets $\tau_c^{(j)}$. Then, the spreading sequence corresponding to source j with estimated time offset $\hat{\tau}_c^{(j)}$ is estimated by taking the principal eigenvector of $\boldsymbol{R}_{\tilde{\boldsymbol{r}}\tilde{\boldsymbol{r}}}(\hat{\tau}_c^{(j)})$. A drawback of the method is that if there are significant differences in the received power corresponding to different sources, local maxima may not be found, and thus the method would fail. This aspect is especially important in any kind of non-cooperative applications, as the transmissions would not be power controlled towards the receiver. Thus near-far effects are unavoidable. Furthermore, when multiple signals are received with approximately the same time offset, the method in [75] fails to distinguish the signals as they would appear as only one maximum in the cost function.

In this thesis, in Publication I and Publication II, an improved method was proposed for the case of multiple signals, avoiding the drawbacks mentioned above. The method is based on a matrix deflation approach in which the timing offset and the spreading code of each source is estimated serially, after which the corresponding contribution of the signal is removed from the covariance matrix $\boldsymbol{R}_{\tilde{\boldsymbol{r}}\tilde{\boldsymbol{r}}}(\boldsymbol{\tau}_c)$. The covariance matrix can be, similarly to (3.16), written as follows:

$$\boldsymbol{R}_{\tilde{\boldsymbol{r}}\tilde{\boldsymbol{r}}}(\boldsymbol{\tau}_c) = \frac{P_{\tilde{s}} N_c}{T} \sum_{j=1}^{K} |\tilde{h}^{(j)}|^2 \Big((T - \tau_c^{(j)}) \tilde{\boldsymbol{u}}_r^{(j)}(\tau_c^{(j)}) \tilde{\boldsymbol{u}}_r^{(j)H}(\tau_c^{(j)}) + \tau_c^{(j)} \tilde{\boldsymbol{u}}_l^{(j)}(\tau_c^{(j)}) \tilde{\boldsymbol{u}}_l^{(j)H}(\tau_c^{(j)}) \Big) + \sigma_{\tilde{v}}^2 \boldsymbol{I}_{N_c}. \tag{3.26}$$

Thus, after estimating the spreading codes and timing offsets for the k:th

source, the matrix can be deflated as

$$\boldsymbol{R}_{\tilde{\boldsymbol{r}}\tilde{\boldsymbol{r}}}^{(k+1)}(\boldsymbol{\tau}_c) = \boldsymbol{R}_{\tilde{\boldsymbol{r}}\tilde{\boldsymbol{r}}}^{(k)}(\boldsymbol{\tau}_c) - \frac{P_{\tilde{s}} N_c |\tilde{h}^{(k)}|^2}{T} \Big((T - \tau_c^{(k)}) \tilde{\boldsymbol{u}}_r^{(k)}(\tau_c^{(k)}) \tilde{\boldsymbol{u}}_r^{(k)H}(\tau_c^{(k)}) + \tau_c^{(k)} \tilde{\boldsymbol{u}}_l^{(k)}(\tau_c^{(k)}) \tilde{\boldsymbol{u}}_l^{(k)H}(\tau_c^{(k)}) \Big). \quad (3.27)$$

where the amplitude-related parameters are obtained from the eigenvalues of matrix $\boldsymbol{R}_{\tilde{\boldsymbol{r}}\tilde{\boldsymbol{r}}}^{(k)}(\boldsymbol{\tau}_c)$. In Publications I and II this method is shown to achieve nearly ideal processing gain in case of multiple users, even at a low signal-to-noise ratio.

Also in [76][77] an improvement of the squared Frobenius norm -based approach is proposed for the asynchronous multi-user DS-CDMA case. The cost function is modified slightly such that the different signals do not mask each other, as in case of the method in [75].

It is noted that the method in [75] as well as the method in Publication I and Publication II require knowledge of the number of signals to be estimated. This number can be estimated using some well-known techniques for model order estimation, for example the information theoretic approaches based on the Akaike information criterion (AIC) or the minimum description length (MDL) [78].

3.1.3 Maximum likelihood -based methods

Maximum-likelihood -based methods for blind synchronization and despreading have also been studied in a few references. First, in [79], an expectation maximization (EM) -based algorithm was studied for the case of synchronous DS-CDMA systems, where multiple signals are received with the same time offset. For a synchronous DS-CDMA system, when $\tau^{(1)} = \ldots = \tau^{(K)} = 0$, the signal model in (3.25) reduces to

$$\tilde{\boldsymbol{r}}[m] = \sum_{j=1}^{K} \tilde{s}_m^{(j)} \tilde{\boldsymbol{h}}_{\tilde{u}}^{(j)} + \tilde{\boldsymbol{v}}[m] = \tilde{\boldsymbol{H}}_{\tilde{u}} \tilde{\boldsymbol{s}}_m + \tilde{\boldsymbol{v}}[m], \quad (3.28)$$

where $\tilde{\boldsymbol{H}}_{\tilde{u}} = \left[\tilde{\boldsymbol{h}}_{\tilde{u}}^{(1)}, \ldots, \tilde{\boldsymbol{h}}_{\tilde{u}}^{(K)}\right]$ and $\tilde{\boldsymbol{s}}_m = \left[\tilde{s}_m^{(1)}, \ldots, \tilde{s}_m^{(K)}\right]^T$. In [79], the spreading sequences are treated as unknown parameters of a Gaussian mixture. The component density functions of the Gaussian mixture are defined by vectors $\tilde{\boldsymbol{s}}_m$, where the symbols are assumed BPSK-modulated, i.e. each $\tilde{\boldsymbol{s}}_m$ is $K \times 1$ binary vector and there are 2^K component density functions. Maximum likelihood estimates of the spreading sequences are found using the EM algorithm. Since the method assumes that the time offset is known, an eigenvalue-based method similar to the one discussed in the previous section is proposed. Furthermore, the number of signals is

assumed known, and it is again mentioned that an estimate of the number of signals can be obtained using the AIC or MDL criteria as discussed also in the previous section.

Other maximum likelihood -based methods for blind despreading have been developed for long-code systems and are described in section 3.2.2. However, since short-code systems can be seen as a special case of long-code systems, the same methods are applicable to short-code systems as well. This has also been mentioned in [80] that deals with ML estimation of spreading sequences in case of long-code systems.

3.2 Blind synchronization and code estimation in long-code DS-CDMA systems

The signal model for long-code DSSS signals is summarized by equations (2.5) and (2.6). It is noted that the difference to short-code signals in equations (3.2) and (3.3) is that the spreading sequence is varying in each symbol. Due to this, most of the methods discussed in the previous section are not directly applicable as they basically rely on the same spreading sequence to repeat in every symbol. For instance, the dominant eigenmode -based methods require that the spreading sequence remains the same as the estimation of the correlation matrix is done by averaging over multiple symbols. Similarly, in the blind channel identification/equalization -based methods, it is assumed that the observation period spans multiple symbols, each spread with the same spreading sequence.

Due to the inherent difficulty of the problem, only a few solutions have been pursued in the literature. The first class of algorithms are extending the dominant eigenmode -based methods by taking into account that the spreading sequence extends over multiple symbol periods. These methods are reviewed in section 3.2.1. Maximum likelihood -based methods are reviewed in section 3.2.2.

3.2.1 Extensions to dominant eigenmode -based methods

As discussed in section 3.1.2, the dominant eigenmode -based methods rely on estimating the covariance matrix of vectors $\tilde{\boldsymbol{r}}[m]$ of length $P = N_c$ where P is the spreading factor. In case of long (aperiodic) spreading codes, this approach would fail as consequent sample vectors (each corresponding to one symbol) are basically pseudo-random, as different spread-

ing codes are utilized. Thus the code sequences can not be found from the eigenstructure of the covariance matrix.

A theoretically simple, yet computationally complex, way of extending the dominant eigenmode -based method to long code case is to utilize the method separately for each different length-P segment of the spreading code. This method is possible when the length of the code sequence is a multiple of the spreading factor, i.e. $N_c = Q_c P$ where Q_c is the number of modulation symbols spanned by the spreading code sequence. The method is computationally very complex as it requires performing the computations of the dominant eigenmode -based method for each of the Q_c segments separately. Furthermore, knowledge of the spreading code length N_c as well as the spreading factor P is required.

Based on a similar principle, in [81] Qui et al. proposed a method which is based on computing multiple covariance matrices, each corresponding to a different short segment of the received signal and of the full spreading sequence. The dominant eigenmode -based approach is then used to obtain segments of the full spreading sequence. Since there is a phase ambiguity between the obtained segments of the spreading sequence, the segments are proposed to be overlapping such that the phase ambiguities can be resolved. Note that in this case there is no relation between the spreading factor and the length of each segment, rather the segments can be even shorter than the spreading factor P. Good performance for signal to noise ratios below 0 dB is shown.

A method extending the dominant eigenmode -based method to the long spreading code case was proposed also in [82]. The method requires computation of a very large correlation matrix reflecting the *whole* code sequence and it is shown that similarly to short code case, synchronization can be achieved by optimizing an eigenvalue -based criterion. Then, the spreading sequence(s) can be estimated from the eigenvectors of the covariance matrix. It is also shown that in fact the method reduces to the same short code dominant eigenmode -based method if $N_c = P$ (i.e. in case short codes are used). Also an extension to multi-user case similar to Publication I and Publication II is discussed.

Finally, the method in [74] based on a frequency-channelized signal is also applicable to long code systems.

3.2.2 Maximum likelihood -based methods

A maximum likelihood -based method for estimation of the spreading code in presence of carrier frequency offset is studied in [80]. The ML cost function is formed and the spreading code is constrained to have a constant modulus. To reduce computational complexity, a semi-definite relaxation -based approach is used, leading to a convex optimization problem which can be solved using traditional optimization methods. The method is then compared to dominant eigenmode -based estimation and clearly better performance is demonstrated in terms of mean square error of spreading code estimation, especially in presence of CFO. The method works also at a very low signal-to-noise ratio.

3.3 Discussion

This chapter has discussed blind methods for synchronization and spreading code estimation in DS-CDMA systems. More specifically, methods that do not require a priori knowledge of the spreading code have been reviewed, both for the short (or periodic) spreading code case as well as for the long (or aperiodic) spreading code case.

Short codes that repeat on every modulation symbol induce cyclostationarity in the DSSS signal that can be taken advantage of in the blind synchronization. Once the synchronization has been achieved, spreading code estimation can be achieved using subspace methods (for example, the dominant eigenmode method), or the signal can be directly equalized using blind equalization methods.

The main contribution of this thesis in this field is in blind synchronization and spreading code estimation in case of asynchronous multi-user DS-CDMA systems. For this case, Publication I and Publication II proposed a method based on covariance matrix deflation, which allows the well-established dominant eigenmode -based method to be used also in multi-user case for blind synchronization and spreading code estimation. The method offers improved performance compared to earlier methods in particular in case the timing offsets of multiple users are very close.

Also the existing methods for long codes were reviewed. Long spreading codes destroy the cyclostationary property of the DSSS signal, and therefore the problem becomes much more challenging. Thus the literature on this topic is also rather scarce. If the length of the spreading

codes is known, it is possible to extend the methods developed for short-code systems to long-code case, even though this comes with a rather high computational complexity. On the other hand, regarding computational complexity it is also noted that in such cases in which it is feasible to estimate the spreading code, the estimation procedure only needs to be performed once.

The results basically show the feasibility of blind synchronization and spreading code estimation in case of short spreading codes. The methods may find applications for instance in interference cancellation in cases where the spreading code of the interfering signal is unknown. Use of such methods could be envisioned also in cognitive radio applications in which the radio parameters of a detected system may need to be estimated. However, such applications are beyond the scope of this thesis. Obviously, in military domain, the methods find application in interception and localization of non-cooperative transmissions. From a different perspective, as the problem is significantly more challenging for long spreading codes, a system designer targeting low probability of intercept DSSS signals should aim at randomizing the spreading codes as much as possible, basically avoiding any kind of repetition in the code sequences.

4. Multi-antenna techniques for initial synchronization

Multiple antenna communications have been studied intensively for almost two decades, and the benefits are well known [14] [15]. In wireless communication, multiple antennas can be either used to increase the data rate (bps/Hz) in linear proportion to the minimum of number of transmit and receive antennas $\min\{N_t, N_r\}$ [15], or to increase robustness by transmitting the same data over multiple transmit-receive antenna pairs. While the benefits of MIMO techniques on achievable data rates and capacity are already rather well known, surprisingly little research has been done before on the benefits of MIMO on synchronization, especially on how to on utilize multiple transmit antennas efficiently in the synchronization process. Still, MIMO techniques are already commonly utilized for improving the actual data rates. Therefore, the transceivers are often equipped with multiple receive and transmit antennas, and thus it is important to be able to utilize those antennas also for synchronization.

As discussed in Chapter 2, typically initial synchronization is done by cross-correlating the received signal with a known synchronization sequence. In this chapter the methods of utilizing multiple antennas for synchronization are discussed. In particular the impacts of receive, transmit and time diversity on the probabilities of synchronization acquisition are reviewed. The main focus is on the cross-correlation -based methods. However, similarly to Chapter 2, for OFDM systems some specific multi-antenna schemes are reviewed as well. Earlier work on the topic is mainly focused on receive diversity, which is reviewed in section 4.1. Methods utilizing multiple antennas at the transmitter side are discussed in section 4.2, including the findings of Publication III and Publication IV related to transmit diversity in context of synchronization sequence transmission. The chapter ends with a discussion in section 4.4.

In this chapter, the impact of frequency offsets is mostly neglected. In

correlation-based synchronization as outlined in section 2, frequency offsets would impact the correlation properties of the sequences, reducing processing gain and hence reducing also the probability of detection. However, there are methods to mitigate these impacts as discussed in Chapter 2. Furthermore, it is assumed that the propagation delays are the same between all transmit and receive antenna pairs. This assumption is verified for instance in [83].

4.1 Multiple receive antennas in initial synchronization

Multiple antennas at the receiver can be used for initial synchronization in multiple ways, depending on, for instance, the type of the antenna array. The methods include antenna diversity techniques, beamforming techniques as well as methods for interference suppression.

Antenna diversity techniques for improving the probability of detection are beneficial mainly when the radio channels to different receive antennas are sufficiently uncorrelated. This holds when the spacing between the receive antennas is larger than the coherence distance, e.g. in the order of multiple wavelengths and/or if the angular spread of the channel at the receive antenna array is sufficiently large. For instance, an antenna array at a small access point or base station in an indoor environment utilizing high carrier frequencies would benefit from antenna diversity techniques. Similarly, around mobile phones the angular spread of the channel can be often large, and therefore antenna diversity techniques may be suitable if multiple antennas are available for reception. Antenna diversity for synchronization is discussed in section 4.1.1.

As opposed to antenna diversity, in beamforming techniques the energy is steered towards a certain angular direction. These techniques are applicable when the antennas of the receive antenna array are closely spaced, for instance by half a wavelength. In addition, the techniques are most effective when the angular spread of the channel at the receive antenna array is small. For instance, base station antenna arrays placed above rooftops could benefit from beamforming techniques, in particular in line of sight situations. Beamforming techniques for initial synchronization are discussed in section 4.1.2.

Finally, the additional degrees of freedom provided by multiple receive antennas could be used for interference suppression. This is discussed in section 4.1.3.

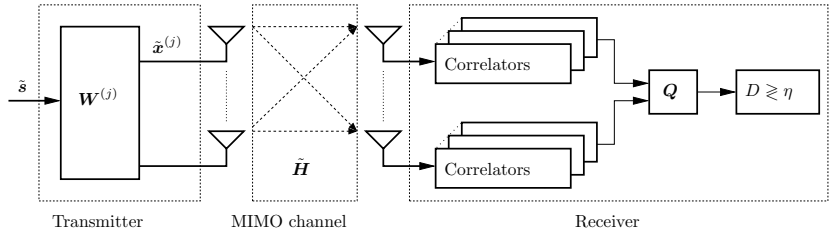

Figure 4.1. Illustration of diversity transmission and reception of synchronization sequences $\tilde{s}$ in a multiple input multiple output system. Cross-correlation based synchronization acquisition at the receiver side is assumed, and matrix $\boldsymbol{Q}$ represents the combiner used to combine the correlator outputs into a single decision statistic D.

It is noted in particular that any techniques requiring channel state information at the receiver side are typically not applicable in the synchronization acquisition phase.

4.1.1 Antenna diversity

The system considered for diversity reception (and transmission) of synchronization signals is illustrated in Figure 4.1. For purposes of this section, single antenna transmission is assumed, i.e. $\boldsymbol{W}^{(j)} = 1$, while other cases are discussed later in section 4.2. In the SIMO case, $\tilde{\boldsymbol{H}} = \tilde{\boldsymbol{h}}$, and the $N_r \times 1$ received signal based on this model is written as follows:

$$\tilde{\boldsymbol{r}}[n] = \tilde{\boldsymbol{h}}\tilde{s}[n-\tau] + \tilde{\boldsymbol{v}}[n]. \tag{4.1}$$

The correlator output can be written as

$$\tilde{\boldsymbol{y}}[n] = \frac{1}{P}\sum_{p=0}^{P-1} \tilde{\boldsymbol{r}}[n+p]\tilde{s}^*[p], \tag{4.2}$$

where P is the spreading factor. Receive antenna diversity schemes target at combining the correlator outputs in vector $\tilde{\boldsymbol{y}}[n]$ into one decision statistic such that the probability of detection is improved.

Receive antenna diversity for PN code acquisition was first addressed in [84]. In the proposed method, the correlator outputs are squared and summed. This is called noncoherent combining. As in the SISO case, the PN code acquisition problem can be then formulated as a hypothesis testing problem. Similarly to equations (2.15) and (2.16), the correlator outputs can be expressed as follows for the null and alternative hypotheses:

$$\mathcal{H}_0 \quad : \quad \tilde{\boldsymbol{y}}[n] = \tilde{\boldsymbol{v}}_0[n] \tag{4.3}$$

$$\mathcal{H}_1 \quad : \quad \tilde{\boldsymbol{y}}[n] = \tilde{\boldsymbol{h}} + \tilde{\boldsymbol{v}}_1[n] \tag{4.4}$$

where $\tilde{\boldsymbol{v}}_0[n] \sim \mathbb{C}(\boldsymbol{0}, \boldsymbol{R}_{\tilde{\boldsymbol{v}},0})$ and $\tilde{\boldsymbol{v}}_1[n] \sim \mathbb{C}(\boldsymbol{0}, \boldsymbol{R}_{\tilde{\boldsymbol{v}},1})$, and $\boldsymbol{R}_{\tilde{\boldsymbol{v}},0}$ and $\boldsymbol{R}_{\tilde{\boldsymbol{v}},1}$ denote the covariance matrices of noise $\tilde{\boldsymbol{v}}$ under each hypothesis. Note that the covariances could also be the same, i.e. $\boldsymbol{R}_{\tilde{\boldsymbol{v}},0} = \boldsymbol{R}_{\tilde{\boldsymbol{v}},1}$. The decision statistic is then formed $D = \tilde{\boldsymbol{y}}^H \tilde{\boldsymbol{y}}$, i.e. the combiner is $\boldsymbol{Q} = \boldsymbol{I}_{N_r}$. In [84], the distributions of the decision statistic D under different hypotheses are derived *conditioned* on a specific realization of the random channel $\tilde{\boldsymbol{h}}$. In that case, under hypothesis $\mathcal{H}_0$ the decision statistic D follows the central χ^2-distribution with $2N_r$ degrees of freedom where the non-centrality parameter is dependent on the channel power. Under $\mathcal{H}_1$, D follows the non-central χ^2-distribution with $2N_r$ degrees of freedom [84]. The results in [84] show significant benefits of receive diversity in all simulated scenarios.

In [84] the channel is assumed uncorrelated between the receive antennas, whereas in [85] the analysis is extended to spatially correlated channels. Still, noncoherent combining is assumed. The distribution of the decision statistic is derived by modeling the channel $\tilde{\boldsymbol{h}}$ as a correlated Gaussian random vector. In this case the decision statistic is, in case of alternative hypothesis $\mathcal{H}_1$, a sum of squared correlated Gaussian random variables. Similar analysis was carried out in [86][87]. An attempt was made to reduce the mean acquisition time in DSSS systems by grouping the multiple receive antennas into groups, each intended for searching a different part of the PN code sequence, in the spirit of the parallel search strategy discussed in section 2. This results in a tradeoff between search time and antenna diversity: Basically, the more the antennas are used to parallelize the search to reduce the search time, the less antenna diversity is obtained. Similar analyses have been made also in [88][89][90][91]. In addition to receive antenna diversity, time diversity utilizing integration of correlator outputs over multiple timeslots is considered in [88][89][90].

Generally the decision statistic based on cross-correlator outputs can be expressed as

$$D = \tilde{\boldsymbol{y}}^H \boldsymbol{Q} \tilde{\boldsymbol{y}}, \tag{4.5}$$

where $\boldsymbol{Q}$ is the used combiner as shown in Figure 4.1. The optimal combiner, obtained by calculating the log-likelihood ratio for the detection problem, can be expressed as $\boldsymbol{Q} = \boldsymbol{R}_{\tilde{\boldsymbol{y}},0}^{-1} - \boldsymbol{R}_{\tilde{\boldsymbol{y}},1}^{-1}$ where $\boldsymbol{R}_{\tilde{\boldsymbol{y}},i}$ denotes the covariance of $\tilde{\boldsymbol{y}}$ under hypothesis i. However, such a combiner would require prior knowledge of the covariance matrices under both hypotheses, and as such is not very practical. Therefore, often the combiner is chosen as $\boldsymbol{Q} = \boldsymbol{I}_{N_r}$ corresponding to noncoherent combining of the correlator out-

puts. In [92], although in a different context, maximum ratio combining (MRC) and equal gain combining (EGC) were studied. In this case, in contrast to normal receive diversity with full channel state information, MRC refers to simply weighting the squared elements of $\tilde{\boldsymbol{y}}$ based on their power before summing. Equal gain combining, on the other hand, is essentially equivalent to noncoherent combining where all weights are equal to one.

The analysis here focuses on the most common and practical case of noncoherent combining. It is noted that in an uncorrelated case, if the receive branches are received with equal power, noncoherent combining in fact corresponds to optimal combining. In the following, the approach of [87] is followed. The same approach has been followed in Publication IV.

In the uncorrelated case, $D = \tilde{\boldsymbol{y}}^H \tilde{\boldsymbol{y}}$ corresponds to a sum of squared independent Gaussian random variables and hence follows the central χ^2-distribution with $2N_r$ degrees of freedom:

$$F_D(\eta|\mathcal{H}_i) = 1 - \exp\left(-\frac{\eta}{\lambda^{(i)}}\right) \sum_{r=0}^{N_r-1} \frac{1}{r!} \left(\frac{\eta}{\lambda^{(i)}}\right)^r . \tag{4.6}$$

where $\lambda^{(i)}$ ($i = 0, 1$) is the power of each element of $\tilde{\boldsymbol{y}}$, also equal to the eigenvalues of the covariance matrix $\boldsymbol{R}_{\tilde{\boldsymbol{y}},i}$.

In the correlated case, the distribution of the decision statistic needs to be derived through its characteristic function. The following has been derived for receive diversity in [87] and generalized to transmit and time diversity in Publication IV:

$$\Phi(\omega|\mathcal{H}_i) = \frac{1}{\prod_{r=1}^{N_r} \left(1 - \jmath\omega\lambda_r^{(i)}\right)}. \tag{4.7}$$

Above, $\lambda_r^{(i)}$ denotes the r:th eigenvalue of $\boldsymbol{R}_{\tilde{\boldsymbol{y}},i}$. The probability distribution function of D is obtained as the inverse Fourier transform of the characteristic function. The resulting cdf can be written as follows:

$$F_D(\eta|\mathcal{H}_i) = \sum_{r_1=1}^{N_r} \left(1 - e^{-\eta/\lambda_{r_1}^{(i)}}\right) \prod_{r_2=1, r_2\neq r_1}^{N_r} \frac{\lambda_{r_1}^{(i)}}{\lambda_{r_1}^{(i)} - \lambda_{r_2}^{(i)}}. \tag{4.8}$$

These distributions can be readily utilized with the expressions for probabilities of detection and false alarm as given in section 2.3. Note that in the general case with combiner $\boldsymbol{Q}$, the analysis can be done similarly via equation (4.7) where $\lambda_r^{(i)}$ denotes the r:th eigenvalue of $\boldsymbol{R}_{\tilde{\boldsymbol{y}},i}\boldsymbol{Q}$.

4.1.2 Beamforming

In beamforming, the correlator outputs are first weighted utilizing specific antenna weights and then summed coherently. Obviously, the problem is that during initial acquisition there is typically no channel knowledge available, and hence computing the antenna weights is difficult. Still, in [93] [94], a beamforming-based algorithm is proposed, aiming at maximizing the array gain, i.e. the SNR gain of the antenna array compared to single antenna reception. In the proposed method, the lack of channel knowledge is overcome by utilizing a normalized least mean square (NLMS) -based adaptive algorithm to compute the beamforming weights on the fly. Essentially, the algorithm penalizes deviations from the full array gain of $10\log(N_r)$ dB, hence it resembles the constant modulus -based adaptive algorithms [69]. The analysis in [93] is done assuming that the algorithm converges to perfect steering vectors, hence basically providing an upper bound for the performance. It is also shown by simulations that the proposed algorithm is able to capture a significant fraction of the full array gain. Similarly in [89], antenna diversity is compared with (ideal) beamforming, and the distribution of the decision statistic D is derived for both cases, taking into account spatial correlation between the receive antennas. Also integration of the correlator outputs in time is considered. It is shown that beamforming outperforms antenna diversity based on noncoherent combining at low SNR values, however non-idealities in the beamformer adaptation are not considered.

Another method of utilizing beamforming without prior knowledge of the channel was proposed in [95]. A two-dimensional search strategy was proposed where the receiver searches for the correct acquisition in both delay and angular domains by forming beams in several directions and attempting to acquire the code timing from each direction. The number of required hypothesis tests increases, however also SNR improves due to beamforming. It is shown that the mean acquisition time can be reduced if the search strategy is properly chosen and if the interference is uniformly distributed spatially.

Here, the distribution of the decision statistic is provided for a detector with knowledge of the ideal steering vector. Hence, the result mainly provides an upper bound. It is assumed that the SIMO channel can be written as $\tilde{\boldsymbol{h}} = \tilde{h}\boldsymbol{a}(\theta)$ where $\boldsymbol{a}(\theta)$ is the steering vector, θ is the direction of arrival and $\tilde{h} \sim \mathcal{N}_{\mathbb{C}}(0, \sigma^2_{\tilde{h}})$ is the fading channel. In such case the ideal

beamformer $\boldsymbol{w}_{\text{ideal}}$ gives the full array gain, i.e. $\boldsymbol{w}_{\text{ideal}}^H \boldsymbol{a}(\theta) = N_r$. Hence, ideally the beamformer is matched to the steering vector as $\boldsymbol{w}_{\text{ideal}} = \boldsymbol{a}(\theta)$. The resulting cdf in case of $\mathcal{H}_1$ follows the exponential distribution [93]:

$$F_D(\eta|\mathcal{H}_1) = 1 - \exp\left(-\frac{\eta}{\sigma_{\tilde{v}}^2 N_r + \sigma_{\tilde{h}}^2 N_r^2}\right). \tag{4.9}$$

Also in the case of null hypothesis $\mathcal{H}_0$, the cdf follows the exponential distribution.

4.1.3 Interference suppression

Especially in dense multi-cell networks, inter-cell interference may become the main limiting factor in acquisition performance. In such case the extra degrees of freedom provided by the multiple receive antennas could be utilized to suppress the inter-cell interference. A study on this aspect was fairly recently conducted in [33] where a comparison of different test statistics for code acquisition was performed in case of a colored interference environment. The test statistics include MMSE-based, LS-based, GLRT-based and spatial invariance -based statistics, in addition to the correlation-based statistic that is used for benchmarking. For the purposes of summarizing these statistics, let us denote $\tilde{\boldsymbol{S}} = [\tilde{\boldsymbol{s}}[0], \ldots, \tilde{\boldsymbol{s}}[P-1]]$, $\tilde{\boldsymbol{Z}}[n] = [\tilde{\boldsymbol{r}}[n], \ldots, \tilde{\boldsymbol{r}}[n+P-1]]$ and $\tilde{\boldsymbol{V}}[n] = [\tilde{\boldsymbol{v}}[n], \ldots, \tilde{\boldsymbol{v}}[n+P-1]]$, where $\tilde{\boldsymbol{s}}[p]$ is now an $N_t \times 1$ vector containing the transmitted synchronization sequences from all N_t antennas. When the received signal is aligned with the synchronization sequences, the $N_r \times P$ matrix $\tilde{\boldsymbol{Z}}[n]$ can be written as

$$\tilde{\boldsymbol{Z}}[n] = \tilde{\boldsymbol{H}}\tilde{\boldsymbol{S}} + \tilde{\boldsymbol{V}}[n]. \tag{4.10}$$

where $\tilde{\boldsymbol{H}}$ is the $N_r \times N_t$ time-domain MIMO channel. In addition, let us define the following projection matrices:

$$\begin{aligned} \boldsymbol{P}_{\tilde{\boldsymbol{Z}}} &= \tilde{\boldsymbol{Z}}^H \left(\tilde{\boldsymbol{Z}}\tilde{\boldsymbol{Z}}^H\right)^{-1} \tilde{\boldsymbol{Z}}, \\ \boldsymbol{P}_{\tilde{\boldsymbol{S}}} &= \tilde{\boldsymbol{S}}^H \left(\tilde{\boldsymbol{S}}\tilde{\boldsymbol{S}}^H\right)^{-1} \tilde{\boldsymbol{S}}. \end{aligned}$$

With these definitions, the test statistics for interference suppressing synchronization are summarized in Table 4.1. The spatial invariance -based tests are based on the observation that the GLRT test statistic is a function of the row spaces of $\tilde{\boldsymbol{Z}}[n]$ and $\tilde{\boldsymbol{S}}$ only. Representing the row spaces of $\tilde{\boldsymbol{Z}}[n]$ and $\tilde{\boldsymbol{S}}$ using matrices $\boldsymbol{K}$ and $\boldsymbol{T}$, respectively, the spatial invariance -based test statistics are constructed based on different subspace distance measures between $\boldsymbol{K}$ and $\boldsymbol{T}$. Each distance measure is a function of the

Table 4.1. Summary of test statistics for interference suppressing synchronization acquisition. Vector $\boldsymbol{a}$ contains the principal angles between the row spaces of $\tilde{\boldsymbol{Z}}[n]$ and $\tilde{\boldsymbol{S}}$.

Method	Test statistic
Correlation	$D_{corr} = \left\| \tilde{\boldsymbol{Z}} \tilde{\boldsymbol{S}}^H \right\|_F^2$
MMSE	$D_{MMSE} = \left\| \tilde{\boldsymbol{S}} \boldsymbol{P}_{\tilde{\boldsymbol{Z}}} \right\|_F^2 / \left\| \tilde{\boldsymbol{S}} \right\|_F^2$
GLRT	$D_{GLRT} = \left\| \boldsymbol{I}_P - \boldsymbol{P}_{\tilde{\boldsymbol{S}}} \boldsymbol{P}_{\tilde{\boldsymbol{Z}}} \right\|^{-P}$
Spatial invariance:	
• Arc length	$D_{AL} = \|\boldsymbol{a}\|^{-1}$
• Minimum angle	$D_{MA} = \min^{-1}(\boldsymbol{a})$
• Chordal distance	$D_{CD} = \|2\sin(\boldsymbol{a}/2)\|^{-1}$
• Product	$D_{prod} = (\prod_m \sin(a_m))^{-1}$

principal angles between the subspaces, obtained using the singular value decomposition as

$$\boldsymbol{K}\boldsymbol{T}^H = \boldsymbol{U}\,\mathrm{diag}\left\{\cos(\boldsymbol{a})\right\}\boldsymbol{V}^H. \tag{4.11}$$

In the above, the vector $\boldsymbol{a}$ contains the principal angles between the subspaces. In [33], the arc length, minimum angle, chordal distance and product -based subspace distance measures are utilized as also summarized in Table 4.1. It is also straightforward to show that the test statistic D_{prod} based on the product of sines of the principal angles is equivalent to the GLRT test statistic up to an exponential coefficient [33]. A review of different subspace distance measures is found for instance in [96].

In [33], the comparisons between the different test statistics were based on simulations. Analytical calculations on probabilities of acquisition or missed detection were not presented. The results basically showed that methods that take into account the spatial structure of the interference, such as GLRT-based and spatial invariance -based detectors, perform significantly better than others, for example better than a noncoherent combining -based correlation detector, in case of spatially colored interference.

In addition to [33], synchronization using multiple antennas in presence of colored co-channel interference was addressed in [97]. The proposed algorithm is correlation-based, and combiner $\boldsymbol{Q}$ (see equation (4.5)) is chosen such that interference is suppressed. More specifically, the combiner

is chosen as follows:

$$\boldsymbol{Q} = \hat{\boldsymbol{R}}_{\tilde{\boldsymbol{r}}\tilde{\boldsymbol{r}}}^{-1}[n] \tag{4.12}$$

$$\hat{\boldsymbol{R}}_{\tilde{\boldsymbol{r}}\tilde{\boldsymbol{r}}}[n] = \sum_{p=0}^{P-1} \tilde{\boldsymbol{r}}[n+p]\tilde{\boldsymbol{r}}^{H}[n+p] \tag{4.13}$$

Thus, the combiner basically approximates the optimal combiner obtained from the log-likelihood ratio.

4.2 Multiple transmit antennas in initial synchronization

As discussed in the previous section, different ways of utilizing multiple receive antennas for synchronization acquisition have been rather thoroughly studied, and the benefits have been quantified in different scenarios both analytically and via simulations. For transmit diversity, however, only very few studies exist and Publications III and IV are filling this gap.

In initial synchronization, multiple transmit antennas can be mainly utilized for (open-loop) transmit diversity purposes. Beamforming is applicable only in some specific point-to-point cases where channel state information happens to be available at the transmitter side when transmitting the synchronization signals. One example of such a case could be uplink synchronization (random access) in TDD-based cellular systems where channel reciprocity could be utilized after first acquiring downlink synchronization based on synchronization signals received in downlink. However, the focus in this section is on transmit diversity schemes. These schemes are most useful in spatially uncorrelated cases where the antenna spacing exceeds the coherence distance.

Transmit diversity for code acquisition was first addressed in [83]. Two transmit diversity schemes, namely the orthogonal transmit diversity - simulcast (OTD-S) and space-time spreading transmit diversity (STSTD) were studied. For code acquisition, two different synchronization receiver structures were studied. The first was the single-user maximum likelihood estimator, i.e. a correlator, and the other was based on the well known MUSIC algorithm. Performance of the transmit diversity schemes was studied only numerically via simulations and it was shown that both transmit diversity schemes improve the acquisition performance over single antenna transmission. However, the results were limited to the relatively high SNR regime above 0 dB. In the low SNR regime where synchronization performance is often most critical, certain transmit diversity

schemes can in fact degrade the performance. This has been noted later by others, e.g. in [98][99][100] as well as in Publication III and Publication IV.

The synchronization performance in MIMO case was addressed in [98] [99] [100] [101] assuming noncoherent combining -based synchronization at the receiver side. In [100], probabilities of detection and false alarm are analytically derived for an OTD-S -based transmit diversity scheme where each transmit antenna is assigned a distinct Walsh code to be used on top of the common PN spreading sequence. Also the impacts on acquisition time were studied. It is observed that, in line with the results in [83], in the high SNR regime multiple transmit antennas provide diversity gain. However, at lower SNR values the diversity gain is outweighed by the required power splitting between the transmit antennas. Due to the power split, the receiver is in fact combining highly noise-contaminated signals and the assumed noncoherent combining at the receiver side does not suppress noise sufficiently. In [99], a similar study is done. However, also differential combining is included in addition to noncoherent combining. Otherwise the studied synchronization setup is basically the same as in [100]. The conclusions are the same even though differential combining slightly outperforms noncoherent combining due to better noise suppression. In [98], also multi-carrier DS-CDMA is included in the study, while [101] studies the impacts of transmit diversity also on the post-initial code acquisition performance. Again, conclusions are the same. The studies in [98] [99] [100] [101] are limited to OTD-S -based transmit diversity and spatially uncorrelated channels. Some of the work is also summarized in [32] and [102]. Based on this work, the overall recommendation of the authors is to rely on single antenna transmission or time-switched transmit diversity, in which one antenna is transmitting at a time, and thus the power splitting loss is not introduced.

In addition to the studies reviewed above, to the author's best knowledge, only Publication III and Publication IV have addressed the benefits of transmit diversity for synchronization. Some of the findings of Publication III and Publication IV are summarized in the following sections 4.2.1 and 4.2.2.

4.2.1 Transmit diversity schemes

In Figure 4.1, transmission of N_{seq} synchronization sequences $\tilde{s}[p]$ simultaneously is expressed as follows:

$$\tilde{\boldsymbol{x}}^{(j)}[p] = \boldsymbol{W}^{(j)}\tilde{\boldsymbol{s}}[p],\ p = 0, \ldots, P-1 \tag{4.14}$$

where the superscript $^{(j)}$ refers to the j:th instance of the synchronization sequence transmission (e.g. the j:th slot or frame) and the $N_t \times N_{seq}$ matrix $\boldsymbol{W}^{(j)}$ is the precoding matrix distributing the N_{seq} synchronization sequences over the $N_{t\_}$ transmit antennas using antenna weights. It turns out that most diversity schemes known to the literature can be expressed as above just by choosing the precoding matrices $\boldsymbol{W}^{(j)}$ appropriately as discussed in the following.

For instance, in time-switched transmit diversity (TSTD), each repetition of the synchronization sequence is transmitted from a different transmit antenna [103]. In other words, the used transmit antenna is changed from synchronization sequence transmission instance to another. Orthogonal transmit diversity - simulcast on the other hand is represented by an identity matrix as the scheme basically means transmission of orthogonal synchronization sequences from all N_t antennas. Different precoding vector switching (PVS) or precoding matrix cycling schemes can be also represented, with the number of synchronization sequences ranging from $N_{seq} = 1$ (PVS) to $N_{seq} = N_t$. Table 4.2 shows examples of precoding matrices $\boldsymbol{W}^{(j)}$ with different transmit diversity schemes in case of four antennas at the transmitter.

Finally, delay diversity at the transmitter side can be used to effectively increase the multipath diversity. By transmitting the same sequence from multiple transmit antennas with different delays, the signal is seen at the receiver side as if it would have passed a more frequency-selective channel. Due to more diverse multipath, the number of valid timing hypotheses is increased, and thus the probability of detection is also increased as given by equation (2.18).

4.2.2 Impact on synchronization performance

The impact of various transmit diversity schemes on the synchronization performance metrics has been studied in [98][99][100][101] which focused only on OTD-S in spatially uncorrelated channels. In Publication III and Publication IV, the study is extended to cover other schemes based on

Table 4.2. Examples of transmit diversity schemes for $N_t = 4$ according to equation (4.14), for three consecutive synchronization sequence repetitions (slots).

Scheme	$\boldsymbol{W}^{(0)}$	$\boldsymbol{W}^{(1)}$	$\boldsymbol{W}^{(2)}$
TSTD	$[1\ 0\ 0\ 0]^T$	$[0\ 1\ 0\ 0]^T$	$[0\ 0\ 1\ 0]^T$
OTD-S	$\frac{1}{2}\boldsymbol{I}_4$	$\frac{1}{2}\boldsymbol{I}_4$	$\frac{1}{2}\boldsymbol{I}_4$
Precoder cycling:			
• $N_{seq} = 1$ (PVS)	$\frac{1}{2}[1\ 1\ 1\ 1]^T$	$\frac{1}{2}[1\ -1\ 1\ -1]^T$	$\frac{1}{2}[1\ 1\ -1\ -1]^T$
• $N_{seq} = 2$	$\frac{1}{2\sqrt{2}}\begin{bmatrix} 1 & 1 \\ 1 & -1 \\ 1 & 1 \\ 1 & -1 \end{bmatrix}$	$\frac{1}{2\sqrt{2}}\begin{bmatrix} 1 & -1 \\ 1 & 1 \\ -1 & 1 \\ -1 & -1 \end{bmatrix}$	$\frac{1}{2\sqrt{2}}\begin{bmatrix} 1 & 1 \\ -1 & 1 \\ 1 & 1 \\ -1 & 1 \end{bmatrix}$

the model in equation (4.14). Also the impacts of spatial correlation are considered in Publication IV. Furthermore the impacts of time diversity are considered in Publications III and IV as some of the schemes improve performance in temporally correlated channels (e.g. low mobility).

The probability of detection can be expressed as in Table 2.1 using the cumulative distribution function of the decision statistic D. In case of multi-antenna transmission and reception the cumulative distribution function $F_D(\eta|\mathcal{H}_i)$ is expressed as follows:

$$F_D(\eta|\mathcal{H}_i) = \sum_{d_1=1}^{N_d} \left(1 - e^{-\eta/\lambda_{d_1}^{(i)}}\right) \prod_{d_2=1, d_2 \neq d_1}^{N_d} \frac{\lambda_{d_1}^{(i)}}{\lambda_{d_1}^{(i)} - \lambda_{d_2}^{(i)}} \tag{4.15}$$

where $N_d = N_r N_{seq} N_{ss}$ is the diversity order when the correlator outputs are integrated over N_{ss} repetitions in time, maximum possible diversity order being $N_d = N_r N_t N_{ss}$. Values $\lambda_d^{(i)}$ are the eigenvalues of the $N_d \times N_d$ matrix $\boldsymbol{R}_{\tilde{\boldsymbol{y}},i}\boldsymbol{Q}$ under hypothesis i, or just matrix $\boldsymbol{R}_{\tilde{\boldsymbol{y}},i}$ if noncoherent combining $\boldsymbol{Q} = \boldsymbol{I}_{N_d}$ is used. Generally for the model in equation (4.14), shown also in Figure 4.1, the $N_d \times N_d$ covariance matrix of $\tilde{\boldsymbol{y}}$ under hypothesis $\mathcal{H}_1$ in case of $N_{ss} = 1$ can be expressed as

$$\boldsymbol{R}_{\tilde{\boldsymbol{y}},1} = \boldsymbol{W}^{(j)T} \boldsymbol{R}_{tx} \boldsymbol{W}^{(j)*} \otimes \boldsymbol{R}_{rx} + \frac{\sigma_v^2}{P} \boldsymbol{I}_{N_{seq} N_r} \tag{4.16}$$

where $\boldsymbol{R}_{tx}$ and $\boldsymbol{R}_{rx}$ are the $N_t \times N_t$ transmit and $N_r \times N_r$ receive side channel covariance matrices, respectively. In Publication IV the corresponding expressions are derived also for multiple instances of the synchronization signal transmission, i.e. $N_{ss} > 1$. Note that the above expression assumes that the channel follows the well-known Kronecker model, i.e. that the

transmit and receive covariances are separable as [104]

$$\boldsymbol{R}_{\tilde{\boldsymbol{H}}} = E\Big\{\mathrm{vec}(\tilde{\boldsymbol{H}})\,\mathrm{vec}^H(\tilde{\boldsymbol{H}})\Big\} = \boldsymbol{R}_{tx} \otimes \boldsymbol{R}_{rx}. \tag{4.17}$$

Transmit diversity impacts the probability of detection through the eigenvalues of matrix $\boldsymbol{R}_{\tilde{\boldsymbol{y}},1}$ according to equation (4.15). In Publication IV, expressions for the eigenvalues are derived explicitly for some of the transmit diversity schemes. Note that under the null hypothesis, the cumulative distribution function is not impacted by the transmit diversity scheme. Consequently, there is no impact on the probability of false alarm if a Neyman-Pearson -based detection strategy is utilized.

The performance of different transmit diversity schemes was studied both analytically and by simulations in Publication III and Publication IV. Basically, the best transmission scheme depends on the operating SNR, channel spatial correlation at the transmitter side as well as the utilization of time diversity. At low SNR, transmit diversity using $N_{seq} > 1$ may even degrade the performance compared to single antenna transmission due to the required power split between the N_{seq} synchronization sequences. However, at a relatively high SNR there is a clear benefit from transmit diversity, unless the transmit correlation is high. The importance of utilizing time diversity by integrating the correlator outputs over several synchronization sequence instances was also demonstrated. In uncorrelated scenarios, precoding vector switching and time-switched transmit diversity perform very well since the benefits of spatial diversity are obtained while the power split between different sequences is avoided. However, the schemes require longer integration of the correlator outputs. In correlated scenarios, PVS may degrade the performance without time diversity because in a given transmission instance the chosen precoder may transmit the signal energy along the null space of the channel.

In Publication IV, transmission schemes maximizing the probability of detection under different channel conditions were studied considering the number of sequences N_{seq} transmitted in parallel and the power allocated to each sequence. The precoders $\boldsymbol{W}^{(j)}$ were selected as a subset of eigenvectors of the transmit covariance matrix $\boldsymbol{R}_{tx}$. Furthermore, given N_{seq}, the subset of sequences and the power α_i^2 allocated to each sequence was chosen by optimizing the following objective function:

$$\min_{\boldsymbol{\alpha}} \quad \sum_{d_1=1}^{N_d} \left(1 - e^{-\eta/\lambda_{d_1}^{(i)}}\right) \prod_{d_2=1, d_2 \neq d_1}^{N_d} \frac{\lambda_{d_1}^{(i)}}{\lambda_{d_1}^{(i)} - \lambda_{d_2}^{(i)}} \tag{4.18}$$

$$\text{s.t. } \|\boldsymbol{\alpha}\|^2 = 1. \tag{4.19}$$

where $\boldsymbol{\alpha} = [\alpha_1, \ldots, \alpha_{N_{seq}}]^T$. The eigenvalues of $\boldsymbol{R}_{\tilde{\boldsymbol{y}},1}$ can be expressed then as follows (see eq. (4.16)):

$$\lambda(\boldsymbol{R}_{\tilde{\boldsymbol{y}},1}) = \alpha_{d_1}^2 \lambda_{d_1}(\boldsymbol{R}_{tx}) \lambda_{d_2}(\boldsymbol{R}_{rx}) + \frac{\sigma_v^2}{P} \tag{4.20}$$

for $d_1 = 1, \ldots, N_{seq}$ and $d_2 = 1, \ldots, N_r$. This optimization problem is non-convex and has no closed-form solution, thus in Publication IV, numerical optimization was used to find the optimum power allocation. A similar optimization was performed in Publication IV also for the case $N_{seq} > 1$ in order to study optimum transmission schemes. The obtained results on the optimum transmission schemes essentially further confirm the findings related to the transmission schemes listed in section 4.2.1. In particular it was found that when integration over time is considered, transmitting constantly using the same eigenvector is not the optimum scheme. Rather, to take advantage of the time diversity, the optimization tends to change the eigenvector from slot to another, especially at low speed. Thus the optimum scheme resembles the precoding vector or matrix switching scheme. On the other hand it was also found that PVS matches the performance of the optimum scheme in the uncorrelated case. This is due to the fact that any precoding vectors chosen from columns of a unitary matrix can be considered as eigenvectors of matrix $\boldsymbol{R}_{tx} = \boldsymbol{I}_{N_t}$. Thus changing the precoding vector does not introduce any power loss but decorrelates the channel in time, providing diversity gain.

4.2.3 Transmit diversity for synchronization in 3GPP cellular systems

3GPP WCDMA and LTE are utilizing MIMO transmission for improving data rates, reliability and coverage. Thus, transmit diversity schemes for synchronization have been studied also for standardization purposes.

In [105], LTE cell search is studied using various transmit diversity methods for the primary and secondary synchronization signals PSS and SSS. The probability of detection as well as the overall cell search time are considered in the simulations. It is demonstrated that transmit diversity is effective in increasing the detection probability and in decreasing the cell search time. The studied transmit diversity schemes include precoding vector switching, time-switched transmit diversity, cyclic delay diversity as well as frequency-switched transmit diversity which is basically equivalent to OTD-S as different sequences are transmitted from different transmit antennas. It is found out that PVS is the most effective

scheme.

The 3GPP LTE specifications do not directly specify the used transmit diversity scheme for PSS and SSS [24]. However, only one synchronization signal is transmitted in each PSS and in each SSS instant ($N_{seq} = 1$), and certain restrictions are specified which the UE receiver can make about the synchronization signal transmission. Essentially, precoding vector switching and time-switched transmit diversity are both applicable in LTE, in addition to single antenna transmission.

In context of 3GPP WCDMA, some studies are reported in [106]. The study shows that time-switched transmit diversity improves the performance of cell search when applied to the different channels/signals in the cell search process. It is also shown that this way more power is left for data channels and thus the overall capacity of the system is improved. Time-switched transmit diversity is explicitly specified as the synchronization channel transmit diversity scheme for WCDMA [107].

The findings of Publication III and Publication IV support the choices of transmit diversity schemes in 3GPP LTE and WCDMA. It is noted that the simulations in Publication III and Publication IV are performed in a setup that resembles LTE synchronization signal transmission. Small modifications to the transmitted sequences were done to enable studying schemes with $N_{seq} > 1$.

4.3 Spatial diversity for coarse synchronization in MIMO-OFDM systems

In section 2.4, initial synchronization methods specific to OFDM systems were reviewed. Some of these methods have been extended to MIMO systems. In particular extensions of the repetitive slots -based method by Schmidl and Cox [42] introduced in section 2.4 have been considered by several authors. First, receive antenna diversity for this method was studied in [108] where different methods for combining the criterion in (2.23) were compared. The studied combining methods include selection combining (SC), maximum ratio combining (MRC) and equal gain combining (EGC). Similar studies have been conducted in [92], [109] and [110]. The methods are summarized in Table 4.3. Basically, selection combining corresponds to selecting the criterion from the receive antenna with the highest received power. Equal gain combining corresponds to averaging the criteria across receive antennas and maximum ratio combining corre-

Table 4.3. Summary of receive diversity schemes for the OFDM synchronization method by Schmidl and Cox [42]. $M_r(d)$, $P_r(d)$ and $R_r(d)$ are the quantities of equations (2.23), (2.24) and (2.25), respectively, computed at receive antenna r. The different criteria have been compared for instance in [92].

Method	Equation
Selection diversity	$M_{SC}(d) = \arg\max_{R_r(d), r \in \{1,\ldots,N_r\}} M_r(d)$
Equal gain combining	$M_{EGC}(d) = \sum_{r=1}^{N_r} M_r(d)$
Maximum ratio combining	$M_{MRC}(d) = \sum_{r=1}^{N_r} M_r(d) R_r(d)$

sponds to a weighted average of the criteria where the weights are chosen based on the received power per receive antenna.

Transmit diversity schemes for the method of Schmidl and Cox were studied in [92] [109] [110] [111]. In [92] [109] [111] it was proposed that if orthogonal sequences are transmitted from the different transmit antennas, the cross-terms between the transmit antennas in the autocorrelation $P(d)$ (see section 2.4) are suppressed, and a transmit diversity gain is achieved. In [110], a study on the sequences suitable for suppressing the cross-terms was conducted in context of IEEE 802.11a/g/n -type of systems. Note that in contrast to section 6.1, it is assumed that the transmitters are utilizing a common local oscillator. Hence the frequency mismatch is common to all transmit antennas. The studies on transmit and receive diversity in [92] [109] [110] show that receive diversity provides significant benefits in terms of synchronization performance, while transmit diversity provides only moderate performance gains.

Finally, the cyclic prefix based OFDM synchronization method by van de Beek et al. [39] is extended to multi-antenna case in [33] and [97].

4.4 Discussion

This chapter has discussed MIMO-assisted initial synchronization, mostly focusing on cross-correlation -based synchronization code acquisition relying on known synchronization signals.

Receive diversity schemes were reviewed. The existing results related to the benefits of utilizing multiple receive antennas for synchronization are in good agreement and show that multiple receive antennas provide benefits in terms of probability of detection in all scenarios. On the other hand it has also been shown that multiple receive antennas may alternatively be used for suppressing co-channel interference during initial acquisition.

The benefits of transmit diversity, however, depend on channel conditions. The analysis in Publication III and Publication IV, as well as in some of the references listed in this chapter, relate the performance of transmit diversity schemes averaged over different channel realizations to the eigenvalues of the covariance matrix of the cross-correlator outputs. These eigenvalues, on the other hand, depend on the spatial correlation both at the transmitter and the receiver side, Doppler spread and signal-to-noise ratio. It was shown that at the low signal-to-noise regime, transmit diversity may in fact degrade the performance in terms of probability of detection, while parallel transmission of multiple synchronization sequences provides diversity benefits at high SNR. However, the precoding vector switching scheme, that does not require power splitting between the transmit antennas, provides performance benefits also at a low SNR in uncorrelated channels. This is due to improving the time correlation properties of the channel, and hence increasing time diversity. By integrating the cross-correlator outputs over multiple synchronization signal transmission instances, the detection performance can be improved. This benefit was observed also by studying the optimum transmission schemes. In highly spatially correlated case it is often best to resort to single antenna transmission. The results of this chapter can be used in the design and implementation of the synchronization part of any wireless systems. Some examples from 3GPP -based systems were presented in section 4.2.3.

5. Effects of time and frequency offsets in multi-antenna wireless systems

As discussed in Chapter 2, synchronization is often subdivided into initial (or coarse) synchronization and fine time and frequency synchronization (or tracking). In OFDM systems, initial time synchronization could mean for instance that the FFT window is set roughly within the cyclic prefix, while some residual error remains. In addition to inaccurate acquisition of the synchronization sequence, such errors may be due to multipath fading: the receiver might for instance not have detected the first tap of the multipath channel. Another source of uncertainty can be changing multipath due to e.g. receiver mobility. In terms of frequency synchronization, similar residual inaccuracies arise from Doppler frequencies, local oscillator drifting as well as errors in the initial frequency offset estimation. As a result of the frequency synchronization, the error is typically at most a few percent of the OFDM subcarrier spacing.

A significantly more demanding synchronization problem needs to be solved when the receiver is simultaneously receiving signals from multiple different transmitters, and accurate time and frequency synchronization to all of them might be required. Such scenarios arise for instance in cooperative MIMO-OFDM systems, if for instance multiple cells are jointly transmitting data to the receiver in order to combat interference, see e.g. [16][17]. Such a system is illustrated in Figure 5.1. Compared to single-link case, time and frequency offsets cause some additional challenges in these scenarios.

In this chapter, the effects of residual time and frequency offsets in MIMO-OFDM systems are discussed. In section 5.1 the effects of time and frequency offsets observed in single-link MIMO-OFDM systems are reviewed. In section 5.2, the additional impacts observed in multi-link/multi-cell scenarios are summarized, with a particular focus on cooperative systems. Also the findings from Publication V and Publication VI are summa-

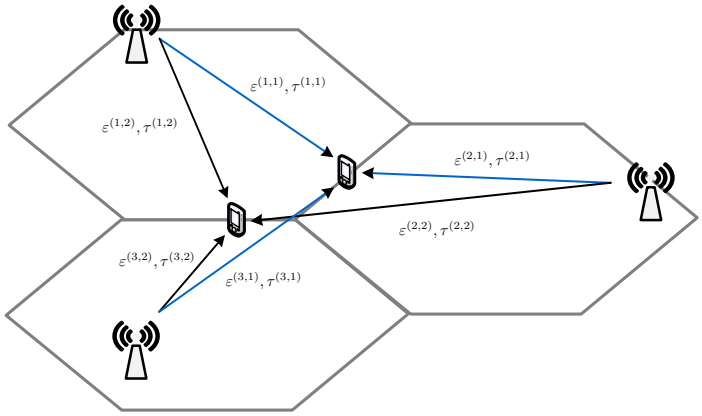

Figure 5.1. Illustration of a cooperative MIMO system in which three cells are jointly transmitting to two receivers in order to combat inter-cell interference. The time and frequency offsets from transmitter k to receiver u are denoted as $\varepsilon^{(k,u)}$ and $\tau^{(k,u)}$, respectively.

rized. Note that the focus in this chapter is solely on the impacts of time and frequency offsets. In the next chapter, estimation and compensation of these offsets is discussed. Note also that other MIMO-OFDM impairments such as for instance the impacts of phase noise and sampling clock offsets are outside the scope of this chapter. A brief review of these can be found in [23].

5.1 Effects of time and frequency offsets in MIMO-OFDM systems

In OFDM systems, time and frequency offsets cause inter-symbol interference and inter-carrier interference, respectively. The effects of this additional interference on the SINR and BER performance in single link MIMO-OFDM systems are already rather well known and several references on the topic exist in the literature. For instance, [23] provides a thorough review. Nevertheless, here the main results are summarized.

5.1.1 Inter-carrier interference

Single-carrier systems are rather sensitive to symbol timing errors, as any non-idealities in the symbol timing induce inter-symbol interference. On the other hand, single-carrier systems tend to be less sensitive to frequency offsets. On the contrary, multi-carrier systems and in particular OFDM systems are more robust in the face of symbol timing errors as inter-symbol interference can be combatted by using a guard period or

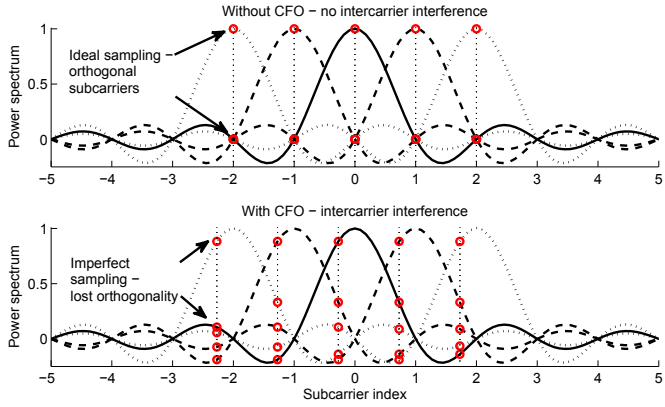

Figure 5.2. Inter-carrier interference arises due to carrier frequency offsets. Without the frequency offsets, subcarriers maintain their orthogonality.

a cyclic prefix. However, OFDM is very sensitive to frequency offsets. Similarly as in single-carrier systems timing offsets induce inter-symbol interference as the orthogonality between the adjacent symbol pulses no longer holds, in OFDM systems the frequency offsets cause loss of orthogonality between subcarriers, and hence inter-carrier interference. This is illustrated in Figure 5.2.

The impacts of carrier frequency offsets in OFDM systems have been analyzed thoroughly in the literature both analytically and via simulations. The impacts have been characterized in terms of SINR as well as in terms of bit error rate (BER) degradation. The SINR degradation is derived also here while for BER impacts only references to literature are made. Similarly to equation (2.2) and assuming rough initial synchronization ($\tau \approx 0$), one can write the received signal in SISO OFDM case. After extracting the cyclic prefix and stacking the N samples of one OFDM symbol (symbol index q) into a $N \times 1$ vector, the received time-domain signal for OFDM symbol q can be written as

$$\tilde{\boldsymbol{r}}^{(q)} = e^{j2\pi\varepsilon\frac{qN_s+G}{N}}\boldsymbol{D}_\varepsilon(\varepsilon)\tilde{\boldsymbol{H}}^{(q)}\tilde{\boldsymbol{x}}^{(q)} + \tilde{\boldsymbol{v}}^{(q)} \tag{5.1}$$

where N is the FFT size, G is the cyclic prefix length and $N_s = N+G$. The $N\times N$ matrix $\boldsymbol{D}_\varepsilon(\varepsilon) = \mathrm{diag}(e^{j2\pi\varepsilon\frac{n}{N}}),\ n = 0,\ldots,N-1$, the $N\times N$ matrix $\tilde{\boldsymbol{H}}^{(q)}$ is a circulant channel matrix and $\tilde{\boldsymbol{x}}^{(q)}$ is the transmitted OFDM symbol q in time domain. All the superscripts $(\cdot)^{(q)}$ refer to OFDM symbol index q.

Taking the FFT, the frequency-domain signal is written as

$$\boldsymbol{r}^{(q)} = e^{\jmath 2\pi\varepsilon\frac{qN_s+G}{N}}\boldsymbol{F}\boldsymbol{D}_\varepsilon(\varepsilon)\tilde{\boldsymbol{H}}^{(q)}\boldsymbol{F}^H\boldsymbol{x}^{(q)} + \boldsymbol{v}^{(q)} \quad (5.2)$$

$$= e^{\jmath 2\pi\varepsilon\frac{qN_s+G}{N}}\boldsymbol{F}\boldsymbol{D}_\varepsilon(\varepsilon)\boldsymbol{F}^H\boldsymbol{H}^{(q)}\boldsymbol{x}^{(q)} + \boldsymbol{v}^{(q)} \quad (5.3)$$

$$= e^{\jmath 2\pi\varepsilon\frac{qN_s+G}{N}}\boldsymbol{\Phi}_\varepsilon(\varepsilon)\boldsymbol{H}^{(q)}\boldsymbol{x}^{(q)} + \boldsymbol{v}^{(q)} \quad (5.4)$$

where $\boldsymbol{H}^{(q)} = \mathrm{diag}(h[k]),\ k = 0, \ldots, N-1$ is the diagonal matrix containing the frequency-domain channel for each subcarrier and $\boldsymbol{\Phi}_\varepsilon = \boldsymbol{F}\boldsymbol{D}_\varepsilon(\varepsilon)\boldsymbol{F}^H$ is an ICI matrix with entries

$$[\boldsymbol{\Phi}_\varepsilon]_{m,n} = \frac{1}{N}\exp\left(\jmath\pi\frac{N-1}{N}(n-m+\varepsilon)\right)\frac{\sin(\pi(n-m+\varepsilon))}{\sin(\pi(n-m+\varepsilon)/N)}. \quad (5.5)$$

The (m,n):th entry of the ICI matrix $\boldsymbol{\Phi}_\varepsilon$ essentially captures the inter-carrier interference from the n:th subcarrier to the m:th subcarrier.

Denoting $\Phi_\varepsilon[m,n] = [\boldsymbol{\Phi}_\varepsilon]_{m,n}$, the average signal to interference and noise ratio for subcarrier m can be expressed as (assuming unit signal power and $E\{|h[m]|^2\} = 1$):

$$\mathrm{SINR}_m = \frac{|\Phi_\varepsilon[m,m]|^2}{\sum_{n=0,n\neq m}^{N-1}|\Phi_\varepsilon[m,n]|^2 + \sigma_v^2}. \quad (5.6)$$

From (5.6) it should be noted that in addition to introducing inter-carrier interference, the frequency offsets also reduce the amplitude of the signal, hence further decreasing SINR. It is also noted that while the symbol-specific phase rotation visible in (5.4) does not impact SINR directly, it complicates channel estimation as will be discussed in more detail in section 5.1.3.

Based on the above, an expression for the approximate SINR degradation D (in decibels) in presence of CFO has been derived by Pollet et al. in [112]. With the notation used in this thesis, the equation reads as follows:

$$D \approx \frac{10}{\ln 10}\frac{(\pi\varepsilon)^2}{3}\mathrm{SNR} \quad [\mathrm{dB}] \quad (5.7)$$

where SNR is the signal to noise ratio without CFO, i.e. $\mathrm{SNR} = 1/\sigma_v^2$, again assuming unit signal power as well as unit average channel power. The approximations used in deriving the equation require that $(\pi\varepsilon)^2 \ll 3$, hence it is valid only at small CFO values. Equation (5.7) has also been derived in [113]. A slightly different approximation to SINR in presence of CFO has also been presented in [43]. In Figure 5.3, the impact of CFO in terms of SINR degradation is plotted for CFO values of $\varepsilon = 0.01$, $\varepsilon = 0.02$ and $\varepsilon = 0.05$, both using the exact SINR expression in (5.6) and the Pollet approximation as in equation (5.7). With such small CFO values the approximation matches reasonably well. It is also seen that the CFO should

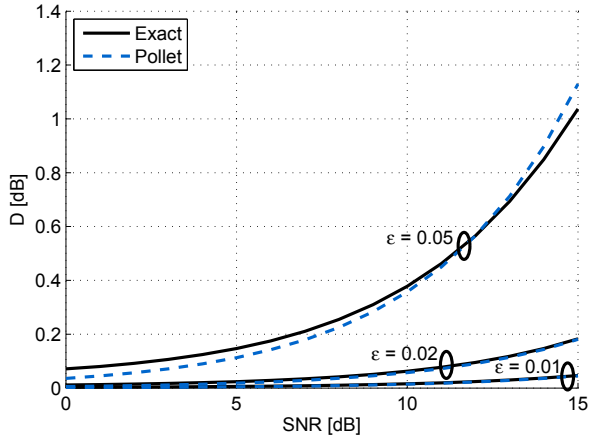

Figure 5.3. SNR degradation D in dB for $N = 256$ and $\varepsilon = 0.01$, $\varepsilon = 0.02$ and $\varepsilon = 0.05$. Both exact values and the Pollet approximation [112] are provided. Especially at high input SNR where ICI dominates, a CFO of a few percent may cause significant degragation in the SNR.

be less than a few percent of the subcarrier spacing in order to avoid significant SINR degradation. Other references studying the SINR impacts are [114] where the SINR degradation due to CFO is compared with impacts of phase noise and sampling clock offsets, and [115] where bounds on the ICI power are derived instead of the exact ICI as in equation (5.5). Such bounds may be useful for instance in determining the OFDM system parameters.

The SINR-based analysis already allows for predicting the impact of CFO on the bit error rate by modeling ICI as additional Gaussian noise, and utilizing the existing bit error rate prediction methods. This approach was first studied by Russell and Stüber [116] where the central limit theorem was utilized to justify the Gaussian approximation of the ICI, and the variance of ICI was based on average SINR similarly to equation (5.6). Average SINR was then utilized to calculate symbol error rate. A similar analysis was carried out in [117]. However, some authors have pointed out some drawbacks of utilizing the Gaussian approximation -based approach in predicting the BER degradation: First, obviously, the Gaussian approximation is valid only for a large number of subcarriers N. Furthermore, in [118] it has been pointed out that average SINR -based BER prediction is not very accurate in frequency-selective channels as the frequency-selectivity impacts also ICI. Hence a more accurate method was proposed, based on calculating the BER first conditioned on channel realization and finally averaging the BER over the channel realizations. More precise

analysis on the BER impacts was also done in [113] for BPSK, QPSK and 16QAM modulations. Essentially all results in the aforementioned papers confirm that OFDM performance starts to degrade when carrier frequency offset exceeds a few percent of the subcarrier spacing, as also shown in Figure 5.3.

The analysis above assumed single-antenna reception at the receiver side. The impacts of multi-antenna reception on ICI have been studied in [116] and [119]. In [116], it is essentially shown that if the radio channels to the multiple receive antennas are uncorrelated, maximum ratio combining averages ICI similarly to averaging noise. On the other hand in [119], it is argued that if there is correlation between receive antennas or heavy frequency correlation in the channel, increasing the number of receive antennas does not help with ICI.

Finally, an uplink OFDMA case was analyzed in [120]. In uplink, multiple users may be transmitting simultaneously on different subcarriers. In this case, the perfect orthogonality between the transmissions from different users is broken, and in addition to self-interference due to each users' own CFO, also multi-user interference (MUI) is induced. Let us write the uplink OFDMA signal model for OFDM symbol q after CP extraction and FFT as follows:

$$\boldsymbol{r}^{(q)} = \sum_{k=1}^{K} e^{j2\pi\varepsilon_k \frac{qN_s+G}{N}} \boldsymbol{F}\boldsymbol{D}_{\varepsilon}(\varepsilon_k)\boldsymbol{F}^H \boldsymbol{H}_k^{(q)} \boldsymbol{x}_k^{(q)} + \boldsymbol{v}^{(q)}. \tag{5.8}$$

In this model, K denotes the number of users and subscript k refers to the k:th user. It is assumed that each user k is allocated a set $\mathcal{S}_k^{(q)}$ of $N_k^{(q)}$ orthogonal subcarriers such that $\mathcal{S}_k^{(q)} \cap \mathcal{S}_l^{(q)} = \emptyset,\ \forall k, l$. Similarly to (5.6), assuming a perfectly power-controlled scenario, the average SINR for subcarrier $m \in \mathcal{S}_k^{(q)}$ allocated to the k:th user can be written as follows [120]:

$$\mathrm{SINR}_m^{(k)} = \frac{|\boldsymbol{\Phi}_{\varepsilon}(\varepsilon_k)[m,m]|^2}{\underbrace{\sum_{n\in\mathcal{S}_k^{(q)}, n\neq m} |\boldsymbol{\Phi}_{\varepsilon}(\varepsilon_k)[m,n]|^2}_{\text{Self-interference}} + \underbrace{\sum_{l=1,l\neq k}^{K} \sum_{n\in\mathcal{S}_l^{(q)}} |\boldsymbol{\Phi}_{\varepsilon}(\varepsilon_l)[m,n]|^2}_{\text{MUI}} + \sigma_v^2} \tag{5.9}$$

Similar conclusions on the impacts of CFOs on the SINR or BER degradation can be drawn as in the single-user (or downlink) case.

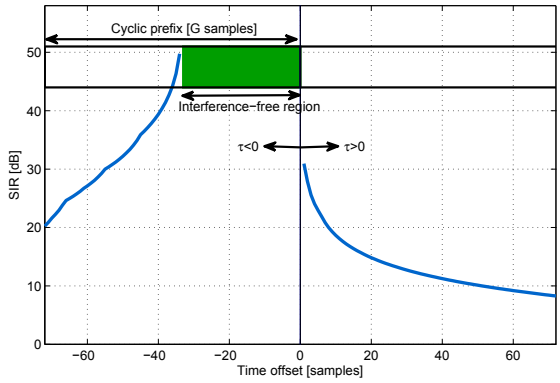

Figure 5.4. Signal to interference ratio with timing offsets in case of $N = 1024$, $G = 72$ and the Extended Vehicular A channel ($L = 40$) according to [122]. To the left of the ideal FFT timing there is an interference-free region of length $G-L+1$ which the ISI from the previous OFDM symbol does not reach.

5.1.2 Inter-symbol interference

As mentioned earlier, OFDM systems are typically considered less sensitive to timing offsets due to use of the cyclic prefix to combat inter-symbol interference. The impact has been studied in [121] [122]. In [121] an approximate expression for the inter-symbol interference was presented, while in [122] an exact expression for the resulting SIR was derived. With the notation used in this thesis and assuming that the total channel power is equal to one $\gamma = \sum_{l=0}^{L-1} \gamma_l = 1$ and that the transmitted signal power is normalized to unity, the SIR due to time offsets can be expressed as [122]

$$\mathrm{SIR}_{\tau>0} = \frac{(N-\tau)^2}{(2N-\tau)\tau - 2(N-\tau)\sum_{k=0}^{\tau-1}\sum_{k'=k+1}^{L-1}\gamma_l} \tag{5.10}$$

$$\mathrm{SIR}_{\tau<0} = \frac{(N-d)^2}{(2N-d)d - 2(N-d)\sum_{k=0}^{d-1}\sum_{k'=0}^{G+\tau+k}\gamma_l} \tag{5.11}$$

where $d = \max\{L-1-(G+\tau), 0\}$. Based on these equations, SIR due to time offsets is illustrated in Figure 5.4 in case of Extended Vehicular A channel ($L = 40$) using the 3GPP LTE parameters ($N = 1024$, $G = 72$) for a 10 MHz system bandwidth [24]. It is noted that the impact of ISI and ICI is asymmetric around the ideal FFT timing $\tau = 0$ due to use of cyclic prefix, and there is an interference-free region, the length of which depends on the channel delay spread. Due to the asymmetric interference, a typical OFDM receiver may use an FFT timing that is shifted to left compared to the estimated FFT timing, to make sure that the timing is within the interference-free region.

5.1.3 Impacts on OFDM channel estimation

As shown in equation (5.4), residual carrier frequency offsets introduce an OFDM symbol -dependent phase rotation into the received signal. While this has no impact on inter-carrier interference, it has an impact on the time correlation properties of the effective radio channel. Adding a time offset to equation (5.4), the equation can be re-written as

$$\boldsymbol{r}^{(q)} = e^{\jmath 2\pi\varepsilon\frac{qN_s+G}{N}}\boldsymbol{\Phi}_\varepsilon(\varepsilon)\boldsymbol{D}_\tau(\tau)\boldsymbol{H}^{(q)}\boldsymbol{x}^{(q)} + \boldsymbol{v}^{(q)} \tag{5.12}$$

where $\boldsymbol{D}_\tau(\tau_c) = \mathrm{diag}(\exp(-\jmath 2\pi\tau_c n/N)),\ n = 0,\ldots,N-1$. This assumes that the time offset is within the region illustrated in Figure 5.4 such that there is no additional inter-symbol interference. From the equation it can be seen that time offsets introduce a phase rotation across the frequency subcarriers. Hence, this time offset has an impact on the frequency correlation properties of the effective radio channel.

When utilizing pilot-assisted channel estimation, typically the channel on the pilot subcarriers can be estimated directly, while the channel on the data subcarriers is interpolated based on the initial channel estimates on the pilot subcarriers. The optimum interpolation in the MSE sense is achieved with the Wiener filter [123]. This method requires knowledge of some channel statistics such as time correlation and frequency correlation.

The initial channel estimates for N_p pilot subcarriers can be estimated, for instance, by using least squares -based estimation, see [23] for a review of other methods:

$$\hat{\boldsymbol{h}}_p = (\boldsymbol{P}^H\boldsymbol{P})^{-1}\boldsymbol{P}^H\boldsymbol{r}_p \tag{5.13}$$

where the $N_p \times 1$ vector $\boldsymbol{r}_p = \boldsymbol{r}_Q(\mathcal{S}_p)$ denotes the received signal on the set of subcarriers $\mathcal{S}_p$ carrying pilots and $\boldsymbol{r}_Q = [\boldsymbol{r}^{(0)T},\ldots,\boldsymbol{r}^{(Q-1)T}]^T$ contains the received frequency-domain signal stacked from multiple OFDM symbols into a single $QN \times 1$ vector. The $N_p \times N_p$ matrix $\boldsymbol{P}$ contains the N_p pilot symbols on the main diagonal. The full $QN \times 1$ channel estimate is then obtained by interpolation as $\hat{\boldsymbol{h}}_Q = \boldsymbol{W}\hat{\boldsymbol{h}}_p$ where $\boldsymbol{W}$ is the interpolation filter of size $QN \times N_p$. As mentioned, the optimum interpolation filter is the Wiener filter obtained by minimizing the mean square estimation error as

$$\boldsymbol{W} = \arg\min_{\boldsymbol{W}} E\left\{\left\|\boldsymbol{h}_Q - \boldsymbol{W}\hat{\boldsymbol{h}}_p\right\|^2\right\} = \boldsymbol{R}_{\boldsymbol{h}_Q\hat{\boldsymbol{h}}_p}\boldsymbol{R}^{-1}_{\hat{\boldsymbol{h}}_p\hat{\boldsymbol{h}}_p} \tag{5.14}$$

where $\boldsymbol{R}_{\boldsymbol{h}_Q\hat{\boldsymbol{h}}_p} = E\left\{\boldsymbol{h}_Q\hat{\boldsymbol{h}}_p^H\right\}$ and $\boldsymbol{R}_{\hat{\boldsymbol{h}}_p\hat{\boldsymbol{h}}_p} = E\left\{\hat{\boldsymbol{h}}_p\hat{\boldsymbol{h}}_p^H\right\}$. Knowledge of channel statistics such as delay spread, Doppler spread and signal to noise ratio

are required to compute these quantities.

The impacts of time and frequency offsets on the channel estimation performance have been studied in [124] [125] [126] and also in Publication VI in case of Wiener filter, while the impacts of mismatched channel statistics are more generally studied in [127]. In [128] [129] the impacts are studied in case of linear interpolation -based filters.

In absence of time and frequency offsets, in case the exact channel statistics are utilized in computing the filter coefficients, the (normalized) channel estimation MSE when the Wiener filter is utilized is expressed as

$$\mathrm{MSE} = 1 - \frac{1}{QN}\mathrm{tr}\left\{\boldsymbol{R}_{\boldsymbol{h}_Q\hat{\boldsymbol{h}}_p}\boldsymbol{R}^{-1}_{\hat{\boldsymbol{h}}_p\hat{\boldsymbol{h}}_p}\boldsymbol{R}^{H}_{\boldsymbol{h}_Q\hat{\boldsymbol{h}}_p}\right\}. \tag{5.15}$$

As mentioned, possible sources of mismatch in the channel statistics are residual time and frequency offsets. Let us denote the effective radio channel (with time and frequency offsets) in symbol q as

$$\boldsymbol{g}^{(q)} = e^{j2\pi\varepsilon\frac{qN_s+G}{N}}\boldsymbol{D}_\tau(\tau_c)\boldsymbol{h}^{(q)}. \tag{5.16}$$

If the time and frequency offsets are not taken into account in the channel estimation, a mismatch occurs and the MSE is written as follows (see Publication VI):

$$\begin{aligned}\mathrm{MSE} = 1 &- \frac{2}{QN}\mathrm{tr}\left\{\Re\left\{\boldsymbol{R}_{\boldsymbol{h}_Q\hat{\boldsymbol{h}}_p}\boldsymbol{R}^{-1}_{\hat{\boldsymbol{h}}_p\hat{\boldsymbol{h}}_p}\boldsymbol{R}^{H}_{\boldsymbol{g}_Q\hat{\boldsymbol{g}}_p}\right\}\right\} \\ &+ \frac{1}{QN}\mathrm{tr}\left\{\boldsymbol{R}_{\boldsymbol{h}_Q\hat{\boldsymbol{h}}_p}\boldsymbol{R}^{-1}_{\hat{\boldsymbol{h}}_p\hat{\boldsymbol{h}}_p}\boldsymbol{R}_{\hat{\boldsymbol{g}}_p\hat{\boldsymbol{g}}_p}\boldsymbol{R}^{-1}_{\hat{\boldsymbol{h}}_p\hat{\boldsymbol{h}}_p}\boldsymbol{R}^{H}_{\boldsymbol{h}_Q\hat{\boldsymbol{h}}_p}\right\}. \end{aligned} \tag{5.17}$$

Figure 5.5 shows the impact of time and frequency offsets on channel estimation MSE (as in (5.17)) in case of SNR of 5 dB and in case of SNR of 15 dB. Clearly, even minor small time/frequency offsets can ruin the channel estimation performance.

This performance degradation has been further studied in Publication VI in case of LTE CoMP. In dynamic cell or transmission point selection, the transmitter may change very rapidly in an attempt to optimize the transmissions to match with the instantaneous radio channel and interference conditions as well as possible. Since time and frequency offsets may also depend on the transmission point, they may also change very rapidly. In LTE this may happen every 1 ms. In Publication VI the impacts of distinct time and frequency offsets to different transmitters on channel estimation performance were studied. Furthermore the consequent LTE link-level throughput degradation was simulated. It was shown that even small residual time and frequency offsets cause significant channel estimation performance degradation, causing the link-level

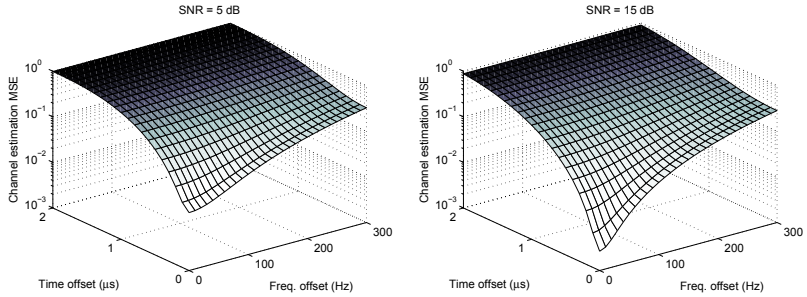

Figure 5.5. Channel estimation MSE in presence of time and frequency offsets at carrier frequency of 2.0 GHz in case of Extended Pedestrian A channel. The correlations are calculated based on LTE UE-specific reference signal patterns [24] using channel estimation over three physical resource blocks, similarly to Publication VI.

performance to collapse, especially in case of higher order modulations. Hence, methods for fast time and frequency error compensation in every 1 ms subframe before channel estimation and symbol detection were studied.

Some methods have been introduced to make the MMSE channel estimator more robust to time and frequency offsets. For instance, in [126] it is shown that if the frequency correlation used in deriving the Wiener filter is based on a uniform power delay profile, the resulting channel estimation MSE becomes independent of the actual PDP. Hence, as long as the time offset and the channel delay spread remain within the uniform power delay profile used to compute the frequency correlation, the filter performs well. Similar observation is made in [127], where it was shown also that if the time correlation is based on a uniform Doppler spread function, the resulting interpolation filter is robust also to mismatches in the time correlation (and hence to frequency offsets). It is shown that MSE performance stays quite close to the MSE performance of the optimum filter. In [125], instead of relying on a uniform power delay profile, the proposed robust interpolation filter takes into account the distribution of the time offset.

5.2 Effects of time and frequency offsets in cooperative wireless systems

In previous sections, the focus has been on the impacts of frequency and time offsets in case of a single radio link and a single time and frequency

offset. However, in cooperative multi-link or multi-cell situations additional challenges may arise. These situations happen in context of cooperative transmission systems such as cooperative relays (see e.g. [130] [131] [132]) or cooperative MIMO (see e.g. [16] [17] [133]). In this section we review the impacts of time and frequency offsets on cooperative MIMO-OFDM systems (section 5.2.1) as well as on cooperative systems utilizing inter-cell interference coordination schemes (section 5.2.2). Note that the topic has been addressed in Publication V and Publication VI.

5.2.1 Effects of time and frequency offsets in cooperative MIMO-OFDM systems

In cooperative MIMO, the problem pertains to the fact that the carrier frequency offsets cause transmitter-specific phase drifts which significantly degrade the performance of any type of transmit precoding aimed at phase coherent transmissions among the different transmitters. It is noted that similar problems do not happen in normal single cell / transmitter -based MIMO systems, because in that case, assuming a common clock source, the CFO is typically common to all MIMO channel branches, and thus does not impact the relative phase between them.

The problem was first noted in [134] [135]. In [134], a simple analysis about SIR degradation due to CFOs was done for a zero-forcing (ZF) -based joint transmission cooperative MIMO system with two transmitters and two receivers, with one antenna each. In [135], the impacts of frequency offsets on the sum-rate capacity of cooperative MIMO were investigated. Let us denote the $N_r \times N_t$ frequency-flat MIMO channel matrix between the transmitter (base station) k and receiver u as $\boldsymbol{H}^{(k,u)}$. Then, denote the effective channel matrix with frequency offsets as $\boldsymbol{H}_{\phi}^{(k,u)} = e^{\jmath\phi^{(k,u)}}\boldsymbol{H}^{(k,u)}$ where $\phi^{(k,u)} = 2\pi\nu^{(k,u)}d$ is the phase offset that depends on the delay d between the CSI acquisition instant and the transmission, as well as on the frequency offset $\nu^{(k,u)}$.

Finally, denote the full $N_r \times KN_t$ effective channel matrix between the K transmitters (base stations) and receiver u as $\boldsymbol{H}_{\phi}^{(u)} = \left[\boldsymbol{H}_{\phi}^{(1,u)}, \ldots \boldsymbol{H}_{\phi}^{(K,u)}\right]$. Then, the sum-rate capacity for U users of the cooperative multi-user

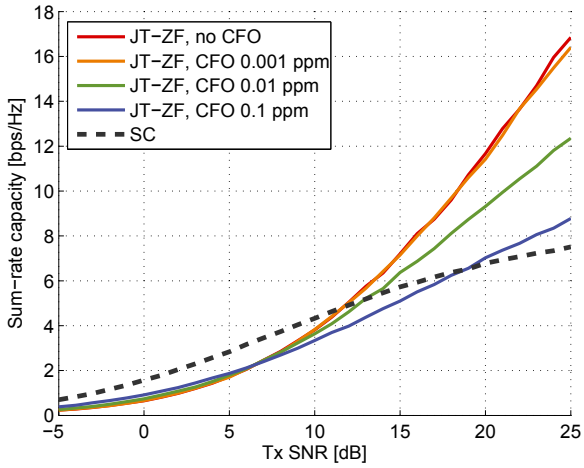

Figure 5.6. Sum-rate capacity of a JT-ZF -based cooperative MIMO system in presence of CFOs at carrier frequency of 2.0 GHz. The CSI delay d corresponds here to 6 ms, based on a typical value in the 3GPP LTE system. Other parameters are $U = 2$, $K = 2$, $N_t = 2$ and $N_r = 2$, and the channels are modeled as uncorrelated Rayleigh fading MIMO channels.

MIMO system in presence of CFOs can be expressed as [133][135]

$$C = \sum_{u=1}^{U} \log_2 \det \Bigg(\boldsymbol{I}_{N_r} + \boldsymbol{H}_{\phi}^{(u)} \boldsymbol{\Psi}^{(u)} \boldsymbol{H}_{\phi}^{(u)H} \Big(\sum_{i=1, i \neq u}^{U} \boldsymbol{H}_{\phi}^{(u)} \boldsymbol{\Psi}^{(i)} \boldsymbol{H}_{\phi}^{(u)H} + \sigma_v^2 \boldsymbol{I}_{N_r} \Big)^{-1} \Bigg) \quad (5.18)$$

where $\boldsymbol{\Psi}^{(u)} = \boldsymbol{W}^{(u)} \boldsymbol{W}^{(u)H}$ comprises the $KN_t \times R$ precoding matrices $\boldsymbol{W}^{(u)}$ for receiver u (R denoting the number of streams). The impact of different carrier frequency offsets on the capacity of a joint transmission ZF -based cooperative MIMO system (based on equation (5.18)) is shown in Figure 5.6. For comparison, also the corresponding single-cell (SC) MIMO capacity is shown, considering the other cell transmission as interference.

In Publication V, a further investigation into impacts of carrier frequency offsets on the SINR at the receiver side in case of cooperative MIMO-OFDM was conducted. The impacts of carrier frequency offsets as well as timing offsets is investigated in terms of SINR degradation, and the impacts of various interference sources (inter-carrier, inter-symbol and multi-user interference) are characterized quantitatively and compared. In the considered case, multi-user interference is due to the CFOs that cause loss of spatial orthogonality among the transmissions to different users. As derived in Publication V, the per-antenna SINR on sub-

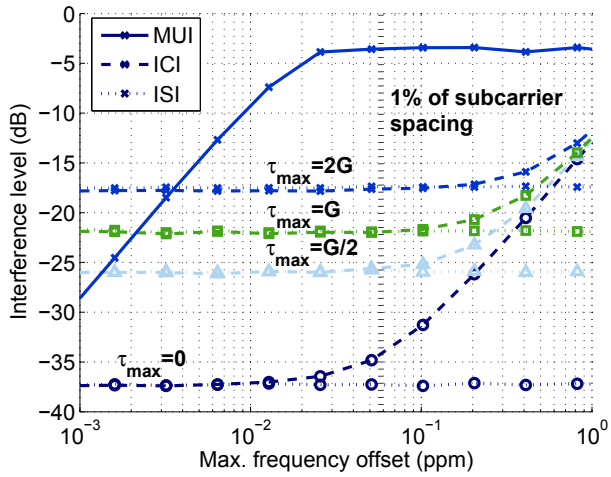

Figure 5.7. Interference level from various interference sources in cooperative MU-MIMO systems [Publication V]. Clearly, such systems are highly sensitive to CFOs due to multi-user interference (MUI). © 2009 IEEE.

carrier k in presence of the aforementioned multi-user interference can be expressed as

$$\mathrm{SINR}[k] = \frac{\mathrm{tr}\left\{\mathcal{S}[k]\right\}}{\mathrm{tr}\left\{\mathcal{I}_{\mathrm{MUI}}[k] + \mathcal{I}_{\mathrm{ICI}}[k] + \mathcal{I}_{\mathrm{ISI}}[k]\right\} + N_r\sigma_v^2} \tag{5.19}$$

where the different interference components $\mathcal{I}_{\mathrm{MUI}}[k]$, $\mathcal{I}_{\mathrm{ICI}}[k]$ and $\mathcal{I}_{\mathrm{ISI}}[k]$ are explained in detail in Publication V. The impact of the different interference sources on the overall SINR is shown in Figure 5.7 [Publication V] which demonstrates that the multi-user interference starts to degrade the performance at several orders of magnitude lower CFOs than the usual OFDM inter-carrier interference.

The result in Figure 5.7 illustrates that in cooperative MIMO systems utilizing multi-user precoding techniques, the multi-user interference resulting from CFOs can be the dominant source of interference. This result also justifies why the sum-rate capacity can be sufficiently accurately evaluated also in OFDM systems by considering only single carrier models as in equation (5.18): the impacts of inter-carrier and inter-symbol interference are several orders of magnitude smaller than those of multi-user interference. Based on the result it can also be concluded that cooperative MIMO-OFDM systems set significantly more strict requirements on then frequency synchronization of the transmitters than in the normal single-link MIMO-OFDM case.

5.2.2 Effects of time and frequency offsets on interference coordination schemes

In OFDM systems, network cooperation may also be used for combatting interference via resource partitioning. For instance, in frequency-domain inter-cell interference coordination (ICIC) schemes (fractional frequency reuse) each transmitter is assigned specific subcarriers or a specific subband of the full system bandwidth on which to transmit [136]. Thus, the transmissions are orthogonalized in frequency domain. In such systems, time and frequency offsets cause loss of orthogonality between the transmissions, reducing the benefits of interference coordination. The impacts of frequency offsets are very similar to the impacts in uplink OFDMA as shown in equation (5.9), with the exception that the transmissions can not be similarly power-controlled. Therefore, signals from certain interfering transmitters may be received even with a higher power than from the serving transmitter.

Taking into account the differences in the overall path gains, the SINR on subcarrier m corresponding to transmissions from transmitter k in presence of CFOs can be expressed as follows:

$$\mathrm{SINR}_m^{(k)} = \frac{\gamma_k |\mathbf{\Phi}_\varepsilon(\varepsilon_k)[m,m]|^2}{\underbrace{\sum_{n\in\mathcal{S}_k^{(q)}, n\neq m} \gamma_k |\mathbf{\Phi}_\varepsilon(\varepsilon_k)[m,n]|^2}_{\text{Self-interference}} + \underbrace{\sum_{l=1,l\neq k}^{K} \sum_{n\in\mathcal{S}_l^{(q)}} \gamma_l |\mathbf{\Phi}_\varepsilon(\varepsilon_l)[m,n]|^2}_{\text{Inter-cell interference}} + \sigma_v^2} \tag{5.20}$$

where γ_j is the path gain corresponding to transmitter j and $\mathcal{S}_j^{(q)}$ is the set of subcarrier assigned to transmitter j.

Large power differences are experienced in practice for instance in heterogeneous cellular networks where the cell association of a user may be offset in order to offload more traffic to small cells on the same frequency. This is called cell range expansion [137][138], illustrated in Figure 5.8. In such case the macro cell signal may be received with e.g. up to 10 dB higher power than the (serving) small cell signal, thus causing severe interference without inter-cell interference coordination schemes.

Since the frequency offsets cause subcarrier power to leak on the neighboring subcarriers, in fractional frequency reuse schemes the frequency offsets cause most problems at the edges of the subbands assigned to different transmitters. The impacts of frequency offsets on fractional frequency reuse schemes are illustrated in Figure 5.9 where two transmitters are considered. The SINR degradation on the first, second and third

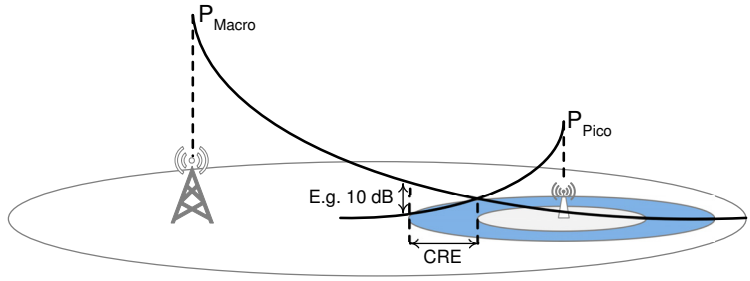

Figure 5.8. Illustration of cell range expansion (CRE) in heterogeneous networks with both high power macro cells and low power pico cells on the same frequency. The receivers within the cell range expansion region suffer from high interference unless interference coordination methods are utilized.

subcarrier closest to the edge of the assigned subbands are shown in case of 3 dB and 10 dB difference between the serving and interfering transmitters. Rather severe SINR degradation can be observed on the closest subcarriers. Hence, unless accurate frequency synchronization can be guaranteed, the number of different assigned subbands should be minimized to also minimize the impacts of frequency offsets. Guard bands between the assigned subbands provide an alternative solution.

5.3 Discussion

This chapter has discussed the effects of time and frequency offsets on MIMO-OFDM systems. In single link MIMO-OFDM systems, the impacts of frequency offsets are already well known: Typically a frequency offset of a few percent of the subcarrier spacing starts to degrade the SINR, and hence also the link-level performance. Also time offsets causing the FFT window start position to fall outside the cyclic prefix may degrade the SINR. In typical systems such as 3GPP LTE, these effects are combatted simply by dimensioning the system parameters appropriately. For instance, the 15 kHz subcarrier spacing in LTE allows frequency errors of up to a few hundreds of Hz. Note that for instance 200 Hz corresponds to 0.1 ppm at a typical carrier frequency of 2.0 GHz. Similarly, in channels typical to LTE in terms of delay spread, the 4.7 μs cyclic prefix length leaves room for time synchronization uncertainties.

The impacts of time and frequency offsets on channel estimation performance were also discussed, and it was shown that even small residual time and frequency offsets may cause the channel estimation performance to degrade significantly. This is in particular true for MMSE channel esti-

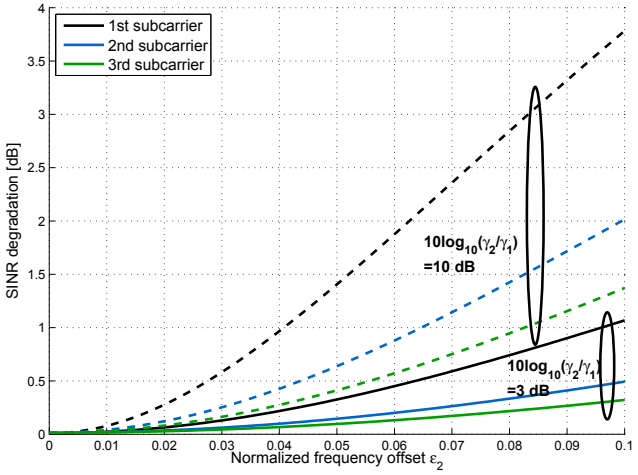

Figure 5.9. Impacts of CFOs on the received SINR (based on equation (5.20)) in case of two transmitters sharing the same band using fractional frequency reuse to combat interference. Parameters are $\varepsilon_1 = 0.01$, $N = 256$, $\gamma_1 = 1$ and $\sigma_v^{(2)} = 0.1$, corresponding to 10 dB SNR. Each transmitter is assigned half of the total bandwidth.

mation methods [123] which rely on the observed channel statistics in calculating the channel interpolation filter. The impacts of this phenomenon were studied in Publication VI in context of LTE CoMP where the time and frequency offsets change whenever a different transmission point or cell is chosen for transmission. Consequently, it was shown that mitigating the residual offsets is crucial for gaining the performance benefits of LTE dynamic point selection CoMP. Clearly, more precise time and frequency synchronization is required from channel estimation perspective than from ICI or ISI perspective. In case of LTE, this was solved by estimating the time and frequency offsets towards multiple transmitters, and informing the (UE) receiver about the originating transmitter of the data transmission. This way the receiver can apply the correct time and frequency offsets prior to channel estimation to mitigate the impacts.

In cooperative MIMO-OFDM systems, in addition to the impacts discussed above, time and frequency offsets cause also other effects. In particular, as shown in Publication V, in cooperative MIMO systems targeting phase coherent transmissions among multiple transmitters, frequency offsets may degrade the performance of the transmit precoding as they cause phase variation that is a function of CSI feedback delay. In cooperative multi-user MIMO schemes, such as zero-forcing joint transmission, this further causes multi-user interference as the spatial or-

thogonality between the transmissions is lost. Thus the capacity potential of cooperative multi-user MIMO schemes can not be exploited. It was shown that the required frequency accuracy is orders of magnitude more precise than what is required for normal single-link OFDM systems. Achieving such an accuracy appears challenging. In [134] it was mentioned that in outdoor cooperative base stations GPS-based solutions could be utilized, while in other cases the Precision Time Protocol (PTP) could be applied. Another possible approach could be distributed network synchronization [139] where the receivers estimate multiple carrier frequency offsets, and report them back to the transmitter side, such that the transmitter-induced CFOs can be corrected in a distributed manner. Whether this approach is feasible depends at least on the accuracy of the CFO estimates which is the topic of the next chapter.

Finally, regarding the impacts of CFOs in cooperative systems, it was further shown that in systems employing fractional frequency reuse or other frequency domain ICIC techniques, CFOs may degrade the SINR and the effectiveness of interference coordination, due to loss of orthogonality between the transmissions from different transmitters. However, the performance degradation is limited to the edges of the assigned subbands, and thus guard bands and careful subband assignment may be used to mitigate the impacts.

To conclude, recent developments in MIMO-OFDM and in particular cooperative MIMO-OFDM clearly place new challenges to time and frequency offset estimation. In the next chapter the estimation of multiple CFOs is discussed, in particular targeting application to cooperative MIMO-OFDM systems.

6. Estimation of time and frequency offsets in cooperative MIMO-OFDM systems

In the previous chapter, the problems caused by time and frequency offsets were discussed, in particular in context of OFDM systems. In single-link cases, the effects can be to a large extent mitigated by the usual OFDM time and frequency offset estimation algorithms discussed in section 2.4. However, as shown in the previous chapter, in cooperative systems the impacts may be much more severe in some cases, potentially requiring even several orders of magnitude more accurate frequency synchronization. Additionally CFOs associated with multiple transmitters may need to be estimated. The problem is made worse by the fact that at the receiver side it is not possible to correct multiple frequency offsets in the traditional way, i.e. by simply counter-rotating the received signal using the estimated CFO. Since in this case the problem is typically mainly the frequency offsets induced by the transmitter side local oscillators (also to some extent by Doppler however the impact of Doppler is typically smaller), in principle the problem could be avoided by more accurate LOs. However, this would require much more expensive hardware and is therefore often not feasible or cost-efficient.

Thus in this chapter, the focus is on estimation of multiple CFOs in cooperative multi-link situations, and also on the mitigation of multiple CFOs. The chapter is organized as follows: In section 6.1 the estimation methods for multiple CFOs are reviewed, including bounds for the estimation performance set by the Cramér-Rao bound. Next, in section 6.2, the mitigation of impacts of multiple carrier frequency offsets is discussed and finally, the chapter is concluded with a discussion in section 6.3.

6.1 Estimation of time and frequency offsets in multi-cell MIMO systems

In cases with multiple links such as in cooperative systems or in any other multi-cell cases, as discussed earlier, the receiver may be required to estimate multiple carrier frequency offsets due to the fact that the different transmitters are driven by distinct local oscillators. Compared to the problem of estimating time and frequency offsets in a single-link case as discussed in section 2.4, estimating multiple frequency offsets incurs some additional challenges: The main problem arises from the fact that the orthogonality between transmissions from the multiple transmitters is lost due to the different CFOs. This loss of orthogonality induces multiple access interference (MAI), complicating the estimation problem.

A similar problem has been studied earlier for uplink OFDMA case in which case the receiver also needs to estimate multiple CFOs due to distinct LOs, e.g. [140] [141]. However, whether the uplink solutions are applicable depends on the assumed subcarrier assignment scheme, as in many cases for uplink it is assumed that each transmitter occupies a certain subband (i.e. a certain number of neighboring subcarriers) of the total bandwidth, which can not be assumed in the downlink case. Still, some solutions are available for CFO estimation in uplink OFDMA with more generalized subcarrier assignment schemes, and those solutions are directly applicable to the problem here. Such uplink OFDMA solutions are also reviewed in this section. The methods can be classified into maximum-likelihood -based methods reviewed in section 6.1.2, subspace-based methods reviewed in section 6.1.3 and correlation-based methods reviewed in section 6.1.4.

Let us write the $N \times 1$ time-domain received signal for symbol q as

$$\tilde{\boldsymbol{r}}^{(q)} = \sum_{k=1}^{K} e^{\jmath 2\pi\varepsilon_k \frac{qN_s+G}{N}} \boldsymbol{D}_\varepsilon(\varepsilon_k)\tilde{\boldsymbol{X}}_k^{(q)}\tilde{\boldsymbol{h}}_k^{(q)} + \tilde{\boldsymbol{v}}^{(q)} \quad (6.1)$$

$$= \tilde{\boldsymbol{X}}^{(q)}(\boldsymbol{\varepsilon})\tilde{\boldsymbol{h}}^{(q)} + \tilde{\boldsymbol{v}}^{(q)} \quad (6.2)$$

where

$$\tilde{\boldsymbol{X}}^{(q)}(\boldsymbol{\varepsilon}) = \left[e^{\jmath 2\pi\varepsilon_1 \frac{qN_s+G}{N}} \boldsymbol{D}_\varepsilon(\varepsilon_1)\tilde{\boldsymbol{X}}_1^{(q)}, \ldots, e^{\jmath 2\pi\varepsilon_K \frac{qN_s+G}{N}} \boldsymbol{D}_\varepsilon(\varepsilon_K)\tilde{\boldsymbol{X}}_K^{(q)}\right]$$

$$\tilde{\boldsymbol{h}}^{(q)} = \left[\tilde{\boldsymbol{h}}_1^{(q)T}, \ldots, \tilde{\boldsymbol{h}}_K^{(q)T}\right]^T$$

and $\tilde{\boldsymbol{X}}_k^{(q)}$ is an $N\times(L+1)$ circular convolution matrix the columns of which are formed from the transmitted signal as $\tilde{x}_k^{(q)}[\langle n-l\rangle_N]$, $n = 0, \ldots, N-1$.

The $(L+1)\times 1$ vector $\tilde{\boldsymbol{h}}_k^{(q)}$ denotes the time-domain channel impulse response associated with transmitter k in symbol q. The task is to estimate the carrier frequency offsets ε_k. Based on these estimates, also the channel coefficients $\tilde{\boldsymbol{h}}_k^{(q)}$ could be estimated, however the channel estimation part is out of scope of this thesis.

6.1.1 Cramér-Rao lower bound

The Cramér-Rao lower bound for the multiple CFO estimation problem, giving the lower bound on the variance of any unbiased estimator $\hat{\varepsilon_k}$, is derived in multiple references: The exact Cramér-Rao bound for the problem was first derived in [142] for a flat-fading channel assuming different CFOs towards different receive antennas. The exact CRB is shown to be a complex function of all K channels and K frequency offsets. Therefore, an asymptotic (i.e. large-sample) CRB is also derived with the assumption that the training signals are zero-mean stationary random processes, leading to a more practical expression. Similar derivations for a frequency-selective channel have been done in [143] [144] and [145]. An exact CRB for the uplink CFO estimation problem, formally the same as the problem here, is also derived in [146]. Here, an approximate expression for the Cramér-Rao lower bound based on [147] is provided as follows:

$$\mathrm{ACRB}(\hat{\varepsilon_k}) = \frac{3N^2}{\pi^2 N_r N(N-1)(2N-1)\cdot \mathrm{SNR}} \tag{6.3}$$

where SNR is now defined as $\mathrm{SNR} = \sigma_v^{-2}$. This expression has been used in the simulations of Publication VII. It is noted that with large N this expression tends to

$$\mathrm{CRB}(\hat{\varepsilon_k}) = \frac{3\sigma_v^2}{2\pi^2 N_r N} \tag{6.4}$$

which is the asymptotic CRB derived in [142] [145]. Both expressions assume that the channels are normalized such that $\left\|\tilde{\boldsymbol{h}}_k^{(q)}\right\|^2 = 1$ for all k. Note that equation (6.4) also coincides with the single CFO bound in equation (2.12) (note that $\varepsilon_k = \nu_k/N$). Basically with large N, estimation of the CFOs associated with different transmitters is decoupled, thus the Cramér-Rao bound for the estimation of multiple CFOs tends to the single CFO CRB.

6.1.2 Maximum-likelihood -based estimation

The maximum-likelihood (ML) estimate for the K frequency offsets is obtained by maximizing the ML cost function (dropping the symbol index

q):

$$\Lambda_{\mathrm{ML}}(\varepsilon) = \tilde{\boldsymbol{r}}^H \tilde{\boldsymbol{X}}(\varepsilon) \left(\tilde{\boldsymbol{X}}^H(\varepsilon) \tilde{\boldsymbol{X}}(\varepsilon) \right)^{-1} \tilde{\boldsymbol{X}}^H(\varepsilon) \tilde{\boldsymbol{r}}. \tag{6.5}$$

Clearly, optimizing the above cost function involves a multi-dimensional (K-dimensional) search over the parameter space, and is thus infeasible in terms of computational complexity. In [142] [143], it was shown that assuming orthogonal training signals, i.e. $\tilde{\boldsymbol{X}}^H(\varepsilon)\tilde{\boldsymbol{X}}(\varepsilon) \approx \boldsymbol{I}_{K(L+1)}$, the ML cost function can be simplified as follows:

$$\Lambda_{\mathrm{ML}}(\varepsilon) \approx \tilde{\boldsymbol{r}}^H \tilde{\boldsymbol{X}}(\varepsilon) \tilde{\boldsymbol{X}}^H(\varepsilon) \tilde{\boldsymbol{r}}. \tag{6.6}$$

Now this cost function can be optimized with K one-dimensional searches, hence it becomes more feasible in terms of computational complexity. Hence, the maximum-likelihood estimator for CFO k is expressed as follows:

$$\hat{\varepsilon}_{k,\mathrm{ML}} = \arg\max_{\varepsilon_k} \; \tilde{\boldsymbol{r}}^H \tilde{\boldsymbol{X}}_k(\varepsilon_k) \tilde{\boldsymbol{X}}_k^H(\varepsilon_k) \tilde{\boldsymbol{r}}. \tag{6.7}$$

However, the problem is that even if the training signals are orthogonal by design, finite-length sequences lose their orthogonality in presence of frequency offsets. In such case, the approximation made above leads to a severe error floor in the CFO estimation performance. In [142], only flat fading channels were considered and thus training signals using symbol-level TDM-based orthogonalization between different transmitters were proposed to overcome this problem. This approach results in the ML cost function of equation (6.6), however is not applicable to frequency-selective channels as the orthogonality would be lost due to multipath. Furthermore, as transmission power can not be shared between different transmitters, the TDM approach leads inevitably to underutilization of transmission resources/power. Due to this reason the training period also becomes longer. A TDM-based approach to solving the multiple CFO estimation problem was considered also in [148]. In [143], the approach of [142] was extended to frequency-selective channels, however the problem with losing the orthogonality of the training signals was not taken into account.

The problem with lost orthogonality of training signals was observed also in [135] [149], in which a different approach to lower the complexity of optimizing the full ML criterion (equation (6.5)) was proposed. Essentially, the multiple access interference (MAI) due to lost orthogonality of the training signals is taken into account by optimizing (6.5) directly by utilizing the Newton method to reduce the computational complexity. It is shown that this is feasible as the cost function remains convex as

long as the CFOs remain within a given interval. Similarly, in [150] the authors proposed lower complexity methods to optimizing the full ML cost function. In this case the optimization was done using the expectation maximization (EM) algorithm [151] and the space-alternating generalized EM (SAGE) algorithm [152]. Finally, in [146], the authors investigated an alternating projection -based [153] approach to optimizing the full ML cost function with a lower complexity. Essentially, the method also reduces the multi-dimensional optimization problem into K one-dimensional problems, though the algorithm still requires multiple cycles for each of the K estimates. This study was done in context of multi-user uplink CFO estimation, however since the scheme assumes nothing about the training signal subcarrier assignment, the problem is equivalent to the problem addressed here.

A different approach was taken in [154][155][156] as well as in Publication VII: Since the assumption $\tilde{\boldsymbol{X}}^H(\varepsilon)\tilde{\boldsymbol{X}}(\varepsilon) \approx \boldsymbol{I}_{K(L+1)}$ essentially means that the training signals retain their orthogonality in presence of frequency offsets, training signal designs to achieve this were studied. As one means of achieving this, in Publication VII as well as in [154][157] it was observed that if the training signal subcarriers of any two transmitters are distant enough, the training signals will remain almost orthogonal also in presence of CFOs. This is because most of the ICI always leaks on the nearest neighboring subcarriers, hence having a few guard subcarriers provides sufficient protection from MAI. Another method discussed in Publication VII and in [155][156] is based on the well-known Zadoff-Chu sequences [158]. It turns out that the Zadoff-Chu sequences retain their orthogonality in presence of time and frequency offsets if the root indices as well as the cyclic shifts are properly chosen. The selection of the Zadoff-Chu sequence parameters was further formalized in [155][156] where sequences that minimize the level of MAI were proposed to be used. In [156], and also in Publication VII, it was then further shown that with this approach good estimation performance very close to the Cramér-Rao bound can be achieved. Finally, in Publication VII, a training signal synthesis method based on minimizing the MAI for a certain range of time and frequency offsets was proposed.

Finally, in [147], it was mentioned that even the simplified ML of equation (6.7) is too complex as it requires K one-dimensional line searches to be performed. Hence, a polynomial rooting -based estimator was proposed. The cost function is first expressed using a polynomial series ap-

proximation, and then the maximum of the polynomial is found using typical polynomial rooting techniques. The algorithm works only with small frequency offsets as otherwise the polynomial approximation will not hold. A low-complexity closed-form expression for the frequency offsets is derived also in [157].

6.1.3 Subspace-based methods

Several subspace-based methods have been proposed in the literature. These methods rely on an interleaved FDMA -based subcarrier mapping, such that the resulting time-domain signal has a repetitive structure. However, the methods are semi-blind in the sense that even though the subcarrier mapping is known, the actual sequences do not need to be known by the receiver.

Subspace methods together with the interleaved subcarrier assignment have been studied first for uplink OFDMA -based systems [140] [141]. However, they are similarly applicable for multiple CFO estimation in cooperative downlink MIMO systems. Each transmitter k is assigned a subchannel starting at subcarrier p_k, see e.g. Figure 6.1. Each subchannel occupies every P:th subcarrier, and hence the time-domain signal will be repetitive with P repetitions within one OFDM symbol. Now, let $\tilde{\boldsymbol{r}} = \sum_{k=1}^{K} \tilde{\boldsymbol{r}}_k + \tilde{\boldsymbol{v}}$, and split $\tilde{\boldsymbol{r}}_k$ in P parts $\tilde{\boldsymbol{r}}_{k,p}$, $p = 0, \dots P-1$, each of which is of length $Q = N/P$ and can, due to the repetitive structure, be expressed as follows:

$$\tilde{\boldsymbol{r}}_{k,p} = e^{\jmath 2\pi\theta_k \frac{p}{P}} \tilde{\boldsymbol{r}}_{k,0} \tag{6.8}$$

where $\theta_k = \varepsilon_k + p_k$ is the effective CFO for transmitter k, accounting also for the subchannel assignment. The subspace methods basically target at estimating θ_k, from which each CFO ε_k can be derived with knowledge of the subchannel assignment.

The methods are based on the observation that the signal can then be arranged in a $P \times Q$ matrix as follows:

$$\tilde{\boldsymbol{Z}}_k = [\tilde{\boldsymbol{r}}_{k,0}, \dots, \tilde{\boldsymbol{r}}_{k,P-1}]^T = \tilde{\boldsymbol{a}}_k \cdot \tilde{\boldsymbol{r}}_{k,0}^T \tag{6.9}$$

$$\tilde{\boldsymbol{Z}} = \sum_{k=1}^{K} \tilde{\boldsymbol{Z}}_k + \tilde{\boldsymbol{V}} = \tilde{\boldsymbol{A}}\tilde{\boldsymbol{S}} + \tilde{\boldsymbol{V}} \tag{6.10}$$

where $\tilde{\boldsymbol{a}}_k = \left[e^{\jmath 2\pi\theta_k \frac{p}{P}}\right]^T$, $p = 0, \dots, P-1$, $\tilde{\boldsymbol{A}} = [\tilde{\boldsymbol{a}}_1 \cdots \tilde{\boldsymbol{a}}_K]$ and $\tilde{\boldsymbol{S}} = [\tilde{\boldsymbol{r}}_{1,0} \cdots \tilde{\boldsymbol{r}}_{K,0}]$. It is noted that matrix $\tilde{\boldsymbol{A}}$ is a $P \times K$ Vandermonde matrix.

In [140], a MUSIC-based CFO estimation algorithm was first proposed. Denoting the l:th column of $\tilde{\boldsymbol{Z}}$ by $\tilde{\boldsymbol{z}}_l = \tilde{\boldsymbol{A}}\tilde{\boldsymbol{s}}_l + \tilde{\boldsymbol{v}}_l$, we can write its covariance

as

$$\boldsymbol{\Psi} = E\{\tilde{\boldsymbol{z}}_l \tilde{\boldsymbol{z}}_l^H\} = \tilde{\boldsymbol{A}}\boldsymbol{\Phi}\tilde{\boldsymbol{A}}^H + \sigma_v^2 \boldsymbol{I} \tag{6.11}$$

where $\boldsymbol{\Phi} = E\{\tilde{\boldsymbol{s}}_l \tilde{\boldsymbol{s}}_l^H\}$. In [140], it is shown that the noise subspace $\boldsymbol{U}_{\tilde{\boldsymbol{z}}}$ of this matrix is orthogonal to $\tilde{\boldsymbol{A}}$, i.e. $\tilde{\boldsymbol{A}}^H \boldsymbol{U}_{\tilde{\boldsymbol{z}}} = \boldsymbol{0}$. Hence, the effective CFOs $\{\theta_k\}_{k=1}^K$ can be found as the K local maxima of the cost function

$$J_{\mathrm{MUSIC}}(\theta) = \frac{1}{\left\| \tilde{\boldsymbol{a}}^H(\theta) \boldsymbol{U}_{\tilde{\boldsymbol{z}}} \boldsymbol{U}_{\tilde{\boldsymbol{z}}}^H \tilde{\boldsymbol{a}}(\theta) \right\|^2}. \tag{6.12}$$

In [159], it was mentioned that with normal IFDMA-based signals, the effective CFOs may be very close to each other at least if the CFOs may be as large as half of the subcarrier spacing. In this case, the MUSIC algorithm may not be able to separate the CFOs reliably. As a solution, the guard subcarrier IFDMA -based signals as shown in figure 6.1 were proposed. This mechanism ensures that the effective CFOs are sufficiently far apart from each other, and can hence be separated by the MUSIC algorithm.

In addition to the MUSIC-based methods, based on a similar interleaved FDMA -based signal structure as in [140], in [141] an ESPRIT-based method for estimating the multiple CFOs was proposed. An ESPRIT-based method was studied also more recently for a cooperative relay downlink case in [160], where the main difference to the method in [141] was the used signal structure. Essentially, the signals are arranged in frequency domain multiplexed tiles instead of single subcarriers. This is to provide better protection from multiple access interference, and thus to decrease the error floor slightly. Hence the method is basically a modification of the method in [141] to a tile-based signal structure.

6.1.4 Correlation-based methods

Similarly to single CFO case, as discussed in section 2.4, several correlation -based methods for estimating the multiple CFOs have been proposed. These methods are again based either on cross-correlation between a training signal and the received signal or between different parts of the received signal itself.

The most straightforward method is based on training signals with a repetitive structure in time domain. For instance, a time domain sequence repeating twice within an OFDM symbol can be obtained by transmitting the training signal on every second subcarrier in frequency domain. Similarly to the single CFO case, the CFOs can be estimated from the phase difference between the two slots. However, as discussed in previous

sections, the problem is that even if the training signals for the multiple transmitters have by design good correlation properties, the carrier frequency offsets cause additional multiple access interference and thus degrade estimation performance. As with the maximum-likelihood -based methods, this can be solved by specifically designing the training signals to maintain good correlation properties in presence of CFOs. Such designs are further discussed in section 6.1.5.

Assume that the training signals are designed to maintain good correlation properties in presence of CFOs. Then, using the notation introduced earlier in this thesis, the estimator for CFO k can be expressed as follows:

$$\hat{\varepsilon}_{k,\mathrm{REP}} = \frac{1}{\pi} \arg \left\{ \tilde{\boldsymbol{z}}_{k,0}^H \tilde{\boldsymbol{z}}_{k,1} \right\} \tag{6.13}$$

where $\tilde{\boldsymbol{z}}_{k,i} = \tilde{\boldsymbol{x}}_{k,1/2}^H \tilde{\boldsymbol{r}}_i$ with

$$\begin{aligned} \tilde{\boldsymbol{x}}_{k,1/2} &= [\tilde{x}_k[0], \ldots, \tilde{x}_k[N/2-1]] \\ \tilde{\boldsymbol{r}}_i &= [\tilde{r}[iN/2], \ldots, \tilde{r}[iN/2+N/2-1]] \,. \end{aligned}$$

In Publication VII, the method of repetitive slots was studied for multiple CFO estimation. Different kinds of training signals minimizing the amount of multiple access interference were considered and good estimation performance nearly achieving the Cramér-Rao bound, especially in case of flat-fading channels, was demonstrated.

Interestingly, by assuming the repetitive training signals and approximating

$$\tilde{\boldsymbol{X}}_k(\varepsilon_k) \approx \left[\tilde{\boldsymbol{X}}_{k,1/2}^T \; e^{\jmath\pi\varepsilon_k} \tilde{\boldsymbol{X}}_{k,1/2}^T \right]^T ,$$

the maximum-likelihood estimator of (6.7) can be expressed as

$$\hat{\varepsilon}_{k,\mathrm{ML}} \approx \arg\max_{\varepsilon_k} \left\| \tilde{\boldsymbol{X}}_{k,1/2}^H \tilde{\boldsymbol{r}}_0 + e^{\jmath\pi\varepsilon_k} \tilde{\boldsymbol{X}}_{k,1/2}^H \tilde{\boldsymbol{r}}_1 \right\|^2 . \tag{6.14}$$

This has a closed-form solution

$$\hat{\varepsilon}_{k,\mathrm{ML}} \approx \frac{1}{\pi} \arg \left\{ \tilde{\boldsymbol{r}}_0^H \tilde{\boldsymbol{X}}_{k,1/2} \tilde{\boldsymbol{X}}_{k,1/2}^H \tilde{\boldsymbol{r}}_1 \right\} . \tag{6.15}$$

Comparing this with equation (6.13), we note that the two are equivalent in case of $L = 1$, and in case of frequency-selective channels $L > 1$, the ML estimator is able to exploit multipath diversity. In other words, the repetitive slots -based estimator is approximately ML for flat-fading channels. This also explains the good performance of the estimator observed in Publication VII.

The method of repetitive slots for estimation of multiple carrier frequency offsets was studied also in [161] where the authors used Walsh

codes to mitigate MAI. However, an error floor remains as the pilot signals do not maintain their orthogonality in presence of frequency offsets. In [160], a weighted repetitive slots method was used for estimating multiple timing offsets before applying a subspace-based CFO estimator. The weights were chosen to take advantage of multipath diversity. Finally, in [162] the authors refine the initial estimates obtained based on (6.13) by utilizing parallel interference cancellation (PIC) for iteratively removing the regenerated MAI. The simulations in the paper show good performance with only very few iterations.

6.1.5 Training signal design for estimation of multiple CFOs

In section 6.1.2, some methods were briefly reviewed for minimizing multiple access interference in presence of CFOs. It turns out that many training-based single CFO estimation methods become applicable if the training sequences are designed to retain their orthogonality in presence of frequency (and time) offsets. Such training sequences were studied in Publication VII. Essentially, the problem boils down to minimizing the correlation between two time-frequency shifted signals. For this purpose, as discussed in Publication VII, the ambiguity function widely utilized in radar signal processing becomes useful. The ambiguity function represents the correlation of the signal with its delayed and frequency-shifted version and can be expressed as follows:

$$\chi(\tau,\varepsilon) = \tilde{\boldsymbol{x}}^H \boldsymbol{D}_\varepsilon(\varepsilon)\tilde{\boldsymbol{x}}(\tau) \quad (6.16)$$

$$= \boldsymbol{x}^H \boldsymbol{F}\boldsymbol{D}_\varepsilon(\varepsilon)\boldsymbol{F}^H \boldsymbol{D}_\tau(\tau)\boldsymbol{x}. \quad (6.17)$$

The cross-ambiguity function between two delay and frequency-shifted signals k and l on the other hand could be expressed as follows:

$$\chi_{kl}(\tau_k,\varepsilon_k;\tau_l,\varepsilon_l) = \tilde{\boldsymbol{x}}_k^H(\tau_k)\boldsymbol{D}_\varepsilon(\varepsilon_l-\varepsilon_k)\tilde{\boldsymbol{x}}_l(\tau_l) \quad (6.18)$$

$$= \boldsymbol{x}_k^H \boldsymbol{D}_\tau^H(\tau_k)\boldsymbol{F}\boldsymbol{D}_\varepsilon(\varepsilon_l-\varepsilon_k)\boldsymbol{F}^H\boldsymbol{D}_\tau(\tau_l)\boldsymbol{x}_l. \quad (6.19)$$

Obviously, in order to minimize the impacts of MAI on the time and frequency offset estimation, one should aim at minimizing $|\chi_{kl}(\tau_k,\varepsilon_k;\tau_l,\varepsilon_l)|^2$ for the relevant value ranges of τ_k, ε_k, τ_l and ε_l.

The ICI power from subcarrier m to subcarrier n essentially decreases as a function of distance $|m-n|$, see e.g. equation (5.5). Therefore, the first method for minimizing the impacts of MAI is to leave a few guard subcarriers between the training signals of different transmitters. This is illustrated in Figure 6.1 for a simple case with two transmitters and

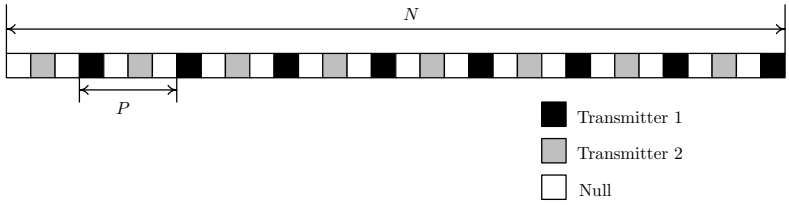

Figure 6.1. Example of training signal design where the distance between training signals of $K = 2$ transmitters is two subcarriers. In this example, $P = 4$, $N = 32$. The guard subcarriers reduce the impact of ICI, thus also the multiple access interference due to CFOs is reduced.

only one guard subcarrier between the corresponding training sequences. Note that in time-domain the signal becomes repetitive with four repetitions ($P = 4$) within one OFDM symbol since the training sequences (per transmitter) are mapped on every fourth subcarrier. In addition to Publication VII, this method has been studied in [154] and [157] in the context of uplink OFDMA.

As an alternative solution, one can rely on the use of the well-known Zadoff-Chu sequences as those possess exactly the desirable correlation properties as long as the sequence parameters are carefully chosen. As an example, the ambiguity function of a Zadoff-Chu sequence of length $N = 128$ with root index $u = 43$ is depicted in Figure 6.2. Let us assume that the transmitters are coarsely synchronized and that the maximum time offset is equal to nine samples (e.g. cyclic prefix length) and the maximum (normalized) frequency offset is 0.5. The ambiguity region for this case is as shown in the figure. Essentially, the training sequence for another transmitter is chosen as a time-frequency shifted version of the base Zadoff-Chu sequence, where the time-frequency shift is large enough to shift the sequence outside of the ambiguity region. Therefore, the sequences will retain their orthogonality in presence of time and frequency offsets as long as the offsets stay within the given interval. This approach basically takes advantage of the prior knowledge of the possible range of time and frequency offsets. The use of Zadoff-Chu sequences for the CFO estimation problem has been studied in Publication VII as well as in [155] [156].

Finally, in Publication VII, suitable training sequences were directly synthesized by optimizing a cost function minimizing the sidelobes in the ambiguity function for the relevant time-frequency offset value range.

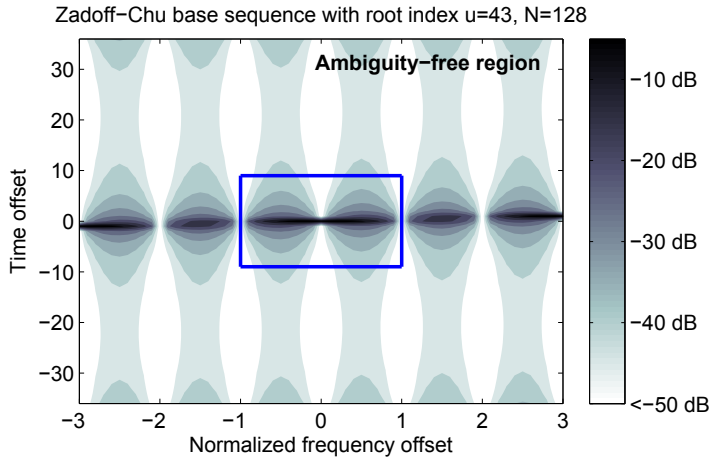

Figure 6.2. Ambiguity function of a Zadoff-Chu sequence of length $N = 128$ with root index $u = 43$. With a CP length of nine samples, the ambiguity region is plotted in blue.

The objective function to be minimized is given as follows:

$$\min_{\boldsymbol{x}} \quad \sum_{\tau \in \Omega_\tau} \sum_{\varepsilon \in \Omega_\varepsilon} \left| \boldsymbol{x}^H \boldsymbol{F} \boldsymbol{D}_\varepsilon(\varepsilon) \boldsymbol{F}^H \boldsymbol{D}_\tau(\tau) \boldsymbol{x} \right|^2 \tag{6.20}$$

$$\text{s.t.} \quad \boldsymbol{x}^H \boldsymbol{x} = 1. \tag{6.21}$$

where Ω_τ and Ω_ε represent the range of time and frequency offset values for which the cross-correlation (and hence multiple access interference) is minimized. In Publication VII, this was solved numerically, resulting in sequences with a low cross-correlation also in presence of time and frequency offsets. In Publication VII, also a similar synthesis of constant modulus training sequences was studied by varying only the phase of the sequence symbols. Again, multiple training signals are then obtained as cyclic shifts of the synthesized base sequence.

6.2 Mitigation of time and frequency offsets in cooperative systems

In case the receiver needs to deal only with a single CFO, it is straightforward to correct the frequency offset in time domain before actual reception by counter-rotating the signal according to the estimated frequency offset. However, in cooperative systems with multiple CFOs this is not possible. There are, however, a few possibilities on how to utilize the estimated CFOs.

6.2.1 CFO feedback loop

First possibility is to utilize a CFO feedback loop back to the transmitters. Essentially, the receiver(s) will estimate the multiple CFOs and feed the CFOs back to the transmitters, which may then correct the transmitter-induced CFOs. This approach has been analyzed in detail in [139], where a ML-based method was utilized at the transmitter side to calculate a representative CFO correction value based on the CFO feedback estimated at and received from the receivers. Also the CFO induced by the receiver itself is taken into account. Highly encouraging results are shown in the paper. However, more studies would be needed to conclude on whether the achieved frequency accuracy is sufficient for cooperative coherent MIMO systems, for instance taking into account the required quantization on the feedback link. As shown in the previous chapter, cooperative coherent MIMO systems require very precise frequency synchronization.

It is noted that the CFO feedback loop -based approach is applicable and a suitable solution to any cooperative transmission systems as long as the CFO feedback loop (i.e. possibility of transmitting the feedback in uplink) exists.

6.2.2 Frequency-domain equalization

Another method is frequency-domain equalization utilizing the multiple CFO estimates as well as channel estimates corresponding to each transmitter. Let us re-write equation (6.1) as

$$\tilde{\boldsymbol{r}}^{(q)} = \sum_{k=1}^{K} \boldsymbol{D}_{\varepsilon}(\varepsilon_k)\tilde{\boldsymbol{H}}_k^{(q)}\boldsymbol{F}^H\boldsymbol{x}_k^{(q)} + \tilde{\boldsymbol{v}}^{(q)} \tag{6.22}$$

where for simplicity the symbol-dependent phase offset has been included into the channel matrix. After FFT, this becomes

$$\boldsymbol{r}^{(q)} = \sum_{k=1}^{K} \boldsymbol{F}\boldsymbol{D}_{\varepsilon}(\varepsilon_k)\tilde{\boldsymbol{H}}_k^{(q)}\boldsymbol{F}^H\boldsymbol{x}_k^{(q)} + \boldsymbol{v}^{(q)}. \tag{6.23}$$

With delay diversity or (non-coherent) joint transmission techniques, $\tilde{\boldsymbol{x}}_k^{(q)} = \tilde{\boldsymbol{x}}^{(q)}$, $\forall k$, and we can write

$$\boldsymbol{r}^{(q)} = \boldsymbol{\Phi}^{(q)}\boldsymbol{x}^{(q)} + \boldsymbol{v}^{(q)} \tag{6.24}$$

where $\mathbf{\Phi}^{(q)} = \sum_{k=1}^{K} \boldsymbol{F}\boldsymbol{D}_{\varepsilon}(\varepsilon_k)\tilde{\boldsymbol{H}}_k^{(q)}\boldsymbol{F}^H$ is the overall ICI matrix. Zero-forcing and MMSE equalization are performed as follows:

$$\hat{\boldsymbol{x}}_{\mathrm{ZF}} = \left(\mathbf{\Phi}^{(q)H}\mathbf{\Phi}^{(q)}\right)^{-1}\mathbf{\Phi}^{(q)H}\boldsymbol{r}^{(q)} \quad (6.25)$$

$$\hat{\boldsymbol{x}}_{\mathrm{MMSE}} = \left(\mathbf{\Phi}^{(q)H}\mathbf{\Phi}^{(q)} + \sigma_v^2\boldsymbol{I}_N\right)^{-1}\mathbf{\Phi}^{(q)H}\boldsymbol{r}^{(q)}. \quad (6.26)$$

Obviously, both of the above are rather complex methods, requiring inversion of an $N \times N$ matrix.

Equalization-based approaches to ICI suppression and cancellation have been studied already for single-link OFDM systems, for equalization of time-variant channels. For instance, in [163], the MMSE as well as LS-based equalizers without any complexity reduction were used for equalization of a time-variant channel. In [164], it was noted that since most of the ICI leaks only a few neighboring subcarriers, the ICI matrix is banded so that most of the interference power is focused on a few subdiagonals next to the main diagonal. This was used to lower the complexity of the matrix inversion. Similarly, in [165], the authors took advantage of the banded structure of the ICI matrix to lower the complexity.

The above methods have been studied further in context of a cooperative delay diversity system in [144][166][167], with various methods for reducing the complexity: In [144], the MMSE equalizer was computed recursively, avoiding the inversion of the full $N \times N$ matrix. In [166], an MMSE-based decision feedback equalizer is proposed. It is noted that basically any of the methods developed for time-variant OFDM systems are applicable to this case. The main difference is that in this case the ICI matrix needs to be constructed based on multiple frequency offset and channel estimates.

Finally, equalization in space-time block coding -based cooperative systems has been studied in [168] [169] [170] [171]. In cooperative STBC-OFDM systems, CFOs introduce inter-symbol interference (ISI) within the STBC block in addition to the ICI within one OFDM symbol [172]. In [168], a low complexity equalizer taking advantage of the banded ICI and ISI matrices was proposed. Similarly in [171], the banded ICI matrix structure is used to develop a low complexity MMSE equalizer for time-reversal STBC-OFDM cooperative systems. In [169], an iterative ML detector for detecting the SFBC blocks in presence of multiple CFOs was proposed. All of these methods require knowledge of the CFOs. However, more detailed treatment of the methods is considered to be outside the scope of this thesis.

6.2.3 SINR-maximizing CFO compensation

In [173], it was proposed to correct CFO at the receiver side using a single CFO value derived from the multiple CFO estimates such that post-FFT SINR (averaged over subcarriers) is maximized. Essentially, the optimal CFO correcting value depends on the multiple CFO values as well as on the corresponding path gains. In [173], a closed-form solution for the optimal CFO is found based on an upper bound on the average ICI power when the difference between the smallest and the largest CFO is less than half of the subcarrier spacing. The optimum CFO correction value is expressed as

$$\varepsilon_{\text{opt}} = \frac{1}{2\pi}\arctan\frac{\sum_{k=1}^{K}\gamma_k \sin(2\pi\varepsilon_k)}{\sum_{k=1}^{K}\gamma_k \cos(2\pi\varepsilon_k)} \tag{6.27}$$

when $\max(\varepsilon_k) - \min(\varepsilon_k) \leq 0.5$. A similar study was done in [174].

Obviously such an approach, while maximizing the SINR, can not completely compensate for the errors and remove ICI. However, the method can be used as a pre-processing method for instance for the equalization schemes presented in section 6.2.2. Since ICI would be minimized, less subdiagonals may need to be taken into account of the ICI matrix, thus reducing the complexity of the frequency-domain equalization schemes.

6.3 Discussion

In this chapter, methods for estimating multiple CFOs in cooperative MIMO systems have been considered. A variety of methods ranging from maximum-likelihood -based and subspace-based methods to correlation-based methods were studied. Especially the ML-based methods suffer from computational complexity problems as a multi-dimensional search is in general required. As discussed in Publication VII, the simplest methods can be made applicable by choosing the training signals carefully such that their orthogonality is maintained in presence of small time and frequency offsets. Publication VII proposed several methods for finding such training signals, assuming that the time and frequency offsets are bounded to certain limited interval. This way, low complexity methods for multiple CFO estimation are applicable as the estimation of the different CFOs can be basically decoupled from each other. In fact, many single CFO estimation methods may be used in this case, thus the problem is significantly simplified. Publication VII also demonstrated estima-

tion MSE very close to the CRB for these methods. On the other hand, this approach requires that the signals received from the different transmitters are received within the cyclic prefix. In other words, coarse time synchronization is required between the transmitters, and propagation delay differences need to be small enough such that the signals remain within the cyclic prefix duration also at the receiver side.

How the multiple CFOs can be utilized depends largely on the application. Basically in any application, it is in principle possible to provide CFO feedback from the receiver to the transmitting nodes in order to correct the CFOs in a distributed manner. Whether the accuracy of such distributed synchronization would be sufficient for cooperative MIMO-OFDM systems with precise frequency synchronization accuracy requirements (as discussed in the previous chapter), remains for further study. In non-coherent joint transmission systems, e.g. in cooperative delay diversity systems or cooperative STBC diversity systems, it is possible to do frequency-domain equalization also at the receiver side, at the cost of increased receiver complexity. This complexity can be slightly reduced by pre-rotating the signal in time-domain based on a carrier frequency offset estimate obtained by a SINR maximization -based approach.

7. Summary

Wireless technologies continue to evolve towards higher data rates, smaller latencies and support of larger number of different devices that will be needed in the near future. Technologies enabling this, such as multiple-input multiple-output (MIMO) antenna technologies and cooperative systems, are bringing new challenges also in the relatively well-developed field of time and frequency synchronization. At the same time, there are also unexplored areas related to synchronization within more mature technologies such as direct sequence spread spectrum. This thesis has addressed specific challenges in the field of time and frequency synchronization that have not been sufficiently studied earlier.

The first part of the thesis addressed blind synchronization and spreading code estimation in direct spread CDMA systems, summarized in Chapter 3. It was shown that in short-code DS-CDMA systems, achieving synchronization without knowledge of the spreading code, as well as estimating the spreading code, are feasible due to the cyclostationarity of the signal induced by the repetitive spreading code sequence. In Publications I and II an algorithm for blindly synchronizing and estimating the spreading code in case of asynchronous multi-user DS-CDMA systems was proposed, showing good estimation performance at signal to noise ratios below 0 dB. Nearly optimal processing gain corresponding to that of the conventional matched filter can be obtained. Also methods for long-code DS-CDMA systems were reviewed.

The methods for blind synchronization and spreading code estimation have significance in the military domain in interception and localization of LPI signals. In addition, in civilian domain, applications are found in spectrum surveillance and localization and characterization of interference sources. In (future) commercial systems, applications could be envisioned in interference cancellation for identification of the signal param-

eters of the interfering transmission (see e.g. [22]), as well as in cognitive radio systems.

As the research area is still rather unexplored despite the relative matureness of the DS-CDMA technology as such, there are several topics that could be further explored related to blind synchronization and spreading code estimation. Future work in this area could, for instance, involve utilization of multiple antennas at the receiver for blind despreading and synchronization. Multiple observations of the same spreading code, even though through independently fading channels, could significantly alleviate the estimation task and improve the estimation performance. In addition to utilization of multiple antennas, application of spreading code estimation in interference-cancelling receivers would be an interesting research area, as in practice it is likely that a receiver facing interference is unaware of the exact spreading codes being applied in the interfering signal.

Next, the thesis addressed multi-antenna methods for initial synchronization in training-based systems in Chapter 4 and Publications III and IV. In particular, transmit diversity schemes for synchronization sequence transmission were studied, both analytically and via simulations. Acquisition performance of the diversity schemes was quantified analytically, and a relation between the probability of detection and the eigenvalues of the covariance matrix of the synchronization correlator outputs was established. These eigenvalues were shown to depend on signal to noise ratio, spatial correlation as well as Doppler spread. Thus, the theoretical relation between these quantities and the detection performance was established. Also optimum schemes were studied based on a cost function optimizing the probability of correct synchronization acquisition. The results provide guidance to system designers for designing the synchronization subsystem, and in particular for deciding on the methods for taking advantage of multiple transmit antennas. Hence, this work is of importance to the design of any wireless system employing multiple transmit antennas. The synchronization subsystem will need to utilize the same transmit antennas and therefore it is crucial to understand the performance impacts of different diversity schemes in various scenarios.

As networks become more and more dense and cell sizes shrink, intercell interference becomes the main performance-limiting factor. Thus, one potential future research direction could be to study synchronization acquisition performance and transmission and reception schemes in pres-

ence of heavy inter-cell interference when multiple antennas are being used at both receiver and transmitter side. So far the main contribution in this field is in [33] that assumed the use of orthogonal transmit diversity at the transmitter side.

Chapters 5 and 6 of the thesis, as well as Publications V, VI and VII, addressed the impacts and mitigation of multiple time and frequency offsets, targeting mainly cooperative transmission systems. It was shown, for example, that cooperative systems requiring phase coherence among the transmissions from multiple transmitters require several orders of magnitude more precise frequency synchronization than what is required in normal single-link OFDM systems. Thus, cooperative MIMO systems set more strict requirements to the transmitter side LO frequency accuracy as the phase variations among the transmitters destroy the desired phase coherence. Also the impacts of time and frequency offsets on channel estimation performance were studied. It was shown that even small time and frequency offsets degrade the channel estimation and consequent link throughput performance significantly. This was demonstrated in context of LTE coordinated multi-point transmission where the transmitting cell may change very rapidly and the UE receiver needs to be able to correct the time and frequency offsets prior to channel estimation in order to maintain the desired link-level performance. These results should be contrasted with the well-established result that in single-link MIMO-OFDM systems the carrier frequency offset should be within a few percent of the subcarrier spacing, and the time offset should remain within the boundaries set by the cyclic prefix length.

In order to solve these problems, Publication VII addressed estimation of multiple carrier frequency offsets. It was proposed to design the training signals used for CFO estimation such that they maintain their orthogonality in presence of small time and frequency offsets. It was shown that with such a design the estimation of multiple CFOs can be decoupled and many well-known single CFO estimation methods become applicable. Thus good estimation performance close to the Cramér-Rao lower bound can be achieved even with low complexity algorithms.

With the further development of 3G and 4G systems as well as with the advent of 5G systems, the significance of cooperative transmission schemes in practical systems can be expected to further increase. Therefore, the findings of this thesis related to time and frequency offset estimation in cooperative systems are relevant for existing and future systems

and will need to be taken into account in the system design phase. Future work in this field could involve, for instance, further studies on utilizing the existing single CFO estimation methods for estimating multiple CFOs when training signals such as those proposed in Publication VII are used. Furthermore, distributed network synchronization based on realistic time and frequency offset estimates and their (quantized) feedback to the transmitters would require further study. Whether synchronization accuracy sufficient even for phase-coherent cooperative systems can be achieved with this approach remains still an open question.

This thesis has addressed time and frequency synchronization primarily in DSSS and OFDM -based systems. These multiple access schemes are employed in current 3G and 4G wireless systems. However, the development of fifth generation (5G) wireless systems has also started, and as of writing this thesis, the choice of multiple access scheme is still an open question. Candidates include for instance generalized frequency division multiplexing (GFDM) -based [175] as well as filter bank multi-carrier -based schemes [176]. Thus one additional potential future research direction would be time and frequency synchronization in such systems.

References

[1] A. Osseiran, F. Boccardi, V. Braun, K. Kusume, P. Marsch, M. Maternia, O. Queseth, M. Schellmann, H. Schotten, H. Taoka, H. Tullberg, M. Uusitalo, B. Timus, and M. Fallgren, "Scenarios for 5G mobile and wireless communications: the vision of the METIS project," *IEEE Communications Magazine*, vol. 52, no. 5, pp. 26–35, May 2014.

[2] Cisco, "Cisco visual networking index: Global mobile data traffic forecast update, 2013-2018," Feb. 2014.

[3] E. Dahlman, P. Beming, J. Knutsson, F. Ovesjo, M. Persson, and C. Roobol, "WCDMA - the radio interface for future mobile multimedia communications," *IEEE Transactions on Vehicular Technology*, vol. 47, no. 4, pp. 1105–1118, Nov. 1998.

[4] 3GPP, "Physical layer procedures (FDD)," 3GPP, Technical Specification 25.214, Mar. 2014, available at http://www.3gpp.org/DynaReport/25214.htm.

[5] H. Holma and A. Toskala, *WCDMA for UMTS: HSPA evolution and LTE, 5th edition*. Wiley, 2010.

[6] S. Willenegger, "cdma2000 physical layer: an overview," *Journal of Communications and Networks*, vol. 2, no. 1, pp. 5–17, Mar. 2000.

[7] 3GPP, "Evolved universal terrestrial radio access (E-UTRA) and evolved universal terrestrial radio access network (E-UTRAN); Overall description; Stage 2," 3GPP, Technical Specification 36.300, Mar. 2014, available at http://www.3gpp.org/DynaReport/36300.htm.

[8] H. Holma and A. Toskala, *LTE for UMTS: evolution to LTE-Advanced, 2nd edition*. Wiley, 2011.

[9] IEEE, "Part 11: Wireless LAN medium access control (MAC) and physical layer (PHY) specifications, High-speed physical layer in the 5 GHz band," IEEE, IEEE Std 802.11a-1999(R2003), 2003.

[10] ——, "IEEE standard for air interface for broadband wireless access systems," IEEE, IEEE Std 802.16-2012, 2012.

[11] K. Etemad and M.-Y. Lai, *WiMAX technology and network evolution*. Wiley-IEEE Press, 2011.

[12] ETSI, "Digital video broadcasting (DVB); frame structure channel coding and modulation for a second generation digital terrestrial television broadcasting system (DVB-T2)," ETSI, ETSI EN 302 755, 2012.

[13] E. Kaplan and C. Hegarty, *Understanding GPS: Principles and Applications*, 2nd ed. Artech House, 2005.

[14] G. J. Foschini and M. J. Gans, "On limits of wireless communications in a fading environment when using multiple antennas," *Wireless Personal Communications*, vol. 6, pp. 311–335, 1998.

[15] I. Telatar, "Capacity of multi-antenna Gaussian channels," *European Transactions on Communications*, vol. 10, pp. 585–595, Nov./Dec. 1999.

[16] D. Gesbert, S. Hanly, H. Huang, S. S. Shitz, O. Simeone, and W. Yu, "Multi-cell MIMO cooperative networks: a new look at interference," *IEEE Journal on Selected Areas in Communications*, vol. 28, no. 9, pp. 1380–1408, Dec. 2010.

[17] D. Lee, H. Seo, B. Clerckx, E. Hardouin, D. Mazzarese, S. Nagata, and K. Sayana, "Coordinated multipoint transmission and reception in LTE-Advanced: deployment scenarios and operational challenges," *IEEE Communications Magazine*, vol. 50, no. 2, pp. 148–155, Feb. 2012.

[18] G. Sun, J. Chen, W. Guo, and K. Liu, "Signal processing techniques in network-aided positioning: a survey of state-of-the-art positioning designs," *IEEE Signal Processing Magazine*, vol. 22, no. 4, pp. 12–23, Jul. 2005.

[19] O. Simeone, U. Spagnolini, Y. Bar-Ness, and S. H. Strogatz, "Distributed synchronization in wireless networks," *IEEE Signal Processing Magazine*, vol. 25, no. 5, pp. 81–97, Sep. 2008.

[20] B. Zarikoff, "Frequency synchronization techniques for coordinated multi-base MIMO wireless communication systems," Ph.D. dissertation, Simon Fraser University, 2008.

[21] Y.-P. Wang and T. Ottosson, "Cell search in W-CDMA," *IEEE Journal on Selected Areas in Communications*, vol. 18, no. 8, pp. 1470–1482, Aug. 2000.

[22] Huawei, HiSilicon, "Study on network-assisted interference cancellation and suppression for UMTS," 3GPP, RP-142250, 2014.

[23] T. Roman, "Advanced receiver structures for mobile MIMO multicarrier communication systems," Ph.D. dissertation, Helsinki University of Technology, 2006, available at http://lib.tkk.fi/Diss/2006/isbn951228104X/.

[24] 3GPP, "Evolved universal terrestrial radio access (E-UTRA); Physical channels and modulation," 3GPP, Technical Specification 36.211, Mar. 2014, available at http://www.3gpp.org/DynaReport/36211.htm.

[25] R. J. Kozick and B. M. Sadler, "Bounds and algorithms for time delay estimation on parallel, flat fading channels," in *IEEE International Conference on Acoustics, Speech and Signal Processing*, Apr. 2008, pp. 2413–2416.

[26] B. M. Sadler and R. J. Kozick, "A survey on time delay estimation performance bounds," in *Fourth IEEE workshop on sensor array and multichannel processing*, Jul. 2006, pp. 282–288.

[27] J. Ziv and M. Zakai, "Some lower bounds on signal parameter estimation," *IEEE Transactions on Information Theory*, vol. 15, no. 3, pp. 386–391, May 1969.

[28] D. Chazan, M. Zakai, and J. Ziv, "Improved lower bounds on signal parameter estimation," *IEEE Transactions on Information Theory*, vol. 21, no. 1, pp. 90–93, Jan. 1975.

[29] A. N. D'Andrea, U. Mengali, and R. Reggiannini, "The modified Cram'er-Rao bound and its application to synchronization problems," *IEEE Transactions on Communications*, vol. 42, no. 2/3/4, pp. 1391–1399, Feb./Mar./Apr. 1994.

[30] A. J. Viterbi, *CDMA - Principles of spread spectrum communication*. Addison-Wesley, 1995.

[31] S. Glisic and B. Vucetic, *Spread spectrum CDMA systems for wireless communications*. Artech House, Inc., 1997.

[32] S.-H. Won and L. Hanzo, "Initial synchronization of wideband and UWB direct sequence systems: single- and multiple-antenna aided solutions," *IEEE Communications Surveys and Tutorials*, vol. 14, no. 1, pp. 87–108, Feb. 2012.

[33] D. W. Bliss and P. A. Parker, "Temporal synchronization of MIMO wireless communication in the presence of interference," *IEEE Transactions on Signal Processing*, vol. 58, no. 3, pp. 1794–1806, Mar. 2010.

[34] L. L. Scharf, *Statistical signal processing - detection, estimation, and time series analysis*. Addison-Wesley, 1990.

[35] J. Moon and Y.-H. Lee, "Rapid slot synchronization in the presence of large frequency offset and Doppler spread in WCDMA systems," *IEEE Transactions on Wireless Communications*, vol. 4, no. 4, pp. 1325–1330, Jul. 2005.

[36] G. E. Corazza, C. Caini, A. Vanelli-Coralli, and A. Polydoros, "DS-CDMA code acquisition in presence of correlated fading - part I: Theoretical aspects," *IEEE Transactions on Communications*, vol. 52, no. 7, pp. 1160–1168, Jul. 2004.

[37] M. Ghogho and A. Swami, "Carrier frequency synchronization for OFDM systems," in *Signal processing for mobile communications handbook*, M. Ibnkahla, Ed. CRC Press, 2005, ch. 8.

[38] M. Morelli, C.-C. J. Kuo, and M.-O. Pun, "Synchronization techniques for orthogonal frequency division multiple access (OFDMA): A tutorial review," *Proceedings of the IEEE*, vol. 95, no. 7, pp. 1394–1427, Jul. 2007.

[39] J.-J. van de Beek, M. Sandell, and P. O. Börjesson, "ML estimation of time and frequency offset in OFDM systems," *IEEE Transactions on Signal Processing*, vol. 45, no. 7, pp. 1800–1805, Jul. 1997.

[40] F. Tufvesson, O. Edfors, and M. Faulkner, "Time and frequency synchronization for OFDM using PN-sequence preambles," in *IEEE 50th Vehicular Technology Conference (VTC)*, vol. 4, Sep. 1999, pp. 2203–2207.

[41] H. Puska and H. Saarnisaari, "Matched filter time and frequency synchronization method for OFDM systems using PN-sequence preambles," in *IEEE 18th International Symposium on Personal, Indoor and Mobile Radio Communications (PIMRC)*, Sep. 2007.

[42] T. M. Schmidl and D. C. Cox, "Robust frequency and timing synchronization for OFDM," *IEEE Transactions on Communications*, vol. 45, no. 12, pp. 1613–1621, Dec. 1997.

[43] P. H. Moose, "A technique for orthogonal frequency division multiplexing frequency offset correction," *IEEE Transactions on Communications*, vol. 42, no. 10, pp. 2908–2914, Oct. 1994.

[44] E. Perahia and R. Stacey, *Next generation wireless LANs: 802.11n and 802.11ac*, 2nd ed. Cambridge University Press, 2013.

[45] M. Morelli and U. Mengali, "An improved frequency offset estimator for OFDM applications," *IEEE Communications Letters*, vol. 3, no. 3, pp. 75–77, Mar. 1999.

[46] M. Ghogho and A. Swami, "Unified framework for a class of frequency-offset estimation techniques for OFDM," in *IEEE International Conference on Acoustics, Speech and Signal Processing*, vol. 4, May 2004.

[47] H. Liu and U. Tureli, "A high-efficiency carrier estimator for OFDM communications," *IEEE Communications Letters*, vol. 2, no. 4, pp. 104–106, Apr. 1998.

[48] B. Chen, "Maximum likelihood estimation of OFDM carrier frequency offset," *IEEE Signal Processing Letters*, vol. 9, no. 4, pp. 123–126, Apr. 2002.

[49] M. Ghogho, A. Swami, and G. B. Giannakis, "Optimized null-subcarrier selection for CFO estimation in OFDM over frequency-selective fading channels," in *IEEE Global Telecommunications Conference (GLOBECOM)*, vol. 1, Nov. 2001, pp. 202–206.

[50] Y.-J. Ryu and D.-S. Han, "Timing phase estimator overcoming Rayleigh fading for OFDM systems," *IEEE Transactions on Consumer Electronics*, vol. 47, no. 3, pp. 370–377, Aug. 2001.

[51] A. J. Coulson, "Maximum likelihood synchronization for OFDM using a pilot symbol: algorithms," *IEEE Journal on Selected Areas in Communications*, vol. 19, no. 12, pp. 2486–2494, Dec. 2001.

[52] M. Luise and R. Reggiannini, "Carrier frequency recovery in all-digital modems for burst-mode transmissions," *IEEE Transactions on Communications*, vol. 43, no. 2/3/4, pp. 1169–1178, Feb./Mar./Apr. 1995.

[53] ——, "Carrier frequency acquisition and tracking for OFDM systems," *IEEE Transactions on Communications*, vol. 44, no. 11, pp. 1590–1598, Nov. 1996.

[54] M. J. F.-G. Garcia, O. Edfors, and J. M. Paez-Borrallo, "Joint 2D-pilot-symbol-assisted-modulation and decision-directed frequency synchronization schemes for coherent OFDM," in *IEEE International Conference on Acoustics, Speech and Signal Processing*, vol. 5, Jun. 2000, pp. 2961–2964.

[55] ——, "Frequency offset correction for coherent ofdm in wireless systems," *IEEE Transactions on Consumer Electronics*, vol. 47, no. 1, pp. 187–193, Feb. 2001.

[56] M. J. F.-G. Garcia, "Tracking of time misalignments for OFDM systems in multipath fading channels," *IEEE Transactions on Consumer Electronics*, vol. 48, no. 4, pp. 982–989, Nov. 2002.

[57] P.-Y. Tsai, H.-Y. Kang, and T.-D. Chiueh, "Joint weighted least-squares estimation of carrier-frequency offset and timing offset for OFDM systems over multipath fading channels," *IEEE Transactions on Vehicular Technology*, vol. 54, no. 1, pp. 211–223, Jan. 2005.

[58] A. V. Dandawate and G. B. Giannakis, "Statistical tests for presence of cyclostationarity," *IEEE Transactions on Signal Processing*, vol. 42, no. 9, pp. 2355–2369, Sep. 1994.

[59] C. A. French and W. A. Gardner, "Spread-spectrum despreading without the code," *IEEE Transactions on Communications*, vol. 34, no. 4, pp. 404–407, Apr. 1986.

[60] M. K. Tsatsanis and G. B. Giannakis, "Blind estimation of direct sequence spread spectrum signals in multipath," *IEEE Transactions on Signal Processing*, vol. 45, no. 5, pp. 1241–1252, May 1997.

[61] C. N. Nzeza, R. Gautier, and G. Burel, "Blind multiuser detection in multirate CDMA transmissions using fluctuations of correlation estimators," in *IEEE Global Telecommunications Conference (GLOBECOM)*, Nov. 2006.

[62] C. Bouder and G. Burel, "A robust synchronization procedure for blind estimation of the symbol period and the timing offset in spread spectrum transmissions," in *IEEE 7th International Symposium on Spread Spectrum Techniques and Applications*, vol. 1, Sep. 2002, pp. 238–241.

[63] G. Burel, "Detection of spread spectrum transmissions using fluctuations of correlation estimators," in *IEEE International Symposium on Intelligent Signal Processing and Communication Systems (ISPACS)*, Nov. 2000.

[64] S. E. Bensley and B. Aazhang, "Subspace-based channel estimation for code division multiple access communication systems," *IEEE Transactions on Communications*, vol. 44, no. 8, pp. 1009–1020, Aug. 1996.

[65] L. Tong and S. Perreau, "Multichannel blind identification: from subspace to maximum likelihood methods," *Proceedings of the IEEE*, vol. 86, no. 10, pp. 1951–1968, Oct. 1998.

[66] R. Johnson, P. Schnitzer, T. J. Endres, J. D. Behm, D. R. Brown, and R. A. Casas, "Blind equalization using the constant modulus criterion: a review," *Proceedings of the IEEE*, vol. 86, no. 10, pp. 1927–1950, Oct. 1998.

[67] J. Treichler, M. Larimore, and J. C. Harp, "Practical blind demodulators for high-order QAM signals," *Proceedings of the IEEE*, vol. 86, no. 10, pp. 1907–1926, Oct. 1998.

[68] Y. Sato, "A method of self-recovering equalization for multilevel amplitude-modulation systems," *IEEE Transactions on Communications*, vol. 23, no. 6, pp. 679–682, Jan. 1975.

[69] D. Godard, "Self-recovering equalization and carrier tracking in two-dimensional data communication systems," *IEEE Transactions on Communications*, vol. 28, no. 11, pp. 1867–1875, Nov. 1980.

[70] T.-H. Li and K. Mbarek, "A blind equalizer for nonstationary discrete-valued signals," *IEEE Transactions on Signal Processing*, vol. 45, no. 1, pp. 247–254, Jan. 1997.

[71] S. Barbarossa and A. Scaglione, "Blind equalization using cost function matched to the signal constellation," in *Conference Record of the Thirty-First Asilomar Conference on Signals, Systems and Computers*, Nov. 1997, pp. 550–554.

[72] G. Burel and C. Bouder, "Blind estimation of the pseudo-random sequence of a direct sequence spread spectrum signal," in *IEEE Military Communications Conference (MILCOM)*, vol. 2, Oct. 2000, pp. 967–970.

[73] Y. Jo and D. Wu, "Blind synchronization, estimation of data symbol, spread sequence, and generator polynomial in direct sequence spread spectrum systems," in *IEEE Military Communications Conference (MILCOM)*, Nov. 2008.

[74] B. G. Agee, R. J. Kleinman, and J. H. Reed, "Soft synchronization of direct sequence spread-spectrum signals," *IEEE Transactions on Communications*, vol. 44, no. 11, pp. 1527–1536, Nov. 1996.

[75] C. N. Nzeza, R. Gautier, and G. Burel, "Blind synchronization and sequences identification in CDMA transmissions," in *IEEE Military Communications Conference (MILCOM)*, vol. 3, Nov. 2004.

[76] ——, "Parallel blind multiuser synchronization and sequences estimation in multirate CDMA transmissions," in *Conference Record of the Fortieth Asilomar Conference on Signals, Systems and Computers*, Nov. 2006, pp. 2157–2161.

[77] ——, "Blind multiuser identification in multirate CDMA transmissions: a new approach," in *Conference Record of the Fortieth Asilomar Conference on Signals, Systems and Computers*, Nov. 2006, pp. 2162–2166.

[78] M. Wax and T. Kailath, "Detection of signals by information theoretic criteria," *IEEE Transactions on Acoustics, Speech, and Signal Processing*, vol. 33, no. 2, pp. 387–392, Apr. 1985.

[79] Y. Yao and H. V. Poor, "Eavesdropping in the synchronous CDMA channel: an EM-based approach," *IEEE Transactions on Signal Processing*, vol. 49, no. 8, pp. 1748–1756, Aug. 2001.

[80] H. Zhang, P. Wei, and Q. Mou, "A semidefinite relaxation approach to blind despreading of long-code DS-SS signal with carrier frequency offset," *IEEE Signal Processing Letters*, vol. 20, no. 7, pp. 705–708, Jul. 2013.

[81] P.-Y. Qui, Z.-T. Huang, W.-L. Jiang, and C. Zhang, "Improved blind-spreading sequence estimation algorithm for direct sequence spread spectrum signals," *IET Signal Processing*, vol. 2, no. 2, pp. 139–146, Jun. 2008.

[82] C. N. Nzeza, B. Himschoot, and R. Gautier, "Blind long spreading codes DS-CDMA signal identification in frequency selective channel," in *9th International Conference on Communications (COMM)*, Jun. 2012, pp. 357–360.

[83] Y. Zhang and S. Miller, "Code acquisition in transmit diversity DS-CDMA systems," *IEEE Transactions on Communications*, vol. 51, no. 8, pp. 1378–1388, Aug. 2003.

[84] R. R. Rick and L. B. Milstein, "Parallel acquisition of spread-spectrum signals with antenna diversity," *IEEE Transactions on Communications*, vol. 45, no. 8, pp. 903–905, Aug. 1997.

[85] P. K. Shamain and L. B. Milstein, "Acquisition of direct sequence spread spectrum signals with correlated fading," *IEEE Journal on Selected Areas in Communications*, vol. 19, no. 12, pp. 2406–2419, Dec. 2001.

[86] H. W. Je, O.-S. Shin, and K. B. Lee, "Acquisition for DS/CDMA systems with multiple antennas in frequency-selective fading channels," *IEEE Transactions on Wireless Communications*, vol. 2, no. 4, pp. 787–798, Jul. 2003.

[87] O.-S. Shin and K. B. Lee, "Use of multiple antennas for DS/CDMA code acquisition," *IEEE Transactions on Wireless Communications*, vol. 2, no. 3, pp. 424–430, May 2003.

[88] H.-R. Park and B.-J. Kang, "On the performance of a maximum-likelihood code-acquisition technique for preamble search in a CDMA reverse link," *IEEE Transactions on Vehicular Technology*, vol. 47, no. 1, pp. 65–74, Feb. 1998.

[89] S. Kim, "Acquisition performance of CDMA systems with multiple antennas," *IEEE Transactions on Vehicular Technology*, vol. 53, no. 5, pp. 1341–1353, Sep. 2004.

[90] ——, "Effect of spatial fading correlation on CDMA code-acquisition performance," *IEE Proceedings on Communications*, vol. 152, no. 1, pp. 103–112, Feb. 2005.

[91] W. H. Ryu, M. K. Park, and S. K. Oh, "Code acquisition schemes using antenna arrays for DS-SS systems and their performance in spatially correlated fading channels," *IEEE Transactions on Communications*, vol. 50, no. 8, pp. 1337–1347, Aug. 2002.

[92] M. Schellmann, V. Jungnickel, and C. von Helmolt, "On the value of spatial diversity for the synchronisation in MIMO-OFDM systems," in *The 16th IEEE International Symposium on Personal, Indoor and Mobile Radio Communications*, vol. 1, Sep. 2005, pp. 201–205.

[93] B. Wang and H. M. Kwon, "PN code acquisition using smart antenna for spread-spectrum wireless communications - part I," *IEEE Transactions on Vehicular Technology*, vol. 53, no. 1, pp. 142–149, Jan. 2003.

[94] ——, "PN code acquisition for DS-CDMA systems employing smart antennas - part II," *IEEE Transactions on Wireless Communications*, vol. 2, no. 1, pp. 108–117, Jan. 2003.

[95] M. D. Katz, J. H. J. Iinatti, and S. Glisic, "Two-dimensional code acquisition in time and angular domains," *IEEE Journal on Selected Areas in Communications*, vol. 19, no. 12, pp. 2441–2451, Dec. 2001.

[96] G. W. Stewart and J. Sun, *Matrix perturbation theory*. Academic Press, 1990.

[97] R. Mhiri, D. Masse, and D. Schafhuber, "Synchronization for a DVB-T receiver in presence of cochannel interference," in *The 13th IEEE International Symposium on Personal, Indoor and Mobile Radio Communications*, vol. 5, Sep. 2002, pp. 2307–2311.

[98] S. Won and L. Hanzo, "Non-coherent code acquisition in the multiple transmit/multiple receive antenna aided single- and multi-carrier DS-CDMA downlink," *IEEE Transactions on Wireless Communications*, vol. 6, no. 11, pp. 3864–3869, Nov. 2007.

[99] S.-H. Won and L. Hanzo, "Non-coherent and differentially coherent code acquisition in MIMO assisted DS-CDMA multi-path downlink scenarios," *IEEE Transactions on Wireless Communications*, vol. 7, no. 5, pp. 1585–1593, May 2008.

[100] ——, "Analysis of serial-search-based code acquisition in the multiple-transmit/multiple-receive-antenna-aided DS-CDMA downlink," *IEEE Transactions on Vehicular Technology*, vol. 57, no. 2, pp. 1032–1039, Mar. 2008.

[101] ——, "Initial and post-initial code acquisition in the noncoherent multiple-input/multiple-output-aided DS-CDMA downlink," *IEEE Transactions on Vehicular Technology*, vol. 58, no. 5, pp. 2322–2330, Jun. 2009.

[102] ——, "Synchronization of noncoherent MIMO systems: synchronization issues," *IEEE Vehicular Technology Magazine*, vol. 7, no. 4, pp. 95–103, Dec. 2012.

[103] D. Rajan and S. D. Gray, "Transmit diversity schemes for CDMA-2000," in *IEEE Wireless Communications and Networking Conference (WCNC)*, vol. 2, Sep. 1999, pp. 669–673.

[104] A. Paulraj, R. Nabar, and D. Gore, *Introduction to space-time wireless communications*. Cambridge University Press, 2003.

[105] S. Nagata, Y. Kishiyama, M. Tanno, K. Higuchi, and M. Sawahashi, "Investigation on transmit diversity for synchronization channel in OFDM based evolved UTRA downlink," in *IEEE 68th Vehicular Technology Conference (VTC)*, Sep. 2008.

[106] S. Brueck and I. Jami, "Impact of transmit diversity on cell search in UMTS," in *5th European Personal Mobile Communications Conference*, vol. 1, Apr. 2003, pp. 266–270.

[107] 3GPP, "Physical channels and mapping of transport channels onto physical channels (FDD)," 3GPP, Technical Specification 25.211, Jul. 2014, available at http://www.3gpp.org/DynaReport/25211.htm.

[108] A. Czylwik, “Synchronization for systems with antenna diversity,” in *IEEE 50th Vehicular Technology Conference (VTC)*, vol. 2, Sep. 1999, pp. 728–732.

[109] T. C. W. Schenk and A. van Zelst, “Frequency synchronization for MIMO OFDM wireless LAN systems,” in *IEEE 58th Vehicular Technology Conference (VTC)*, vol. 2, Oct. 2003, pp. 781–785.

[110] T. J. Liang, X. Li, R. Irmer, and G. Fettweis, “Synchronization in OFDM-based WLAN with transmit and receive diversities,” in *The 16th IEEE International Symposium on Personal, Indoor and Mobile Radio Communications*, vol. 2, Sep. 2005, pp. 740–744.

[111] A. N. Mody and G. L. Stuber, “Synchronization for MIMO OFDM systems,” in *IEEE Global Telecommunications Conference (GLOBECOM)*, vol. 1, Nov. 2001, pp. 509–513.

[112] T. Pollet, M. V. Bladel, and M. Moeneclaey, “BER sensitivity of OFDM systems to carrier frequency offset and Wiener phase noise,” *IEEE Transactions on Communications*, vol. 43, no. 2/3/4, pp. 191–193, Feb./Mar./Apr. 1995.

[113] K. Sathananthan and C. Tellambura, “Probability of error calculation of OFDM systems with frequency offset,” *IEEE Transactions on Communications*, vol. 49, no. 11, pp. 1884–1888, Nov. 2001.

[114] B. Stantchev and G. Fettweis, “Time-variant distortions in OFDM,” *IEEE Communications Letters*, vol. 4, no. 10, pp. 312–314, Oct. 2000.

[115] Y. Li and L. Cimini, “Bounds on the interchannel interference of OFDM in time-varying impairments,” *IEEE Transactions on Communications*, vol. 49, no. 3, pp. 401–404, Mar. 2001.

[116] M. Russell and G. L. Stuber, “Interchannel interference analysis of OFDM in a mobile environment,” in *IEEE 45th Vehicular Technology Conference (VTC)*, vol. 2, Jul. 1995, pp. 820–82.

[117] T. Keller and L. Hanzo, “Adaptive multicarrier modulation: a convenient framework for time-frequency processing in wireless communications,” *Proceedings of the IEEE*, vol. 88, no. 5, pp. 611–640, May 2000.

[118] L. Rugini and P. Banelli, “BER of OFDM systems impaired by carrier frequency offset in multipath fading channels,” *IEEE Transactions on Wireless Communications*, vol. 4, no. 5, pp. 2279–2288, Sep. 2006.

[119] M. Speth and H. Meyr, “Synchronization requirements for COFDM systems with transmit diversity,” in *IEEE Global Telecommunications Conference (GLOBECOM)*, vol. 3, Dec. 2003, pp. 1252–1256.

[120] W. Zhang and J. Lindner, “SINR analysis for OFDMA systems with carrier frequency offset,” in *IEEE 18th International Symposium on Personal, Indoor and Mobile Radio Communications (PIMRC)*, Sep. 2007.

[121] M. Speth, F. Classen, and H. Meyr, “Frame synchronization of OFDM systems in frequency selective fading channels,” in *IEEE 47th Vehicular Technology Conference (VTC)*, vol. 3, May 1997, pp. 1807–1811.

[122] Y. Mostofi and D. Cox, "Mathematical analysis of the impact of timing synchronization errors on the performance of an OFDM system," *IEEE Transactions on Communications*, vol. 54, no. 2, pp. 226–230, Feb. 2006.

[123] P. Hoeher, S. Kaiser, and P. Robertson, "Two-dimensional pilot-symbol-aided channel estimation by Wiener filtering," in *IEEE International Conference on Acoustics, Speech and Signal Processing*, vol. 3, Apr. 1997, pp. 1845–1848.

[124] S. Y. Park, B. S. Seo, and C. G. Kang, "Effects of frequency offset compensation error on channel estimation for OFDM system under mobile radio channels," *Signal Processing*, vol. 83, no. 12, pp. 2621–2630, Dec. 2003.

[125] C. R. N. Athaudage and A. D. S. Jayalath, "Enhanced MMSE channel estimation using timing error statistics for wireless OFDM systems," *IEEE Transactions on Broadcasting*, vol. 50, no. 4, pp. 369–376, Dec. 2004.

[126] V. Srivastava, C. K. Ho, P. Ho, W. Fung, and S. Sun, "Robust MMSE channel estimation in OFDM systems with practical timing synchronization," in *IEEE Wireless Communications and Networking Conference*, vol. 2, Mar. 2004, pp. 711–716.

[127] Y. Li, L. J. Cimini, and N. R. Sollenberger, "Robust channel estimation for OFDM systems with rapid dispersive fading channels," *IEEE Transactions on Communications*, vol. 46, no. 7, pp. 902–915, Jul. 1998.

[128] J. Park, J. Kim, M. Park, K. Ko, C. Kang, and D. Hong, "Performance analysis of channel estimation for OFDM systems with residual timing offset," *IEEE Transactions on Wireless Communications*, vol. 5, no. 7, pp. 1622–1625, Jul. 2006.

[129] D.-C. Chang, "Effect and compensation of symbol timing offset in OFDM systems with channel interpolation," *IEEE Transactions on Broadcasting*, vol. 54, no. 4, pp. 761–770, Dec. 2008.

[130] A. Nosratinia, T. E. Hunter, and A. Hedayat, "Cooperative communication in wireless networks," *IEEE Communications Magazine*, vol. 42, no. 10, pp. 74–80, Oct. 2004.

[131] A. Sendonaris, E. Erkip, and B. Aazhang, "User cooperation diversity: Part I: System description," *IEEE Transactions on Communications*, vol. 51, no. 11, pp. 1927–1938, Nov. 2003.

[132] ——, "User cooperation diversity: Part II: Implementation aspects and performance analysis," *IEEE Transactions on Communications*, vol. 51, no. 11, pp. 1939–1948, Nov. 2003.

[133] H. Zhang and H. Dai, "Cochannel interference mitigation and cooperative processing in downlink multicell multiuser MIMO networks," *EURASIP Journal on Wireless Communications and Networking*, vol. 2004, no. 2, pp. 222–235, Dec. 2004.

[134] V. Jungnickel, T. Wirth, M. Schellmann, and T. Haustein, "Synchronization of cooperative base stations," in *IEEE International Symposium on Wireless Communication Systems*, Oct. 2008, pp. 329–334.

[135] B. Zarikoff and J. Cavers, "Carrier frequency offset in coordinated multi-base MIMO narrowband systems," in *IEEE 67th Vehicular Technology Conference (VTC)*, May 2008, pp. 872–877.

[136] G. Boudreau, J. Panicker, N. Guo, R. Chang, N. Wang, and S. Vrzic, "Interference coordination and cancellation for 4G networks," *IEEE Communications Magazine*, vol. 47, no. 4, pp. 74–81, Apr. 2009.

[137] A. Damnjanovic, J. Montojo, Y. Wei, T. Ji, T. Luo, M. Vajapeyam, T. Yoo, O. Song, and D. Malladi, "A survey on 3GPP heterogeneous networks," *IEEE Transactions on Wireless Communications*, vol. 18, no. 3, Jun. 2011.

[138] A. Ghosh, N. Mangalvedhe, R. Ratasuk, B. Mondal, M. Cudak, E. Visotsky, T. Thomas, J. Andrews, P. Xia, H. Jo, H. Dillon, and T. Novlan, "Heterogeneous cellular networks: from theory to practice," *IEEE Communications Magazine*, vol. 50, no. 6, Jun. 2012.

[139] B. Zarikoff and J. K. Cavers, "Coordinated multi-cell systems: carrier frequency offset estimation and correction," *IEEE Journal on Selected Areas in Communications*, vol. 28, no. 9, pp. 1490–1501, Dec. 2010.

[140] Z. Cao, U. Tureli, and Y.-D. Yao, "Deterministic multiuser carrier-frequency offset estimation for interleaved OFDMA uplink," *IEEE Transactions on Communications*, vol. 52, no. 9, pp. 1585–1594, Sep. 2004.

[141] J. Lee, S. Lee, K.-J. Bang, S. Cha, and D. Hong, "Carrier frequency offset estimation using ESPRIT for interleaved OFDMA uplink systems," *IEEE Transactions on Vehicular Technology*, vol. 56, no. 5, pp. 3227–3231, Sep. 2007.

[142] O. Besson and P. Stoica, "On parameter estimation of MIMO flat-fading channels with frequency offsets," *IEEE Transactions on Signal Processing*, vol. 51, no. 3, pp. 602–613, Mar. 2003.

[143] S. Ahmed, S. Lambotharan, A. Jakobsson, and J. A. Chambers, "MIMO frequency-selective channels with multiple-frequency offsets: estimation and detection techniques," *IEE Proceedings on Communications*, vol. 152, no. 4, pp. 489–494, Aug. 2005.

[144] ——, "Parameter estimation and equalization techniques for communication channels with multipath and multiple frequency offsets," *IEEE Transactions on Communications*, vol. 53, no. 2, pp. 219–223, Feb. 2005.

[145] J. Chen, Y.-C. Wu, S. Ma, and T.-S. Ng, "Joint CFO and channel estimation for multiuser MIMO-OFDM systems with optimal training sequences," *IEEE Transactions on Communications*, vol. 56, no. 8, pp. 4008–4019, Aug. 2008.

[146] M.-O. Pun, M. Morelli, and C.-C. J. Kuo, "Maximum-likelihood synchronization and channel estimation for OFDMA uplink transmissions," *IEEE Transactions on Communications*, vol. 54, no. 4, pp. 726–736, Apr. 2006.

[147] L. Haring, S. Bieder, A. Czylwik, and T. Kaiser, "Estimation algorithms of multiple channels and carrier frequency offsets in application to multiuser OFDM systems," *IEEE Transactions on Wireless Communications*, vol. 9, no. 3, pp. 865–870, Mar. 2010.

[148] M.-K. Oh, X. Ma, G. B. Giannakis, and D.-J. Park, "Cooperative synchronization and channel estimation in wireless sensor networks," in *Conference Record of the Thirty-Seventh Asilomar Conference on Signals, Systems and Computers*, vol. 1, Nov. 2003, pp. 238–242.

[149] B. Zarikoff and J. Cavers, "Multiple frequency offset estimation for the downlink of coordinated MIMO systems," *IEEE Journal on Selected Areas in Communications*, vol. 26, no. 6, pp. 901–912, Aug. 2008.

[150] T.-H. Pham, A. Nallanathan, and Y.-C. Liang, "Joint channel and frequency offset estimation in distributed MIMO flat-fading channels," *IEEE Transactions on Wireless Communications*, vol. 7, no. 2, pp. 648–656, Feb. 2008.

[151] T. K. Moon, "The expectation-maximization algorithm," *IEEE Signal Processing Magazine*, vol. 13, no. 6, pp. 47–60, Nov. 1996.

[152] J. A. Fessler and A. O. Hero, "Space-alternating generalized expectation-maximization algorithm," *IEEE Transactions on Signal Processing*, vol. 42, no. 10, pp. 2664–2677, Oct. 1994.

[153] I. Ziskind and M. Wax, "Maximum likelihood localization of multiple sources by alternating projection," *IEEE Transactions on Acoustics, Speech, and Signal Processing*, vol. 36, no. 10, pp. 1553–1560, Oct. 1988.

[154] Y. Zeng, A. R. Leyman, and W. S. Leon, "Multiple frequency offset estimations in multiuser OFDMA," in *IEEE 65th Vehicular Technology Conference (VTC)*, Apr. 2007, pp. 2741 – 2745.

[155] Y. Wu, J. W. M. Bergmans, and S. Attallah, "Carrier frequency offset estimation for multiuser MIMO OFDM uplink using CAZAC sequences: performance and sequence optimization," *EURASIP Journal on Wireless Communications and Networking*, vol. 2010, Mar. 2010.

[156] Y.-R. Tsai, H.-Y. Huang, Y.-C. Chen, and K.-J. Yang, "Simultaneous multiple carrier frequency offsets estimation for coordinated multi-point transmission in OFDM systems," *IEEE Transactions on Wireless Communications*, vol. 12, no. 9, pp. 4558–4568, Sep. 2013.

[157] Y. Zeng and A. R. Leyman, "Pilot-based simplified ML and fast algorithm for frequency offset estimation in OFDMA uplink," *IEEE Transactions on Vehicular Technology*, vol. 57, no. 3, pp. 1723–1732, May 2008.

[158] D. Chu, "Polyphase codes with good periodic correlation properties," *IEEE Transactions on Information Theory*, vol. 18, no. 4, pp. 531–532, Jul. 1972.

[159] S.-W. Keum, D.-H. Kim, and H.-M. Kim, "An improved frequency offset estimation based on companion matrix in multi-user uplink interleaved OFDMA systems," *IEEE Signal Processing Letters*, vol. 21, no. 4, pp. 409–413, Apr. 2014.

[160] Q. Huang, M. Ghogho, J. Wei, and P. Ciblat, "Practical timing and frequency synchronization for OFDM-based cooperative systems," *IEEE Transactions on Signal Processing*, vol. 58, no. 7, pp. 3706–3716, Jul. 2010.

[161] Y. Yao and T.-S. Ng, "Correlation-based frequency offset estimation in MIMO system," in *IEEE 58th Vehicular Technology Conference (VTC)*, vol. 1, Oct. 2003, pp. 438–442.

[162] Y.-J. Liang, G. L. Stuber, J.-F. Chang, and D.-N.Yang, "A joint channel and frequency offset estimator for the downlink of coordinated MIMO-OFDM systems," *IEEE Transactions on Wireless Communications*, vol. 11, no. 6, pp. 2254–2265, Jun. 2012.

[163] Y.-S. Choi, P. J. Voltz, and F. A. Cassara, "On channel estimation and detection for multicarrier signals in fast and selective Rayleigh fading channels," *IEEE Transactions on Communications*, vol. 49, no. 8, pp. 1375–1387, Aug. 2001.

[164] W. J. Jeon, K. H. Chang, and Y. S. Cho, "An equalization technique for orthogonal frequency-division multiplexing systems in time-variant multipath channels," *IEEE Transactions on Communications*, vol. 47, no. 1, pp. 27–32, Jan. 1999.

[165] L. Rugini, P. Banelli, and G. Leus, "Simple equalization of time-varying channels for OFDM," *IEEE Communications Letters*, vol. 9, no. 7, pp. 619–621, Jul. 2005.

[166] D. Veronesi and D. L. Goeckel, "Multiple frequency offset compensation in cooperative wireless systems," in *IEEE Global Telecommunications Conference (GLOBECOM)*, Nov. 2006, pp. 1–5.

[167] N. Benvenuto, S. Tomasin, and D. Veronesi, "Multiple frequency offsets estimation and compensation for cooperative networks," in *IEEE Wireless Communications and Networking Conference*, Mar. 2007, pp. 891–895.

[168] Z. Li, D. Qu, and G. Zhu, "An equalization technique for distributed STBC-OFDM system with multiple carrier frequency offsets," in *IEEE Wireless Communications and Networking Conference (WCNC)*, Apr. 2006, pp. 839–843.

[169] Q. Huang, M. Ghogho, and J. Wei, "Data detection in cooperative STBC-OFDM systems with multiple carrier frequency offsets," *IEEE Signal Processing Letters*, vol. 16, no. 7, pp. 600–603, Jul. 2009.

[170] Y. Yao and X. Dong, "Multiple CFO mitigation in amplify-and-forward cooperative OFDM transmission," *IEEE Transactions on Communications*, vol. 60, no. 12, pp. 3844–3854, Dec. 2012.

[171] T. Liu, S. Zhu, and F. Gao, "A simplified MMSE equalizer for distributed TR-STBC systems with multiple CFOs," *IEEE Communications Letters*, vol. 16, no. 8, pp. 1300–1303, Aug. 2012.

[172] J. Mietzner, J. Eick, and P. A. Hoeher, "On distributed space-time coding techniques for cooperative wireless networks and their sensitivity to frequency offsets," in *ITG Workshop on Smart Antennas*, Mar. 2004, pp. 114–121.

[173] K. Deng, Y. Tang, S. Shao, and K. Sun, "Correction of carrier frequency offsets in OFDM-based spatial multiplexing MIMO with distributed transmit antennas," *IEEE Transactions on Vehicular Technology*, vol. 58, no. 4, pp. 2072–2077, May 2009.

[174] Y.-J. Won and B.-S. Seo, "Compensation of multiple carrier frequency offsets in amplify-and-forward cooperative networks," in *IEEE 24th International Symposium on Personal, Indoor and Mobile Radio Communications (PIMRC)*, Sep. 2013, pp. 159–163.

[175] N. Michailow, M. Matthé, I. S. Gaspar, A. N. Caldevilla, L. L. Mendes, A. Festag, and G. Fettweis, "Generalized frequency division multiplexing for 5th generation cellular networks," *IEEE Transactions on Communications*, vol. 62, no. 9, pp. 3045–3061, Sep. 2014.

[176] B. Farhang-Boroujeny, "OFDM versus filter bank multicarrier," *IEEE Signal Processing Magazine*, vol. 28, no. 3, pp. 92–112, May 2011.

Errata

Publication II

Publication II contains two errors. First, in the first as well as in the last paragraph of Section 2 it is mentioned that the employed modulation scheme is assumed known. However, in fact the method does not require this information. Second, after equation (3.7) the condition for the expression to form an eigendecomposition of matrix $\boldsymbol{R}_x(\tau)$ should read as $\boldsymbol{u}_{k_1}^{rH}\boldsymbol{u}_{k_2}^{l} = 0$, $\forall k_1, k_2$, meaning that the vectors should be orthogonal to each other.

Publication VI

Publication VI contains an error in equations (7) and (8). In equation (7), the term Δ_K should be placed in the denominator, and the imaginary unit should be removed. Thus, the equation should read as follows:

$$\hat{\tau} = -\frac{N}{2\pi\Delta_K} \arg\left\{ \sum_{r=0}^{N_r-1} \sum_{t=0}^{N_t-1} \sum_{q=0}^{Q_p-1} \sum_{k=0}^{K_p(q)-2} \hat{g}_{r,t}(k,q)\hat{g}_{r,t}^{*}(k+1,q) \right\}.$$

In equation (8), the imaginary unit should be removed and the equation should read as follows:

$$\hat{\varepsilon} = \frac{N}{2\pi N_s\Delta_Q} \arg\left\{ \sum_{r=0}^{N_r-1} \sum_{t=0}^{N_t-1} \sum_{k=0}^{K_p-1} \sum_{q=0}^{Q_p(k)-2} \hat{g}_{r,t}(k,q)\hat{g}_{r,t}^{*}(k,q+1) \right\}.$$

Aalto-DD 114/2015

ISBN 978-952-60-6332-4 (printed)
ISBN 978-952-60-6333-1 (pdf)
ISSN-L 1799-4934
ISSN 1799-4934 (printed)
ISSN 1799-4942 (pdf)

Aalto University
School of Electrical Engineering
Department of Signal Processing and Acoustics
www.aalto.fi

BUSINESS + ECONOMY

ART + DESIGN + ARCHITECTURE

SCIENCE + TECHNOLOGY

CROSSOVER

DOCTORAL DISSERTATIONS